

Liquid Crystalline Carbon Nanotube Suspensions

—

From Unique Challenges to Unique Properties

Dissertation

zur Erlangung des

Doktorgrades der Naturwissenschaften (Dr. rer. nat.)

der

Naturwissenschaftlichen Fakultät II

Chemie, Physik und Mathematik

der Martin-Luther-Universität

Halle-Wittenberg

vorgelegt

von Herrn Stefan Schymura

geb. am 14.07.1982 in Ludwigsburg

Tag der Verteidigung: 04.07.2013

Ich erkläre hiermit an Eides statt, dass ich die vorliegende Dissertation selbstständig und nur unter Verwendung der angegebenen Literatur und Hilfsmittel angefertigt habe.

Die Arbeit wurde bisher in gleicher oder ähnlicher Form keiner anderen Prüfungsbehörde vorgelegt.

Leipzig, den

Unterschrift:

Die vorliegende Arbeit wurde am Institut für Chemie – Physikalische Chemie der Martin-Luther-Universität Halle-Wittenberg angefertigt.

Hauptberichterstatter: Prof. Dr. Jan Lagerwall

Berichterstatter: Prof. Dr. Rudolf Zentel

Berichterstatter: Prof. Dr. Alfred Blume

To my Family and Friends

For any comments, questions and criticisms feel free to contact the author:
Email: S.Schymura@gmx.de

At first I want to thank my supervisor Prof. Dr. Jan Lagerwall for giving me the chance of working in the interesting field of carbon nanotube liquid crystal composites and for his support and motivation, which brought light into the darkness of failed experiments and difficult analysis of complex data throughout the course of this thesis.

I greatly appreciated the scientific and social atmosphere in the group and had the chance of working on various fields also not directly linked to this thesis like microfluidics and electrospinning. I want to thank my colleagues Sarah Dölle, Eva Enz, Martin Kühnast and Hsin-Ling Liang (in alphabetical order) for creating said atmosphere. Specifically I want to thank Martin Kühnast for the synthesis of 6T7 and for the help with the dispersion experiments and UV/Vis measurements, Eva Enz for help with DSC measurements, first dispersion experiments and for mastering the challenge of sharing an office with me. Also I want to thank Sarah Dölle, Eva Enz, Hsin-Ling Liang for the coproduction on the topics of lyotropic LC/CNT composites, electrospinning and LC microfluidics, which found no space in this thesis.

Furthermore I thank the whole group of Prof. Dr. Alfred Blume at the Physical Chemistry department at the University of Halle for discussion and hardware support contributing to this work in various ways and making my time in Halle as pleasant as it was.

I am grateful also to Prof. Dr. Giusy Scalia, as well as the group of Prof. Dr. Frank Gießelmann for introducing me to the LC and CNT research field during my diploma thesis and the continuing support during this PhD thesis. Specifically I want to thank Alberto Sanchez-Castillo for help with the Raman measurements, Florian Schörg for the co-operation on the lyotropic LC/CNT composites and Dr. Stefan Jagiella for the calculation of the dipole moments for the various thermotropic LCs.

Thanks as well to Dr. Per Rudquist at Chalmers University for making the visit to Sweden possible and letting me use the glue dispenser.

Prof. Dr. Alan Guymon and Bradley Forney from the University of Iowa are thanked for providing of the polymerizable surfactants. We kindly thank Dr. M. Czanta (Merck) and Dr. R. Eidenschink (Nematel) for samples of E7 and PCH7, respectively

Furthermore financial support of the “Exzellenzcluster nanostrukturierte Materialien” of the Land Sachsen-Anhalt is gratefully acknowledged.

Last but not least I want to thank my family and friends for the support I have gotten throughout this thesis and my whole life in general, which altogether made the preparation of this work possible.

Parts of this thesis were published in the following articles:

„Macroscopic-scale carbon nanotube alignment via self-assembly in lyotropic liquid crystals“, S. Schymura, E. Enz, S. Roth, G. Scalia, J. Lagerwall, *Synthetic Met.* 159(21-22), 2177-2179, **2009**

„Towards Efficient Dispersion of Carbon Nanotubes in Thermotropic Liquid Crystals“, S. Schymura, M. Kühnast, V. Lutz, S. Jagiella, U. Dettlaff-Weglikowska, S. Roth, F. Gießelmann, C. Tschierske, G. Scalia, J. Lagerwall, *Adv. Funct. Mat.* 20(19), 3350-3357, **2010**

„Filament formation in carbon nanotube-doped lyotropic liquid crystals“, S. Schymura, S. Dölle, J. Yamamoto, J. Lagerwall, *Soft Matter* 7, 2663-2667, **2011**

Further investigations made during the course of this work which are not incorporated in this thesis were published here:

„Nematic-Smectic Transition under Confinement in Liquid Crystalline Colloidal Shells“, H.-L. Liang, S. Schymura, P. Rudquist, J. Lagerwall, *Phys. Rev. Lett.* 106(24), 247801, **2011**

„ Effects of chain branching and chirality on liquid crystalline phases of bent-core molecules: blue phases, de Vries transitions and switching of diastereomeric states“, H. Ocak, B. Bigin-Eran, M. Prehm, S. Schymura, J. Lagerwall, C. Tschierske, *Soft Matter* 7, 8266-8280, **2011**

„Utilizing the Krafft phenomenon to generate ideal micelle-free surfactant-stabilized nanoparticle suspensions“, S. Dölle, B.-D. Lechner, J.H. Park, S. Schymura, J. Lagerwall, G. Scalia, *Angew. Chem. Int. Ed. Engl.* 51(13), 3254-3257, **2012**

Table of content

1. Introduction	1
2. Background	3
2.1. Liquid crystals	3
2.1.1. Thermotropic liquid crystals	4
2.1.2. Lyotropic liquid crystals	9
2.2. Carbon Nanotubes	12
2.3. LC/CNT composites	16
2.4. Percolation	21
2.5. Depletion attraction	24
3. Methods	27
3.1. Raman spectroscopy	28
3.2. Conductivity measurements	31
3.3. Rheology	33
3.4. Polarizing microscopy	35
4. Results and Discussion	39
4.1. Producing lyotropic LC/CNT composites	40
4.1.1. The same procedure as every time?	41
4.1.2. Substantial matters	46
4.2. Towards efficient dispersion of CNTs in thermotropic liquid crystals	52
4.2.1. Results	53
4.2.2. Discussion	61
4.3. Filament formation in carbon nanotube-doped lyotropic liquid crystals	72
4.3.1. Understanding the filament formation process	73
	IX

4.3.2. Application of LC/CNT-filaments	81
4.4. CNT percolation in thermotropic LCs	86
4.5. CNTs and fullerenes in chiral thermotropic LCs	91
5. Conclusions and Outlook	99
6. Bibliography	101
7. Appendix	116
7.1. Materials	116
7.2. Equipment	119
7.3. Procedures	120
7.3.1. Dispersion procedures	120
7.3.2. Preparation of lyotropic LC/CNT composite	122
7.3.3. Checking for polarizer effect	123
7.3.4. Polymerization of lyotropic LCs	124
7.3.5. High Speed camera measurements	124
7.3.6. Percolation measurements	125
7.3.7. UV/Vis Measurements on thermotropic LC/CNT mixtures	126
7.3.8. Calculation of dipole moments of thermotropic LCs	127
7.4. Additional data	127
7.4.1. Degrees of protonation of surfactants	127
7.4.2. Viscosity of thermotropic LCs	128
7.4.3. Klopman-Salem Equation	129
8. Curriculum Vitae	130
9. List of Publications	131

1. Introduction

The topic of the here presented work is the combination of two interesting and different materials. The first is liquid crystals, discovered already in 1888 [1] and known to the general public for their main application in the liquid crystal display (LCD) technology. Although our modern informational society would be unimaginable without LCs, this development could not be foreseen in the decades of research following their discovery. In 1924, more than 30 years after their discovery, Daniel Vorländer, main liquid crystal synthesist of his time, on the question if he can imagine an application for this sort of material gave the answer: “I see no possibility for that.” This statement remained essentially true until 1969 when Hans Kelker synthesized the first room temperature LC [2]. With the subsequent invention of the twisted nematic LCD by Martin Schadt and Wolfgang Helfrich in 1970 [3] the starting point for widespread liquid crystal application was set, about 80 years after their discovery, and led to LCDs becoming a part of our everyday life.

In very strong contrast to this development stands the second material that is the topic of this thesis, the carbon nanotubes (CNTs). This new modification of elemental carbon, discovered about 100 years after the LCs in 1991 [4], quickly caught the interest of the whole scientific community. Following their discovery a vast variety of possible applications were introduced into the scientific discussion. From nano computer, new super materials, cure for cancer [5-9], cause of cancer [10-12] (not as an application) to space elevator [13,14], nanotubes were proposed to revolutionize almost every scientific field known to man, inspiring research teams all around the world with a steep rise of publications in the field to over 11000 publications per year in 2012*. Among others, carbon nanotubes even contributed to making

* Web of Science search: Topic: carbon nanotube

the general public outside the scientific community aware of the word “nano”, as it became a key word for various marketing strategies. It even achieved the prime ennoblement for new technologies possible in modern western society; outright fear of hypothetical risks.

Yet, despite all the proposed applications, almost two decades after their discovery the only commercially available applications of CNTs are composites of CNTs in polymer matrixes (which are conducting due to the CNTs), as filling material in batteries (where they prolong the lifetime) and their incorporation into tennis rackets and golf clubs (where they serve the purpose of a unique selling point). Compared with other revolutionizing technologies such as the transistor technology and the high expectations raised by the multitude of possible applications this outcome seems rather disappointing, especially when having in mind that the CNTs currently loose their rank as revolutionary material to their little brother, graphene [15].

The main problems in CNT application today is their selective synthesis, their lasting separation into single tubes rather than aggregates of tubes and the control of their orientation. Incorporating the CNTs into an LC matrix could solve the two latter. But how does the liquid crystal act as a problem solver?

The answer to this question is self-assembly. Although this term by some is referred to as a euphemism for “and magic happens here” [16] the concept provides a great potential for overcoming two of the prime obstacles of CNT utilization and the remark should be countered by quoting Arthur C. Clarke:

“Any sufficiently advanced technology is indistinguishable from magic.” [17]

The goal of this work is therefore to explore the magic of self-assembly of CNTs in LCs and to show that in fact magic is a concept that is not needed to explain the interesting and unique properties of the resulting composites. In order to produce such composites one has to overcome unique challenges. Thus the outline of this thesis is to first explain in more detail the background of LCs and CNTs and their composites as well as an introduction of important concepts such as percolation and depletion attraction (chapter 2) and the experimental methods (chapter 3). This will be followed by a description of the results of my research done on LC/CNT composites and the related discussion, focusing first on the challenges that the preparation of these composites hold (chapters 4.1 and 4.2) and then on the properties of said compounds (chapters 4.3 – 4.5). As last point before the literature and appendix there will be a conclusion and outlook (chapter 5).

2. Background

2.1. Liquid crystals

In 1888 Austrian botanist Friedrich Reinitzer reported his observation that cholesteryl benzoate has two melting points [1]. At 145.4 °C it melts into a cloudy liquid, not turning into a clear liquid, as would be expected for any normal solid to liquid phase transition, until at 178.5°C. Although there have been similar reports before, this is generally acknowledged to be the birthing hour of liquid crystal research, a term that was eventually coined by the German physicist Otto Lehmann in 1904 [18] and prevailed ever since. But what is meant by the seemingly schizophrenic term liquid crystal? Can a substance be liquid and crystalline at the same time?

The shortest explanation for what liquid crystals actually are would be to label them as anisotropic fluids. The liquid crystalline phase is fluid like a liquid while showing direction dependent physical properties otherwise only known of crystals, the most striking of which is optical birefringence. One distinguishes between thermotropic liquid crystals – where the liquid crystalline phase behavior occurs with temperature – and lyotropic liquid crystals, which are multi-component mixtures, the liquid crystallinity of which depends on the concentration of the different components.

2.1.1. Thermotropic liquid crystals

In thermotropic liquid crystals the liquid crystallinity occurs at temperatures between the crystal phase and the isotropic liquid – therefore liquid crystalline phases are often called mesophases (Greek, ‘μεσο’ (meso): in between). An ideal crystal shows a perfect order (disregarding defects), meaning that from knowing the position and orientation of one molecule one could theoretically calculate the position and orientation of any other molecule inside the crystal. The crystal possesses perfect long-range positional and orientational order. The liquid in contrast shows neither positional order nor orientational order with long range. In the liquid crystalline state of matter however a certain amount of the perfect ordering of the crystal prevails upon melting until the substance turns into an isotropic liquid at the clearing point with only short-range order remaining (Fig. 2.1).

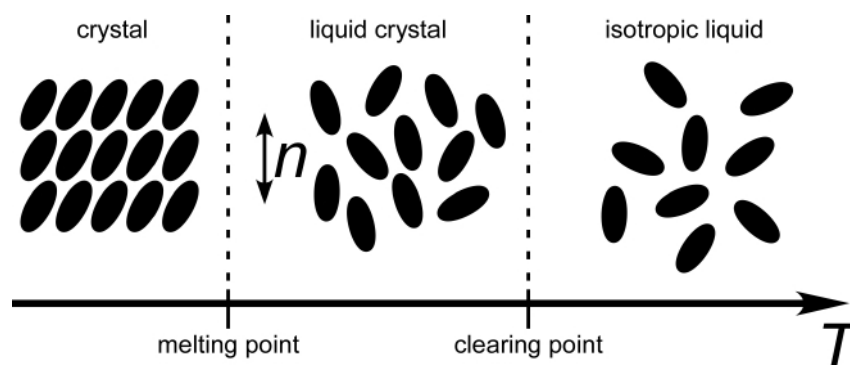


Fig. 2.1: Schematic 2D depiction of the phase sequence of a simple thermotropic calamitic LC.

Materials showing liquid crystallinity are composed of molecules with highly anisometric shapes such as rods or discs. The molecules are called mesogens, calamitic or discotic, respectively (Fig. 2.2 a, b). Such molecules are in general composed of a stiff core, the mesogenic unit, with flexible wing groups attached to it. In the simplest LC phase, the nematic phase N (Fig. 2.3 a) these molecules show no positional ordering but tend to orient along a preferential direction, the director \mathbf{n} , resulting in a long-range orientational order in the phase, rendering it anisotropic. An illustrative picture for a bulk sample in the case of calamitic LCs is a bowl of rice (coins in the case of discotic LCs) (Fig. 2.2 c) in which the rice grains, while not pointing all in the same direction, preferably align along a certain direction. Yet this direction varies from place to place in the bowl. This kind of director modulation in bulk samples is the reason for the turbidity of a bulk LC sample, because as the director

changes throughout the sample, the optical properties experienced by a light beam passing through it varies, resulting in various scattering processes. While the rice picture may catch the orientational ordering of nematic phases it completely fails on the other aspect of liquid crystallinity, the fluidity. It is important to have in mind that such pictures can only resemble a freeze frame of an LC. In reality the molecules at all time retain mobility in all directions while statistically the probability of orientation along the director is slightly higher than for any other single direction.

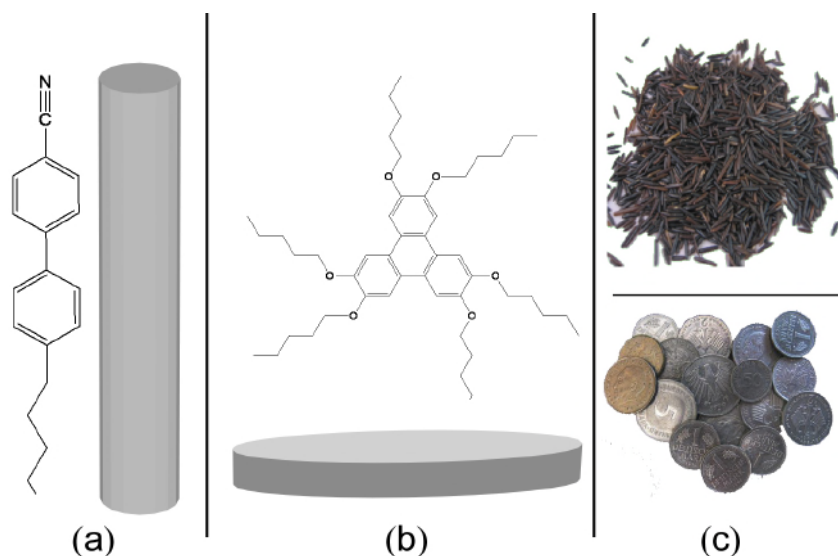


Fig. 2.2: Typical anisometric shape of mesogenic molecules, (a) rodlike calamitic 4-pentyl-4'-cyanobiphenyl (5CB) and (b) disklike discotic hexapentyloxytriphenylene (HAT5) and (c) illustrative pictures for their nematic phase, rice grains and coins, respectively.

The orientational ordering has its physical origin mainly in steric and electrostatic interactions between the molecules. With the anisometric shape of the molecules comes an anisotropy of the electric polarizability. Thus the induced dipoles that are responsible for the basic van der Waals forces between any nearby molecules also tend to point along the long axis of the molecule. And as dipoles in general align parallel, more accurately antiparallel, to each other to minimize the energy the molecules will align with their long axes parallel to each other. This also explains some basic structural principles of LCs such as the beneficial influence of large systems of delocalized thus polarizable electrons as in the common biphenyl cores or permanent dipoles as in the cyano groups, both of which are common structural features of LC-forming materials although by no means mandatory. These features promote ordering while the long flexible wing groups prevent crystallization.

Mathematically the ordering can be described by an orientational distribution function (ODF) considering a mean field of force acting on every molecule of the phase as done by

Maier and Saupe [19]. By developing the ODF using Legendre polynomials the first non-trivial parameter S_2 can be used for quantifying the degree of orientational order:

$$S_2 = \frac{1}{2} \langle 3 \cos^2 \beta - 1 \rangle \quad (2.1)$$

The variable β is the angle that the long axis of a single molecule confines with the director. For perfect orientational order, i.e. all molecules perfectly aligned along the director, S_2 equals 1. For no orientational order, i.e. an isotropic liquid, S_2 equals 0. S_2 is also called the order parameter and typically is in the range of 0.4 to 0.7 for nematic LCs.

The nematic phase is not the only LC phase. There are plenty of other phases showing varying degrees of order. Below the nematic phase often the so-called smectic phases can be found that in addition to the orientational order show also a certain amount of positional order, meaning that the molecules arrange in layers. Inside the layers there is no long-range positional order only between the layers, making each layer a two dimensional fluid. The director can either point in the same direction as the layer normal as in the smectic A phase (SmA, Fig. 2.3 b) or tilt away of it as in the smectic C phase (SmC, Fig. 2.3 c). In other smectic phases the degree of positional order increases further for example by the formation of hexagonal domains inside the layers.

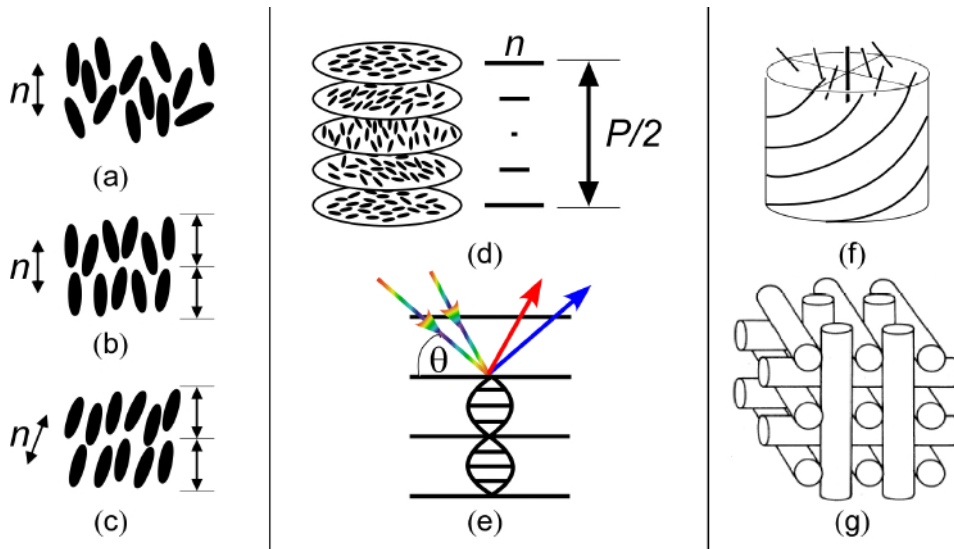


Fig. 2.3: Schematic depiction of LC phases (a) N, (b) SmA, (c) SmC, (d) N* and (f, g) BP*, respectively and (e) selective reflection at N*-helix.

Interesting effects can be observed when one adds chirality, also called handedness, to the system of a nematic LC either by using chiral molecules from the start or by adding chiral dopants. In this case the nematic director exhibits a twisted configuration. In the chiral nematic-

ic phase or N* phase (chiral phases are indicated by an asterisk), commonly also called the cholesteric phase as it was first observed in cholesterol derivatives, the molecules do not prefer being exactly parallel to each other but tend to align at a slight angle to each other along one direction. The director therefore rotates throughout the sample forming a helix (Fig. 2.3 d), which in normal nematics would be a deformation of the director field connected to an energy penalty. The distance over which a full turn is performed is called the pitch P . The optical periodicity is however $P/2$ since the director is not a vector and so a physically similar state is already reached after a rotation of 180° rather than a full rotation.

This has an interesting outcome on the interaction of a cholesteric LC with light. In a simplified depiction the half-turns of the helix can be compared to layers at which reflection of light occurs. Yet only light gets reflected which is circular polarized with the same handedness of the helix leading to a phenomenon called selective reflection (Fig. 2.3 e). Depending on the angle of incidence only a certain wavelength of light gets reflected in the same fashion as X-rays get diffracted at crystal planes. Analogously one can formulate Bragg's law [20]:

$$\lambda = 2d \sin \theta \quad (2.2)$$

with λ being the wavelength of light incident in the medium at an angle of θ and d the optical periodicity, i.e. $P/2$ in the case of a cholesteric LC. With the incident light along the helix, thus at an angle of 90° , this comes to:

$$\lambda = P \quad (2.3)$$

When taking into account that λ here is the wavelength of the light inside the medium the wavelength of the reflected light that an observer actually sees can be calculated using the average refractive index n of the material as:

$$\lambda_r = nP \quad (2.4)$$

This means that when the pitch of the helical modulation of the director field shown by a particular cholesteric LC is in the range of the wavelengths in the visible electromagnetic spectrum the LC also shows a variety of colors depending on the viewing angle and temperature. The pitch most often decreases hyperbolically on heating as can be understood by the fact that the phase usually following the N*- phase on cooling, the SmA* phase, does not allow any twist of the director as this would interfere with the layer configuration. So the pitch typically decreases steeply from infinity – or no helix – in the SmA* phase as the substance enters the cholesteric phase in a fashion that can often be described by a hyperbola

$$\lambda_r = \frac{k}{(T - T_{NA})} \quad (2.5)$$

with T being the temperature, T_{NA} the transition temperature from SmA* to N* and an adjustable parameter k .

With increasing tendency for twisting additional phases can be formed at temperatures above the N* phase, the so-called blue phases BP*. As for the colorful appearance of the normal N* phases the first observation of blue phases was already reported by Reinitzer who stated that the cholesteryl benzoate turned blue shortly before the clearing point. Yet the recognition that this observation indicated separate, thermodynamically stable phases took until the mid 1970s. There are three different blue phases not all of which are well understood [21]. As a prime example for blue phase structure the BPI phase shall be explained in more detail. BPI is composed of building blocks called double twist cylinders (Fig. 2.3 f). These are cylinders in which the director is parallel to the long axis in the center, twisting in every direction when going outwards from the center. These cylinders then pack into a complex structure with defects – places where the director field is undefined (the phase is thus effectively isotropic here) – wherever different double twist cylinders meet. These defects form a cubic lattice (Fig. 2.3 g) rendering the whole phase optically isotropic. The color of the blue phase depends on the lattice constants and the domain orientation with respect to the viewing direction (blue phases do not have to be blue). The blue phases generally occur only in a small temperature range of about one degree right below the clearing point.

2.1.2. Lyotropic liquid crystals

Just like thermotropic LCs, lyotropic LCs are fluids that show anisotropy in their physical properties. Exactly as with thermotropic LCs this is due to the anisometric shape of the building blocks of the LC phases. The basic difference between thermotropic and lyotropic LCs is the nature of said building blocks. Whereas in thermotropic LCs the mesogens are individual molecules, in lyotropic LCs they are generally agglomerates of many individual molecules in a solvent that is different from these molecules.

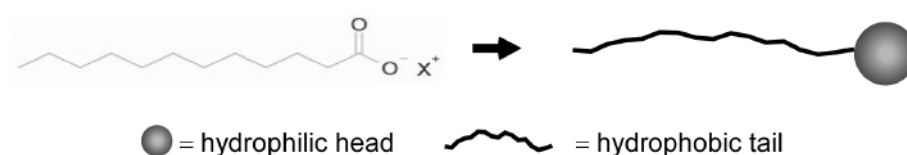


Fig. 2.4: Structure of the surfactant laurinat and its schematic depiction.

Typically these phases are composed of amphiphilic molecules in water. These molecules generally have two distinct features, a hydrophilic and a hydrophobic part. Most common is the combination of a hydrophilic, meaning polar (often ionic), head group paired with a non-polar tail, typically an alkyl chain (Fig. 2.4). Such molecules combine two different tendencies in one entity. The ionic head group interacts very well with the surrounding water. The alkyl chains however cause the water molecules to find themselves in a frustrated environment, as the chains cannot participate in hydrogen bonding, thus reducing the interaction space of the water molecules. Thus the water primarily for entropic reasons expels the alkyl chains. This has as result that amphiphilic molecules move to the surface so that the polar head group can interact with the water while the alkyl chains get exposed to the air. That is why these molecules are generally called surfactants for surface-active agents. These molecules will move to whatever surface more non-polar than water to which the solution is exposed to, making it possible for the surfactants to cover non-polar substances and to promote their dissolution, which is the principle of using soap for cleaning. This phenomenon is called the hydrophobic effect.

A different mechanism to avoid the frustrating presence of alkyl chains of amphiphilic molecules in a polar solvent is for amphiphiles to cluster together and to form associates where the polar head groups are exposed to the water while the alkyl chains are surrounded by other alkyl chains inside the associated structure, which is called micelle. This however can

only happen above a concentration threshold, the critical micelle concentration (CMC). The lowest temperature at which this concentration can be reached is called the Krafft temperature.

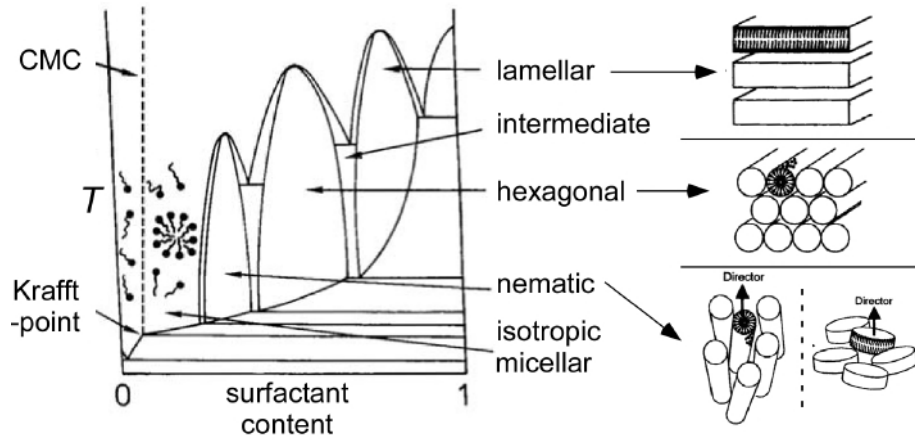


Fig. 2.5: Typical phase diagram of the lyotropic system surfactant/water [22] and phase structures [23].

These micelles can form various shapes from simple spherical micelles to disks, rods or layer structures. This variety of structures can be made plausible by simple geometrical considerations of the size of the polar head group in relation to the volume of the hydrophobic tail. With knowledge of these factors a packing parameter p can be defined as [24]:

$$p = V / la_0 \quad (2.6)$$

with V the volume of the hydrophobic tail, l the length of the hydrophobic tail (alkyl chain in all-trans conformation) and a_0 the effective area the polar head group occupies at the water/micelle border. Hence the packing parameter represents a comparison of the theoretical volume the molecule would have if the head group and the tail had the same breadth and the actual volume the tail occupies and is thus a direct representation of the shape of the micelle building blocks. If the head group is much larger than the hydrophobic tail the shape of the molecule resembles a cone, which acts as building block for a sphere and would have a packing parameter typically around 1/3. The more the head-to-tail ratio grows to 1 the more the building block resemble wall stones (bricks) which produce just that, walls, e.g. layer structures. The size of the head group is very dependent on the composition of the mixture, mainly the amount of hydratization and the presence of other electrolytes or co-surfactants, so that the same substance can form various structures at different concentrations.

At high enough concentrations rod-like or disk-like micelles lead to nematic ordering of these associates rendering the whole phase liquid crystalline. At even higher concentrations

rod-like micelles will eventually extend to quasi-infinite length and pack closely together with long-range positional ordering in a columnar phase, often with hexagonal lattice. Even higher concentrations can lead to lamellar phases where the associates form a layer structure corresponding to the smectic phases known from thermotropic LCs.

2.2. Carbon Nanotubes

For a long time the world of allotropes of elemental carbon was rather stable. Graphite and diamond were the two main forms of carbon. Graphite with its layer structure of condensed planar 6-atomic-rings of sp^2 -hybridized carbon (Fig. 2.6 a) being the thermodynamically stable modification in a standard environment opposed to diamond, only metastable, composed of sp^3 hybridized carbon atoms (Fig. 2.6 b). The idea of another carbon modification in the form of a soccer ball was first revealed only to a small audience in a Japanese journal in the 1970s [25] and thus was not widely observed. This changed in 1985 when Harry Kroto found a stable cluster of 60 carbon atoms to be formed during the evaporation of graphite [26], which was subsequently named buckminsterfullerene (Fig. 2.6 c) after the architect Buckminster Fuller for its similarities to Fuller's roof-constructions. With the subsequent discovery of other fullerene structures with 70 or 80 carbon atoms that formed increasingly cylindrical looking structures a general interest rose in the possible structures accessible to graphitic carbon sheets which 1991 lead to the synthesis of "helical microtubules of graphitic carbon" by Sumio Iijima [4] or carbon nanotubes as they are generally called today (Fig. 2.6 d).

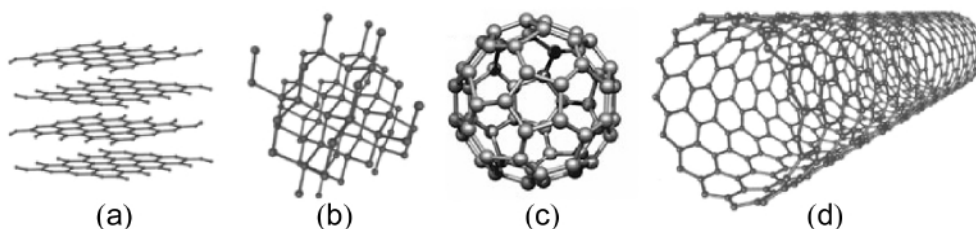


Fig. 2.6: Allotropes of elemental carbon, graphite (a), diamond (b), C_{60} -buckminsterfullerene (c) and CNT (d).

These carbon nanotubes typically have a diameter of about 1 nm (in case of single-wall tubes) and lengths up to several micrometers – but also lengths of several centimeters are possible [27] – and possess very interesting physical properties that predestine them for a wide variety of applications. They have superior electrical and thermal conductivity to many materials in use. For example their thermal conductivity is about twice that of diamond, previously the material with the highest thermal conductivity. Also their mechanical properties are amazing, being a thousand times stronger than steel at a considerably lower density [28,29].

An illustrative picture for the structure of an individual CNT is to roll up a graphene sheet (one individual layer of graphite) into a cylinder, which is not to be misunderstood as the mechanism of synthesis. CNTs are synthesized by evaporation/decomposition of carbon or a carbon-containing precursor and consequent recondensation, sometimes in the presence of metal catalysts. This evaporation/decomposition can be achieved by heat (chemical vapor deposition, CVD [30]), laser light (laser ablation [31]) or electrical discharges (arc discharge [32]). Yet the rollup picture is suitable to explain several structural features of CNTs. Depending on the roll-up angle CNTs with different helical conformation of the carbon atom arrangement result. These different types of nanotubes can be characterized by appointing them a pair of integers (n,m) , which together with the lattice constants of the graphene sheet define the “chiral vector”. This vector connects two crystallographically equivalent points on the CNT and is identical in length to the circumference of the nanotube (Fig. 2.7):

$$\vec{C} = n\vec{a}_1 + m\vec{a}_2 \quad (2.7)$$

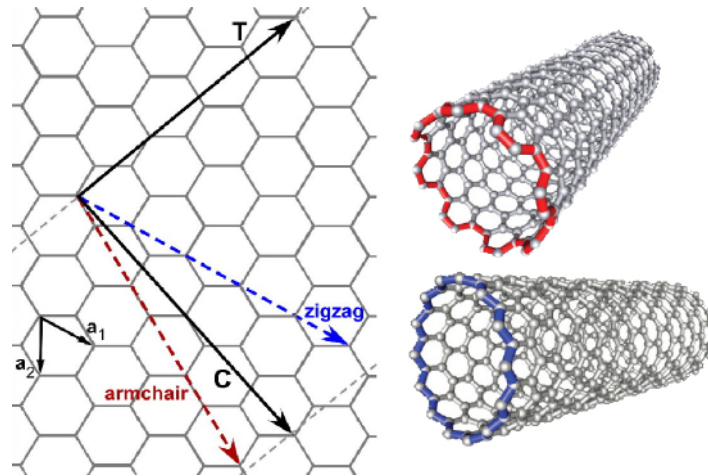


Fig. 2.7: Construction of CNTs by rolling up a graphene layer along the chiral vector C and depiction of CNTs of armchair and zigzag chirality [33].

Three general types of CNTs can be deduced from this:

$n = m$: armchair CNTs

$m = 0$: zigzag CNTs

other: chiral CNTs

The pair of integers or the deduced type – armchair, zigzag or chiral – characterizing a CNT are often called its chirality although armchair and zigzag CNTs are not chiral, they possess mirror symmetry. It is important to recognize that CNTs so far cannot be produced as

unichiral samples. Samples of CNTs are always mixtures of different chiralities in the above mentioned sense and the fraction of a particular “chirality” is normally not chiral in the sense of only being composed only of one enantiomer (only tubes with one handedness of the helix); usually this would still be a racemic mixture of equal amounts of left- and right handed tubes, but with the same pitch of the helical arrangement.

The type of the so far described single wall carbon nanotubes (SWCNTs) greatly influences their physical properties, most importantly the electrical properties. Depending on their chirality CNTs are either metallic or semiconducting. CNTs are metallic if n equals m or if n minus m is a multiple of 3. This means that every armchair CNT and every third zigzag CNT is metallic. By rolling up several graphene sheets into cylinders one would obtain multi wall carbon nanotubes (MWCNTs) which by many are considered to always be metallic because statistically at least one layer will be metallic and this will dominate the whole CNT in its electrical behavior. Another school of thought maintains that it is the outermost layer that determines the electrical properties of MWCNTs. If the synthesis would arbitrarily produce every chirality with the same likeliness a standard SWCNT sample should contain two thirds semiconducting CNTs and one third metallic CNTs [28].

Both metallic and semiconducting CNTs show the electronic properties of a 1-dimensional quantum wire with, in contrast to the continuous energy-dependency of the density of states (DOS) of bulk materials, sharp spikes with descending flanks of the DOS, called Van Hove singularities [34]. The difference between metallic and semiconducting CNTs is the DOS at the Fermi energy [35]. The conduction and the valence band are separated by a band gap for semiconducting CNTs while for metallic CNTs there is no band gap. The optical transitions of CNTs are transition between the Van-Hove-Singularities (Fig. 2.8).

CNTs are generally depicted as perfect long cylindrical rods, a picture that can be misleading considering that real nanotubes have defects such as heptagons or pentagons in the otherwise hexagon-based structure which lead to kinks in the cylinder. Also a widening or narrowing of CNTs can be observed as if two different types of CNTs had been welded together. These defects greatly influence the physical properties. Centers of sp^3 -type inside the otherwise pure sp^2 -structure will disturb the delocalized π -electron system which is responsible for the good electrical conductivity, they can act as fracture points under mechanical stress and they provide attack points for chemicals [36].

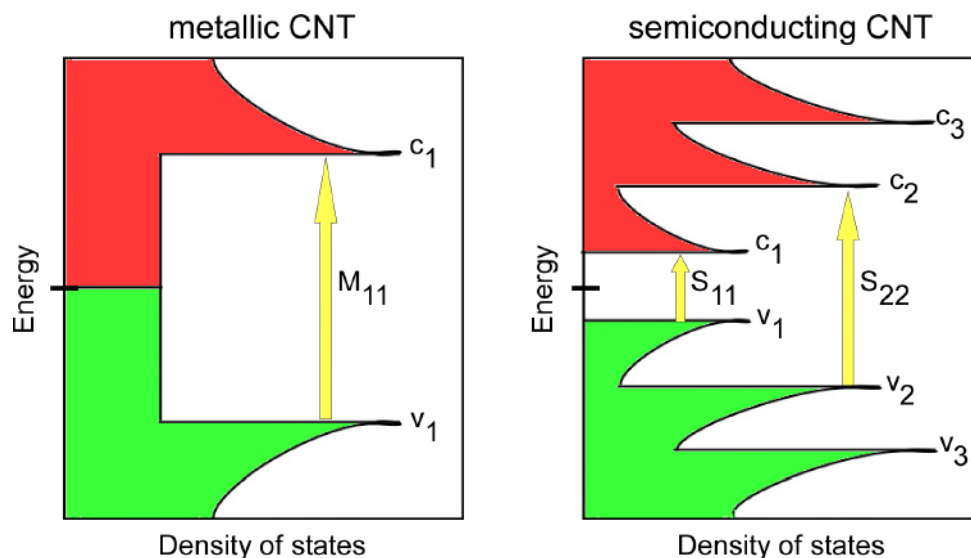


Fig. 2.8: Diagrams of DOS for metallic and semiconducting CNTs, respectively. Possible optical transitions between the Van Hove singularities of the valence band (green) and the conduction band (red) are denominated with an M for metallic and S for semiconducting and are indexed with the number of the respective transitions. Only equal-numbered transitions are allowed.

All the so far described properties of CNTs are, reflecting their anisometric shape, highly anisotropic. The polarizability of a CNT is much greater along its axis than perpendicular to it, as are the electrical and thermal conductivities. Therefore control over the tube orientation is highly desirable for many applications.

2.3. LC/CNT composites

Despite their great potential so far few applications of CNTs have actually been realized outside of the laboratory. The most limiting problems in CNT application that have to be overcome are today the selective synthesis of high quality CNTs or the subsequent separation of the different CNT types, the efficient separation of CNTs into single tubes rather than large aggregates of tubes and the control of the tube orientation. While synthesis gets better and more selective – one can actually buy CNTs and be sure that one gets CNTs rather than a crude mixture of every carbon species known, which was not that obvious only a few years ago – samples of only one type of CNT, let alone truly unichiral (only one enantiomer) samples, are still not available commercially or in academic laboratories. First promising steps are taken in separating CNTs after synthesis by ultracentrifugation [37,38] or chromatography [39] but these methods currently are far away from a possible up-scaling to provide large samples of uniform CNTs (which still would not be unichiral) for technical application.

The efficient dispersion and thus breaking up of CNT aggregates is also a great challenge that is far from being solved to everyone's satisfaction. Singular dispersed nanotubes are often only possible at minute concentrations and the stability over time is often unsatisfactory. In general the search for a suitable solvent for CNTs is still going on and is to some extent an enigma to be solved. Apart from the use of surfactants such as sodium dodecylsulfate (SDS) or sodium dodecylbenzenesulfonate (SDBS) to yield metastable dispersions in water, which is an established procedure, only few solvents have been identified that are able to disperse CNTs at notable concentration. Dimethylformamide (DMF), N-methylpyrrolidone (NMP) [40], γ -butyrolactone (GBL) [41] long being the most notable ones, only recently being topped by NMP derivatives with an outstanding reported maximum concentration as high as 3.5 mg/ml in cyclohexyl-pyrrolidone (CMP) [42]. It is speculated that the lone-pair at the nitrogen atom present in all those solvents may play a role for the solubility [43] but a convincing theory that allows certain predictions is still lacking. Surfactant stabilized CNT dispersions in contrast, while being metastable in the thermodynamic sense, are stable for years at high CNT loadings although there can be large differences between different surfactants [44]. The first choice of readily available SDS and SDBS still is among the most efficient options. In all cases it takes high mechanical force to debundle CNT-aggregates. Although simple stirring has been reported to be efficient [45] most procedures include ultrasound treatment.

Also the control of the tube orientation still proves to be a very challenging obstacle, maybe **the** obstacle together with synthesis that is preventing nanotubes from revolutionizing computer technology – reported CNT transistors [46-48] and logic circuits are sadly more of a random occurrence or tedious to assemble. Today the ability to control the orientation of nanotubes is still far from satisfactory. Orientation by electrical or magnetic fields has been proposed but is not generally applicable because the CNTs react differently to applied electrical fields depending on their chirality [49] and for magnetically controlled orientation high fields are normally needed [50,51] (on the scale of tens of Tesla), although scarce reports of low-field orientation exist. Moreover the orientation only prevails in the presence of the field.

Mechanical methods for orientation such as shear flow [52,53] or “molecular combing” [54], where a substrate is immersed into a suspension of CNTs and slowly removed again, so that the CNTs orient along the drawing direction, are either poor in outcome – order parameter below 0.1 have been reported for shear flow alignment of CNTs – or only applicable at small concentrations. CNTs have been moved using an AFM tip [55], or even aligned by using normal tweezers [56] but an easily up-scalable method for application is still lacking.

The best method, with results undeniably impressive, is the orientation-controlled growth of CNTs. It is possible to grow CNTs parallel [57-59] as well as perpendicular [60-62] to a substrate. Through additional treatment that involves the addition and evaporation of solvent one can produce complex CNT microarchitectures such as concentric microwells, blooming flowers, CNT microhelices or thin-walled lattices of CNT-forests [63]. Yet the controlled growth of CNTs makes a substrate mandatory and is thus incompatible with current methods of CNT-purification and –separation, which only work with unsupported nanotubes.

These are the reasons why CNTs so far still are mostly of academic interest, despite the many potential applications, that reach from the next step in computer technology over materials of never before known mechanical strength, finally making solar power profitable [64] to their application in medicine [6,9]. Up to now CNTs are mainly used academically as fillers for polymers – mostly to make them conductive, not so much for their mechanical properties – , as new thin, thus better resolving AFM tips [65-67] or field emitters.

And this is where liquid crystals enter the picture. LCs have the potential to solve two of the three main challenges of CNT application, efficient dispersion of CNTs and controlling their orientation. The LC’s inherent order can be transferred to CNTs dispersed in it. The anisotropic elastic forces of an LC lead to a situation where the minimal free energy for a CNT in a LC matrix is reached for a configuration where the CNT points along the director of the LC. Other orientations lead to a distortion of the director field and an increase of the free

energy of the system thus to a torque acting to reorient the tube towards the state of lower energy, causing the uniform alignment of the CNTs along the liquid crystal director (Fig. 2.9). This principle mechanism is applicable for both thermotropic and lyotropic LCs. Several studies have shown that CNTs dispersed in LCs – thermotropic as well as lyotropic – adopt about the same order parameter as the LC [68-70].

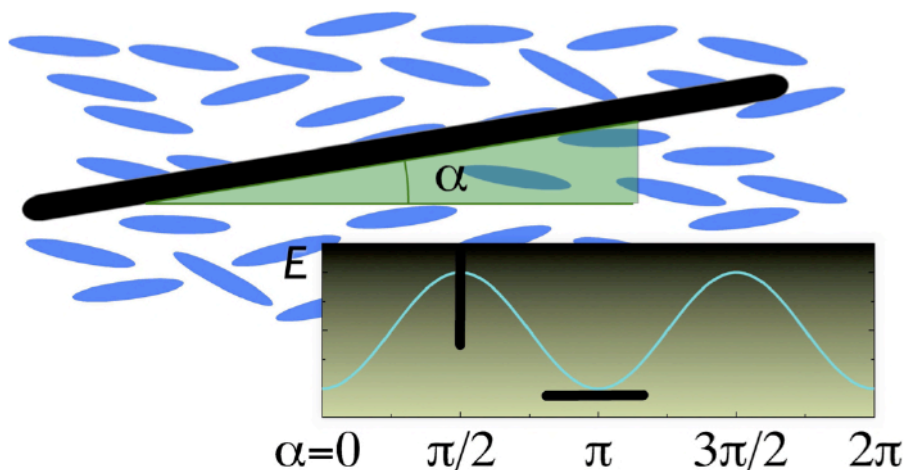


Fig. 2.9: Scheme of order transfer from LC-matrix to CNT; the free energy of the system is lowest for tube orientation along the director since this minimizes the distortion of the director field.

For thermotropic LCs highly developed techniques for macroscopic LC alignment are available through their wide usage in LCDs and this allows for flexible control of the ground state of the LC. In addition their fast response to external electric or magnetic fields open the possibility of fast, dynamic switching of CNTs together with the LC matrix [71]. A major drawback in thermotropic LC/CNT composites so far has been that efficient dispersion is only possible at small concentration – 0.1 mg/ml seem already to be too much (the rare studies that claim that such high concentrations are possible generally omit microscopic pictures for evaluating dispersion quality) – and that even low-concentration dispersions are not stable and sediment over a time-scale of hours to weeks. All the studies performed however used standard off-the-shelf LCs such as 5CB or the E7 mixture none of which is optimized for CNT dispersion. LCs designed specifically for CNT dispersion should be able to improve the situation considerably and first results are already published that follow the concept of adding dopants which combine anchor-groups such as pyrene with standard cyanobiphenyl moieties, thereby promoting CNT dispersibility [72].

In the case of thermotropic LCs a number of reports also suggest a reverse benefit. CNT doping is found to improve the display performance of the LC, e.g. by decreasing the Fredericks threshold (the voltage needed for the LC to respond to an applied field) and reducing the

switching time [73-78]. It is speculated that this is due to a reduction of free ions in the LC as the CNTs scavenge ions out of the LC fluid matrix in which they are dispersed. Yet these processes are far from understood and contradicting reports exist.

The approach to incorporate CNTs in lyotropic LCs is a quite natural step since the CNT dispersion in isotropic aqueous surfactant solution is a widespread, established procedure. Just by adding more surfactant a lyotropic phase can be built up. Lyotropic LCs have the advantage that they allow for higher CNT loading up to about 3 mg/ml and that the LC matrix may be more easily removed than for thermotropic LCs (at least the solvent is readily evaporated and the surfactant may be more or less completely rinsed away, if necessary, with solvents like water or ethanol). The deposition of oriented CNTs onto a target substrate and subsequent removal of the LC, required since it is not compatible with most applications of CNTs, is in fact one of the largest problems of this concept. Careful rinsing with water can be applied to lyotropic LC/CNT composites although many CNTs are typically removed in the process. For thermotropic LCs rinsing with organic solvents may be useful, but no experiments in this direction have yet been performed. The possible high loading of CNTs in lyotropic LCs results in a very apparent effect of the CNT alignment. These composites act as linear polarizers (Fig. 2.10, left). When the LC matrix is uniformly aligned by slight vacuum suction of the composite into an optically flat capillary the thus aligned CNTs, which only absorb light polarized along their axis, fulfill the purpose of absorbing the fraction of the incident light polarized parallel to the CNTs rendering the transmitted light linearly polarized. Yet the contrast of these polarizers is very weak which is mainly due to the poor flow-induced overall alignment that is possible for lyotropic LC phases.

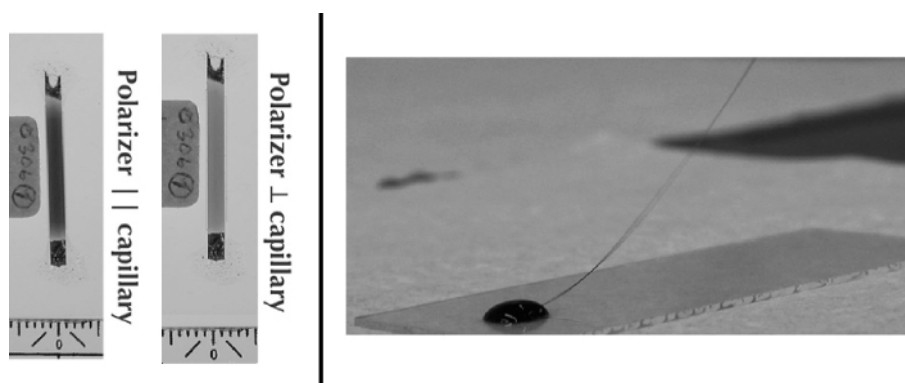


Fig. 2.10: Polarizer effect of a shear aligned lyotropic LC/CNT composite [70] (left) and filament drawn out of a bulk drop of a lyotropic LC/CNT composite [79] (right).

Such composites show another interesting phenomenon. Long thin filaments can be extracted from the bulk samples and deposited on any substrate available (Fig. 2.10, right). LC and CNTs are highly aligned in these filaments and remain on the substrate after rinsing away the water. Both effects, the polarizer effect and the filament formation, are only shown with CNT dispersion of high quality.

2.4. Percolation

Percolation theory is a mathematical theory that describes clustering in randomly occupied lattices [80-83]. The interesting and physically relevant results of the mathematical considerations are about the number of clusters, the properties of these clusters (dimensions, shape, etc.) and the occurrence of continuous clusters that extend throughout the whole system, connecting a boundary with the opposite one, when the fraction of occupied lattice sites exceeds what is referred to as the percolation threshold. Imagine a polymer that gets filled with conducting particles that are distributed randomly throughout the polymer matrix. The amount of filler one needs to form a conductive path – an infinite cluster – throughout the polymer marks the percolation threshold. The composite becomes conductive when the filler concentration reaches the threshold value. This theory is applicable to a wide variety of transitions, from the already mentioned transition from insulator to conductor in multi-component materials, gelation processes and thermal transitions such as crystallization (transition from many clusters with short-range order to one infinite cluster = crystal) but also to such macroscopic phenomena as forest fires, disease spreading and even the developing of star constellations in galaxies.

Obviously the theory has its relevance in CNT research, where it is largely concerned with the properties of more or less randomly formed CNT networks. And the percolation problem for CNTs indeed holds some interesting results. For a simple cubic lattice the percolation threshold for randomly distributed spherical particles is calculated to be about 31%, that means that 31% of the lattice sites have to be filled with particles at random in order for these particles to form a continuous network [84,85]. These high loadings are reflected in reality by the fact that, for example, when using carbon black as filler for polymers often volume fractions as high as 50% have to be used to yield a suitable conductivity. Of course such a high filler concentration greatly influences the mechanical and flow properties of said polymer [86]. For CNTs however the situation is very different. Experimental studies have established percolation thresholds below 1% of CNT volume fraction [87,88] and calculations suggest percolation thresholds as low as 0.1% [89].

The fundamental difference between the mentioned carbon black particles and CNTs is that nanotubes, being highly anisometric, possess a high aspect ratio of typically 1:1000, and this substantially lowers the percolation threshold. This can easily be made plausible by imagining a squared area with an edge of one centimeter. Bridging from one edge to the opposite could be done with one shape the length of one centimeter. Considering an aspect ratio of

1:1000 such a shape would occupy an area fraction of 0.1%. The same considerations for a circular shape would yield an area fraction of 78,5%. Fig. 2.11 shows a more sophisticated example of percolating rods in contrast to non-percolating spheres.

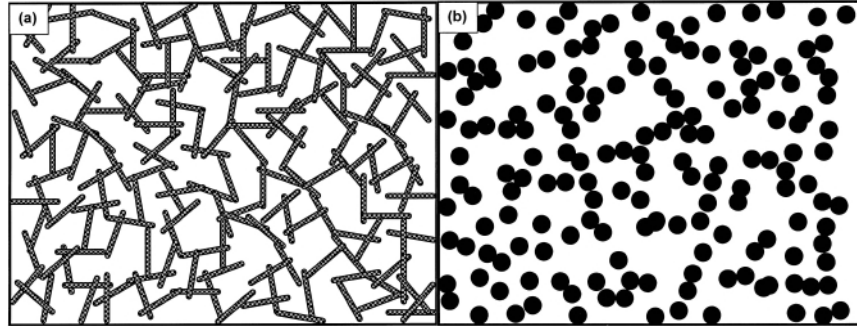


Fig. 2.11: Two-dimensional schematic of the percolation of randomly distributed high aspect ratio particles (a), the corresponding non-percolating structure for circular particles at the same area fraction [89].

For the case of LC/CNT composites yet another factor is to be considered. Here the matrix is anisotropic and the CNTs orient along a preferential direction. For this problem there is a bit of confusion in the literature. In general calculations [90] and many experimental studies conclude that isotropic (random) orientation of CNTs should lead to a lower percolation threshold than aligned tubes. This is also in accordance with a simple thought experiment. Considering the extreme case of perfectly aligned CNTs, percolation can only occur when CNTs meet head-to-head which is not likely at low loadings.

Despite these results there are also reports of a lower percolation threshold for aligned CNTs [91]. The major factor for these discrepancies seems to be the consideration of attractive forces between the CNTs. If well dispersed CNTs, at low enough concentrations to avoid large-scale aggregation, attract each other they will connect, thereby causing a certain alignment which will lead to a lower percolation threshold than for unaligned non-interacting or weakly interacting CNTs (Fig. 2.12) [92,93]. Depletion attraction (see next section) or field-induced polarization of CNTs could provide these interactions. This could also explain why many of the lowest reported percolation thresholds are studies with percolation under an electrical field [94,95]. One should note that the naturally strong van der Waals interactions between CNTs are very short-ranged and should not play too much of a role in a situation of well dispersed CNTs, but they will definitely cause large-scale aggregation at higher concentration or over long periods of time when CNTs eventually come into close vicinity of each other. An illustrative picture may be the efficiency of a plumber who carefully connects tubes to each other and also makes sure that they point in the same direction in contrast to a plumb-

er who places randomly oriented tubes in random places. Who will need fewer pipes to reach the canalization?

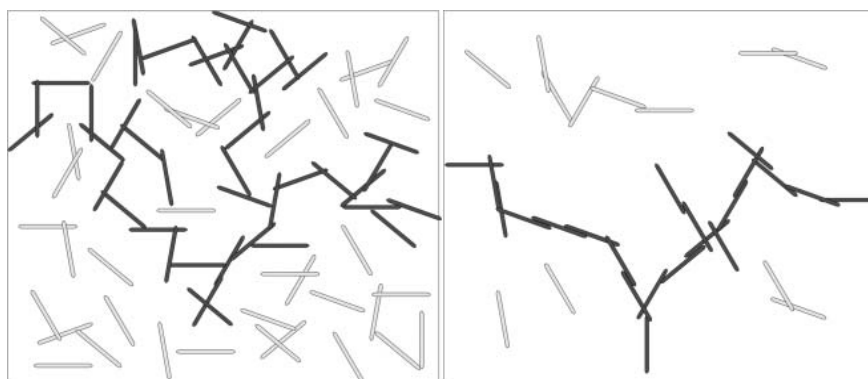


Fig. 2.12: Schematic representation of percolated networks of nanotubes. The dark grey rods show continuous conductive paths through the sample. Left: when interactions are weak, or when the particle aspect ratio is small, the nanotubes form a random network. Right: in the presence of strong attractive interactions or for high aspect ratio, the nanotubes align when they stick to each other. The percolation threshold is lower and more nanotubes are parallel. Sketches of the nanotubes belonging to a percolated cluster, which connects two sides of the box sample, are indicated as darker rods [93]

2.5. Depletion attraction

Depletion attraction is a not widely known force that can play a deciding role in colloidal systems. It has a major function in self-assembly processes – in the sense of aggregation processes - taking place in colloidal suspensions of differently sized particle species [96,97]. In systems that contain some large particles in the presence of many small particles, which do not interact with the large particles and a particle loading of at least 20-30% of the volume a mysterious force, seems to drive aggregation of the large particles [98]. This force is the depletion attraction, and it stems from the osmotic pressure that the small particles exhibit on the larger ones. The osmotic pressure in general is the same from every direction so that there is no resulting force on the larger particles. This however changes when two large particles get so close to each other that the volume between them becomes inaccessible for the small particles. The volume is then depleted of the small particles, which are also called the depletants. In this situation a resulting force occurs that pushes the two large particles together thus causing aggregation (Fig. 2.13 a). The effect can also be understood as an entropic problem. In the vicinity of each large particle there exists a volume that is inaccessible for the small particles, as they cannot occupy the same space as any of the large particles (Fig. 2.13 b). At high particle loading this excluded volume can become very large, thus reducing the degree of freedom of the small particles and as a consequence the entropy of the system. The excluded volume gets minimized when aggregation of the large particles occurs. The depletion attraction is thus an entropically driven aggregation force that occurs in highly concentrated colloidal systems of particles of different size.

Depletion attraction may be expected to play a major role in the system of a lyotropic LC/CNT composite. The two particle species here are the surfactant covered CNTs (large particles) and free micelles (depletants) between them. Although the CNTs technically are only large in one dimension their large surface area results in a high excluded volume that can be considerably reduced by aggregation (Fig. 2.13 c). To some extent this can be avoided by the approach of catanionic complexation where the CNTs are dispersed using an anionic surfactant while the LC matrix is formed by cationic species or in the reverse fashion. In such a system the supposedly depleting micelles actually are now attracted to the surfactant-covered CNTs and thus cannot act as depletant as effectively as in the case mentioned above. This is reflected in the higher CNT loading possible in such catanionic systems in comparison with

only anionic or cationic species as has been shown for the system of SDBS and cetyltrimethylammonium bromide (CTAB).

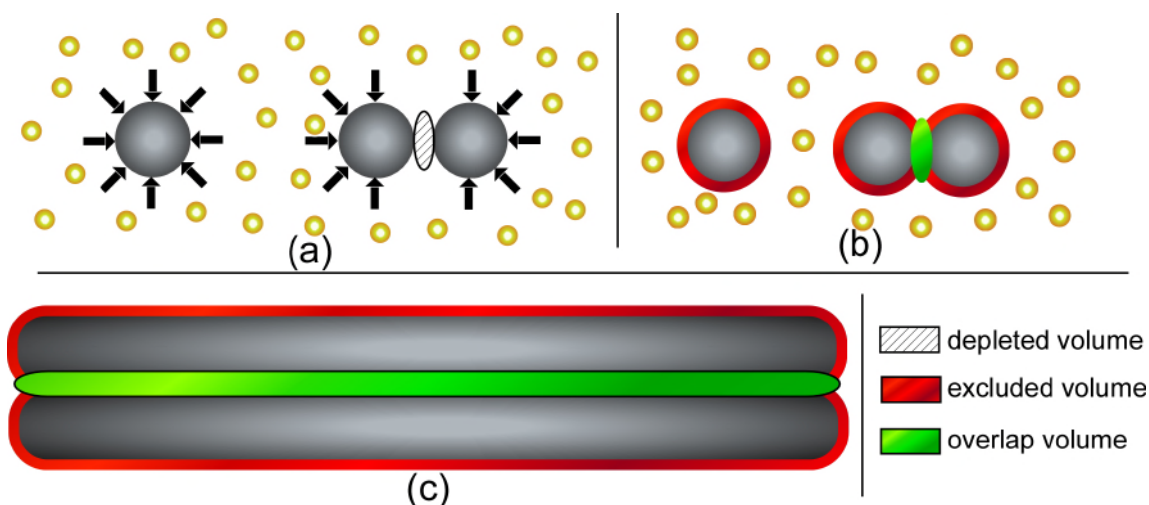


Fig. 2.13: Scheme of depletion attraction, small particles exhibit an osmotic pressure on large particles in the same solution, which leads to aggregation when two large particles are so close to one another that the volume between them is depleted of small particles. The close vicinity of the large particles is an excluded volume for the small particles, which gets reduced if the large particles aggregate, and their excluded volumes overlap. The effect is exceptionally large for the aggregation of rodlike particles.

Another factor that has to be taken into account for lyotropic LC/CNT composites is the fact that depletion attraction is strongly anisotropic in the LC phases [99]. Along the director depletion forces are much larger than perpendicular to it. This will rather lead to a CNT chain formation than to a forming of large more or less isotropic bundles of CNTs.

3. Methods

The purpose of this chapter is to give the reader an introductory overview of the analytical methods used in this thesis, as far as it is necessary in order to understand how these are linked to the topic at hand if they are not explained in the results part. Purely experimental details like materials, equipment specifications and experiment build-up will be given in the appendix.

3.1. Raman spectroscopy

In contrast to standard spectroscopy methods like UV/Vis or IR spectroscopy, Raman spectroscopy relies not on the analysis of the light absorbed by a certain sample but on the analysis of the inelastic scattering of light at molecules. This is also known as the Raman effect. A molecule that is brought into an electric field of the strength E will get polarized corresponding to its polarizability α . A dipole moment will be induced

$$\vec{\mu}_{ind} = \alpha \cdot \vec{E} \quad (3.1)$$

In the case of an incident electromagnetic wave with the frequency ν_0 this field is the oscillating electric field vector and the induced dipole moment equals

$$\vec{\mu}_{ind} = \alpha \vec{E}_0 \cos(2\pi\nu_0 t) \quad (3.2)$$

The oscillating charges lead to the emission of an electromagnetic wave of the same frequency ν_0 (Rayleigh scattering). However if the polarizability of the molecule is subject to a periodic change due to internal movement of the molecule because of rotations or oscillations, an additional oscillation is superimposed on the induced dipole moment. The change of the polarizability can be expressed by a serial development

$$\alpha = \alpha_0 + \left(\frac{\partial \alpha}{\partial Q} \right)_1 Q + \dots \quad (3.3)$$

with Q being the normal coordinate of the superimposed oscillation with the frequency ν_R

$$Q = Q_0 \cos(2\pi\nu_R t) \quad (3.4)$$

Neglecting the higher terms, for the overall induced dipole moment this leads to

$$\vec{\mu}_{ind} = \left[\alpha_0 + \left(\frac{\partial \alpha}{\partial Q} \right)_1 Q_0 \cos(2\pi\nu_R t) \right] \vec{E}_0 \cos(2\pi\nu_0 t) \quad (3.5)$$

which can be expressed as

$$\vec{\mu}_{ind} = \alpha_0 \vec{E}_0 \cos(2\pi\nu_0 t) \quad \text{Rayleigh scattering} \quad (3.6)$$

$$+ \frac{1}{2} \left(\frac{\partial \alpha}{\partial Q} \right)_1 Q_0 \vec{E}_0 \cos(2\pi(\nu_0 - \nu_R)t) \quad \text{Stokes scattering} \quad (3.7)$$

$$+ \frac{1}{2} \left(\frac{\partial \alpha}{\partial Q} \right)_1 Q_0 \vec{E}_0 \cos(2\pi(\nu_0 + \nu_R)t) \quad \text{Anti-Stokes scattering} \quad (3.8)$$

The first term describes the elastic scattering of light without a change in wavelength while the two other terms describe the inelastic scattering where a change of wavelength/frequency of $\nu_0 \pm \nu_R$ takes place. This is only the case if $\partial\alpha/\partial Q \neq 0$, i.e. when the polarizability of the molecule changes during the oscillation, which is for instance the case for so called „breathing modes“ which are oscillations in which the molecule changes size in a similar fashion as the thorax widens during breathing.

In a quantum mechanical view the scattering of a photon with the energy $h\nu_0$ either leads to elastic scattering, with no energy change of the photon or molecule, or inelastic scattering where energy is either transferred from the photon to the molecule (Stokes lines) or from the molecule to the photon (anti-Stokes lines), corresponding to a vibrational transition of the molecule. Since at room temperature molecules in general are in their vibrational ground state typically only the Stokes lines are observed where the molecule gets excited into a higher vibrational state. The measured signal thus is corresponding to photons, which transferred some of their energy to the molecule. The shift in energy of the scattered photon is called Raman shift and is typically measured in wave numbers.

Raman lines in general have a very small intensity, which however can be substantially increased if the energy of the incident light is equal (resonance Raman effect) or close (pre-resonance Raman effect) to an electronic transition of the molecule. Because of the higher energy intake of the molecule due to the resonant interaction of the incident photon with the excited molecule the scattering signal can show an increase in intensity by a factor of up to 10^6 .

The resonance Raman spectra of carbon nanotubes are very characteristic and contain only a few signals which can directly be linked to the structural features of the CNTs [100,101]. The three most important features in a CNT Raman spectrum are the so called radial breathing modes (RBMs) around 75 to 300 cm^{-1} , the D-band between 1330 and 1360 cm^{-1} and the G-band around 1580 cm^{-1} (Fig. 3.1).

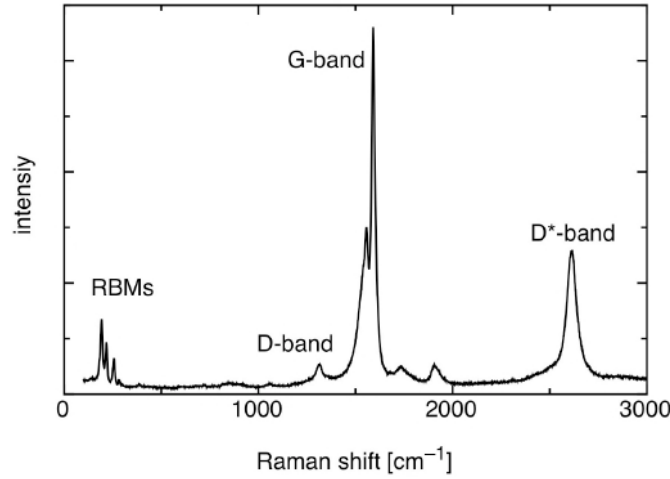


Fig. 3.1: Raman spectrum of HiPCO SWCNTs used in this study.

The RBMs stem from vibrations perpendicular to the long axis of the CNT in which the nanotube widens and thins, it breathes, hence the name. They are directly linked to the diameter d of the nanotube, which can be calculated from the location of the modes in the spectrum using the empirical formula as given by Maultzsch et al. [102]

$$\omega_{RBM} = \frac{c_1}{d} + c_2 \quad c_1 = 215 \pm 2 \text{ cm}^{-1}\text{nm}; \quad c_2 = 18 \pm 2 \text{ cm}^{-1} \quad (3.9)$$

A single nanotube thus has only one radial breathing mode whereas a sample of nanotubes has several RBMs corresponding to the diameter distribution. The D-band is linked to defects in the CNT structure, the letter D standing for disorder. The G-band is due to tangential stretching-oscillations in the graphitic plane. It is also present in pure graphite which is the meaning of the G in its naming. The ratio of G- to D-band holds information about how defect-rich the CNTs are [103].

Raman spectroscopy using linear polarized light is a useful tool for getting information about the tube orientation. The intensity of all Raman bands is the highest if the polarization of the incident light is parallel to the tube axis [104]. Studying the polarization-dependent Raman mode intensity thus allows probing for the orientation of the CNTs and we can even calculate an order parameter S by analyzing the dichroism of the Raman signal analogously to how the order parameter of dichroitic dyes in LCs is calculated [69,105]. Using the dichroic ratio $D = I_{||} / I_{\perp}$, with $I_{||}$ as the Raman intensity for incident polarization along the director and I_{\perp} the Raman intensity for excitation polarized perpendicular to the director, the order parameter can be approximated as

$$S = \frac{D - 1}{D + 2} \quad (3.10)$$

3.2. Conductivity measurements

The electric conductivity of samples was measured using a dielectric bridge that allows the automatic measurement of the conductivity at different frequencies of the measuring field and varying DC bias settings. The measurement circuit is composed of two series of impedances which get balanced against each other automatically allowing the establishment of the unknown component (Fig. 3.2), in our case a set of two square electrodes facing each other, the gap being filled with a thermotropic LC/CNT composite. If the measured voltage between the two legs of the bridge is zero the value of the unknown impedance can be deduced, with the reciprocal being the conductance G of the sample, which is multiplied by the cell constant l/A , with l the sample thickness and A the electrode area, to yield the conductivity σ [106].

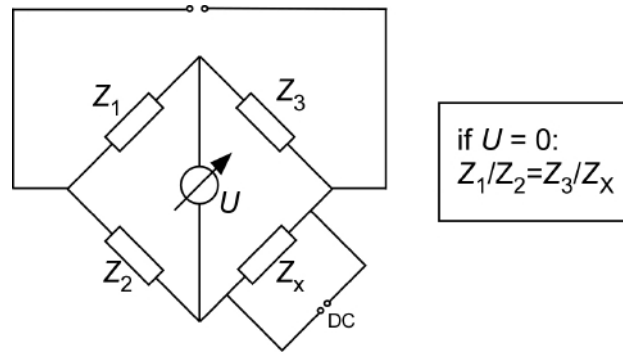


Fig. 3.2: Measuring circuit of the dielectric bridge.

In general the frequency dependence of such a setup is as follows: at low frequencies the conductance G is mainly dependant on the ohmic resistance R of the sample, as the slowly changing field is similar to a DC field, and therefore constant:

$$G = 1/R \quad (3.11)$$

With increasing frequency the setup is mainly acting as a capacitance C the conductance of which increases linearly with the frequency f :

$$G = 2\pi f C \quad (3.12)$$

At very high frequencies a leveling off of the conductance or even a decrease of the conductance can be seen as the inductive properties of the wiring counteract any further increase.

A percolating CNT network inside the cell will increase the low frequency conductivity by at least one order of magnitude in comparsion to a sample with CNT concentrations below the percolation threshold (Fig. 3.3).

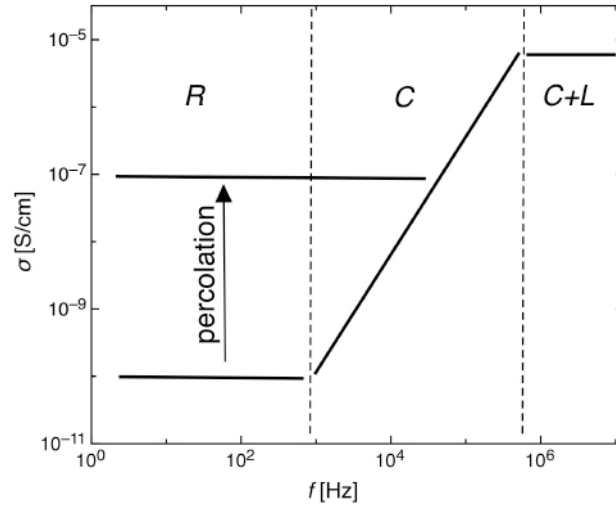


Fig. 3.3: Typical frequency dependency of the electrical conductivity of a thermotropic LC/CNT composite inside an LC cell. At low frequencies the setup acts as a resistor R , at medium frequencies as a capacitor C and at the highest frequencies as a combination of a capacitor and an inductor L .

3.3. Rheology

Rheology is best defined as the science of the flow and deformation properties of materials. In flow different points of a material move relative to each other thereby deforming the material. Two basic kinds of flow can be identified. In shear flow different points in a material are moving past each other while in elongational flow different points are moving towards or away from each other (Fig. 3.4).

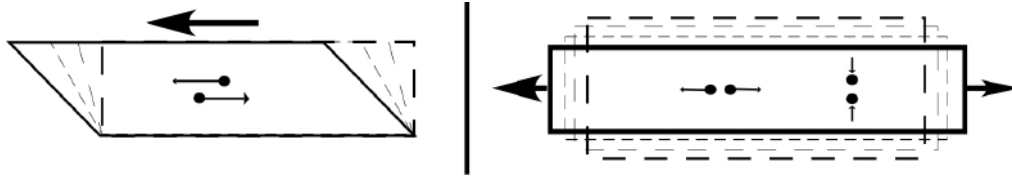


Fig. 3.4: schematic depiction of the two basic kinds of flow, shear flow (left) and elongational flow (right).

The viscosity of the system, also often dubbed the internal friction, counteracts every flow. Colloquially spoken the viscosity η is the factor that determines how much applied force is required for a certain velocity of flow. More exactly, in the case of shear flow, it is the proportionality factor between the shear stress σ and the shear rate $\dot{\gamma}$:

$$\sigma = \eta \dot{\gamma} \quad (3.13)$$

As seen in Fig. 3.5 the shear stress is defined as the applied force F divided by the sheared area A while the shear rate is the rate of the deformation – the shear γ – of the system and thus defined as the velocity gradient over the sheared sample

$$\dot{\gamma} = v / h \quad (3.14)$$

In the case of uniaxial, extensional flow the definitions are analogous, with the elongational stress or tension σ_e , the extension rate $\dot{\epsilon}$ and the extensional viscosity η_e .

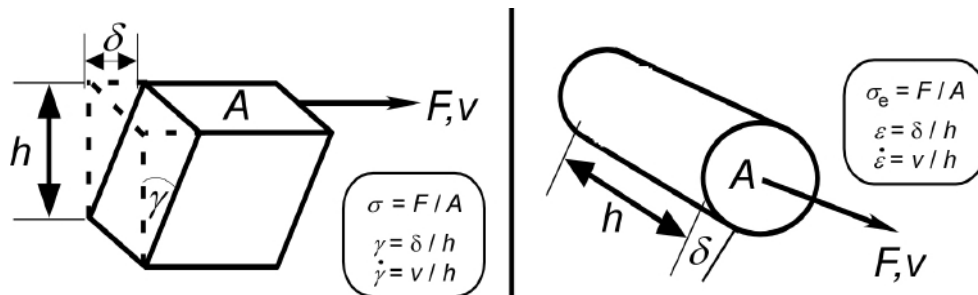


Fig. 3.5: Definitions diagram of shear flow (left) and elongational flow (right).

For standard fluids, so-called Newtonian fluids, the viscosity is constant for all shear rates. Non-Newtonian fluids however show a shear rate dependency of the viscosity. This means that the flow properties change depending on the force exerted on the liquid. An increase of the viscosity with shear rate is called shear-thickening while the opposite behavior is called shear-thinning. Everyday examples of fluids showing one of the two are honey and ketchup which are shear-thickening and shear-thinning, respectively. Non-Newtonian fluids are often multi-component mixtures like starch-water mixtures, quicksand, blood or polymer solutions. The changes of viscosity result from microscopic structural changes in the fluid which alter the internal interactions of the fluid [107].

In the case of rodlike particles dispersed in a fluid or phases composed of rodlike building blocks – e.g. liquid crystal phases – the shear forces cause an alignment of the particles along the shear direction in order to minimize the viscosity opposing the flow [108]. In the case of liquid crystalline phases this results in a shear induced orientation of the director along the shear flow [109].

3.4. Polarizing microscopy

Polarizing microscopy is a technique to study birefringent materials, materials with anisotropic optical properties. In contrast to normal light microscopy polarizing microscopy uses linearly polarized light and the sample to investigate is placed between crossed polarizers. The first polarizer polarizes the light linearly while the other polarizer, also called the analyzer, is set at a 90° angle to the first thereby normally filtering out all the light and giving a dark picture. This remains true if any optically isotropic sample, like an isotropic liquid for example, is placed between the crossed polarizers. However, if a birefringent material, for example most crystals and LCs, is brought between the crossed polarizers light can pass the analyzer under certain circumstances.

Depending on the direction in which the light passes through the sample it can be that it experiences different refractive indices. The light will split into components with polarization parallel to the two axes in the plane perpendicular to the light propagation direction that correspond to maximum and minimum refractive index, respectively. In the case of a planar-aligned (director in the plane of the sample) uniaxial material like a uniformly aligned nematic LC phase, linearly polarized light will split up into two rays with their electric field vectors polarized parallel and perpendicular to the optic axis, respectively. The optic axis is the axis of symmetry of a uniaxial material and it corresponds to either the highest (positive uniaxial) or lowest (negative uniaxial) refractive index of the material. Because the light propagation speed scales inversely with the refractive index, the two rays travel with different speed through the material, causing a certain retardation between the two rays when they leave the material again. This retardation depends on the thickness of the sample and the difference in the refractive indices that the two rays experience. Upon recombination of the rays the polarization state of the light is thus changed. In effect the formerly linearly polarized light may now have also a component polarized perpendicular to the original polarization. This component now can pass the analyzer causing a bright image (Fig 3.6).

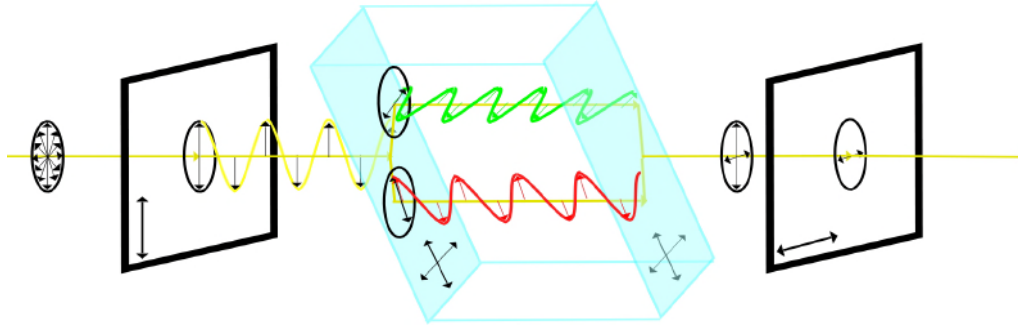


Fig. 3.6: Schematic depiction of polarizing microscopy with a uniaxial birefringent material. Unpolarized light passes a polarizer and gets linearly polarized. Upon entering the birefringent material it splits into two rays with polarization parallel and perpendicular to the optic axis of the material. The two rays travel with different speed. When leaving the material the reunited beam has now also components perpendicular to its original polarization which can pass the second polarizer which is rotated 90° with respect to the first. (Double arrows indicate the polarization planes).

The aforementioned is the case for a sample of a uniformly planar-aligned nematic LC when the light is polarized neither perpendicular nor parallel to the director. If, on the other hand, the incoming polarization is parallel or perpendicular to the director, then no separation into two components occurs and no effect from the birefringence is seen. Consequently the sample will appear dark when viewed in the polarizing microscope. There are two main situations when this happens. First, if the alignment is homeotropic, i.e. the director is perpendicular to the substrate, the light is always polarized perpendicular to the director, hence the image will always be dark (Fig. 3.5 left). Second, in the case of uniform planar alignment, i.e. the director is parallel to the substrate and thus perpendicular to the direction of light propagation, there are still four orientations of the sample in which the linearly polarized incoming light will be either parallel or perpendicular to the director, yielding dark states. When rotating such a sample it will show a dark image every 90° (Fig. 3.5 middle).

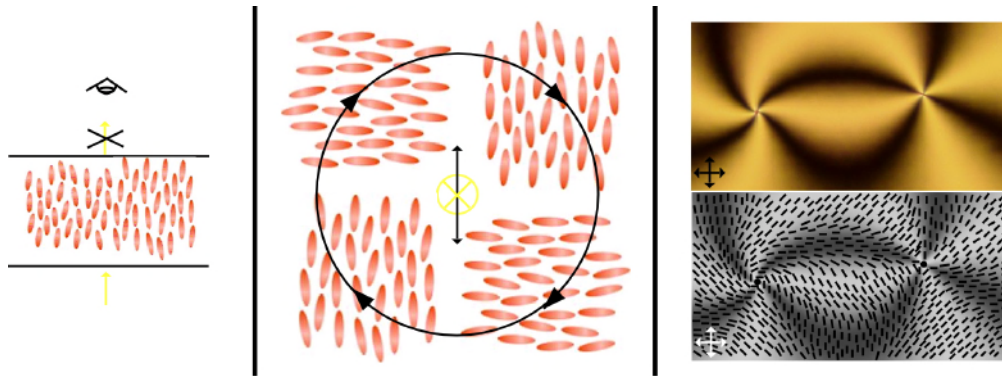


Fig. 3.7: Homeotropic alignment of an LC sample (left), the four dark states of a uniformly planar aligned sample of a nematic LC as viewed from above with vertically linearly polarized (double arrow at center) light coming out of the paper plane (middle) and the picture of a defect structure in a non-uniformly planar aligned nematic LC with a possible corresponding director configuration (right).

In the case of a non-aligned LC, a variety of colors can be seen depending on the thickness of the sample, the director orientation with respect to the viewing direction and the magnitude of the birefringence (defined as the difference between the refractive indices of the system) [110]. A non-uniformly planar aligned LC sample of even thickness shows uniform color but can exhibit defects that are connected by dark brushes. Defects are points where the director field is not defined, i.e. it is isotropic and they occur at points where the director field has no possibility for uniform alignment because areas of different alignment meet. The brushes that connect these defects are areas where the director is parallel or perpendicular to the polarizer.

4. Results and Discussion

The here presented work touches a variety of topics in the world of LC/CNT composites from mainly technical questions of the production of these composites, via the fundamental physical chemistry issues of the dispersion process and choice of material, to the resulting properties and potential applications of LC/CNT composites. The order of the following subchapters can be seen as following the subtitle of this thesis. The main focus of the first two subchapters is thus the unique challenges, such as the production of lyotropic LC/CNT composites (chapter 4.1) and the dispersion of CNTs in thermotropic LCs (chapter 4.2) with respect to the choice of LC and dispersion method. The next three subchapters are devoted to the exploration of the unique properties of these compounds, beginning with the filament formation of lyotropic LC/CNT composites (chapter 4.3) followed by the percolation-characteristics of CNTs dispersed in thermotropic LCs (chapter 4.4) and ending with the treatment of the properties of CNTs and fullerenes in cholesteric thermotropics (chapter 4.5).

4.1. Producing lyotropic LC/CNT composites

The incorporation of CNTs in lyotropic phases is today a well-proven concept [79]. Yet for reproducibly good results, meaning well dispersed CNTs, and further optimizations such as increase of CNT content, improved CNT alignment and general handling, further research is needed. The standard procedure for the production of a lyotropic LC/CNT composite consists of two principle steps:

1. The production of an isotropic aqueous CNT dispersion with whatever method that does the job of efficiently debundling CNT aggregates using whatever surfactant suitable for stabilization of the CNTs in the dispersion and compatible with step 2.
2. The transformation of this dispersion into a lyotropic liquid crystal with prevailing dispersion quality using a suitable LC-forming material.

This outline allows the identification of several target points for optimization, which can be generalized into two different routes, the first of which is the choice of used substances, the second of which is finding optimal dispersion procedures. As mentioned above the first step of composite production is the dispersion of CNTs in an aqueous surfactant solution. The choice of surfactant is therefore an important issue, influencing both the maximum CNT content and the quality of dispersion. In the decision how this dispersion is achieved equipment- and procedure-wise one has to take several points into account. For example, high power dispersion methods may have a time advantage, but the risk of CNT damage is higher. The same questions are posed in the second step when the LC phase is formed. Here again the choice of LC forming material influences stability, dispersion quality and maximum CNT content while the procedure has to be carefully chosen to ensure a homogeneous CNT distribution in the sample.

Some of these questions have already been partially answered. Ionic surfactants in general seem to give better results concerning the maximum CNT content. A catanionic approach, using a surfactant of different charge to form the LC phase compared to that used for stabilizing the CNT dispersion, is superior to an approach where the LC phase is formed by the same surfactant used for getting the initial isotropic CNT dispersion. And of course there is the basic observation that the two-step procedure outlined above is advisable: adding dry CNT powder to a preformed LC phase works poorly [79].

In the next two sub-chapters the results of our optimization work will be shown and discussed following the two-topic approach of procedure and substances.

4.1.1. The same procedure as every time?

For procedure variation the standard outline allows two points of attack. The production of the initial isotropic CNT dispersion and the homogenization after the second surfactant is added to build up the LC phase (even the details of how the surfactant is added are not without importance). Dispersion of CNTs in a certain medium is done by applying mechanical force to the sample with CNT aggregates in the host fluid, such that the CNT aggregates are torn apart and eventually split into singular tubes [111]. The power of the applied force and the time of treatment are the most critical variables. Obviously, if the force is too low the strong van der Waals forces between the CNTs will not be overcome, yet with an increase in power also the probability for potential CNT damage will rise [112]. The homogenization step after adding the LC-forming surfactant to the isotropic dispersion is equally important in order to achieve the polarizer effect mentioned in chapter 2.3.

The different means of dispersion were all tested on samples of HiPCO CNTs in aqueous solutions of the surfactant SDBS whose suitability for CNT dispersion is well proven and make it one of the most widely used substances for this purpose [113,114]. As a standard testing procedure samples consisting of 2.5 mg/mL HiPCO CNTs in 1 ml aqueous SDBS solution (the mass ratio SDBS : CNTs = 5 : 1) were chosen. The methods evaluated were, in sequence of increasing mechanical power, magnetic stirring, Vial Tweeter sonication (the Vial Tweeter is a device specially designed for sonicating Eppendorf vials) and tip (sonotrode) sonication.

These methods vary in strength/energy input, dispersion mechanism and homogeneity of the energy input. Magnetic stirring works by producing a gentle shear flow inside the sample which is supposed to tear the aggregates apart and distribute the CNTs throughout the host fluid, while the Vial Tweeter, like a conventional ultrasonic bath, works mainly by inducing cavitation inside the liquid (the energy input is however much higher than in an ultrasonic bath). Cavitation, bubble evolution through localized heating and consequent collapse of these bubbles, can tear solids apart as the bubbles tend to nucleate at particles. This mechanism is also a driving force in the case of tip sonication, yet in contrast to the Vial Tweeter treatment the applied force is now even stronger and more localized. A defined cavitation zone is

formed directly beneath the sonotrode and a circular shear flow is built up that in addition to promoting deaggregation also transports particles into the cavitation zone where the high-energy forces upon bubble collapse literally rip the bundles apart.

As much as gentle dispersion methods would be preferable, the magnetic stirring turns out not to be sufficiently powerful to overcome the strong intertube interactions. The initial aggregates do not substantially decrease in size even though the liquid turns slightly darker after hours of treatment. The suspension will however clear quickly upon standing. The two sonication methods, in contrast, can both be used to achieve good dispersions, the quality of which was evaluated by optical microscopy and centrifugation. Both methods can yield dispersions with the bundle size below optical resolution, which are resistant to sedimentation by centrifugation (Fig. 4.1). For a decision between the two one has to take into account several points as each of them has its own set of advantages and disadvantages.

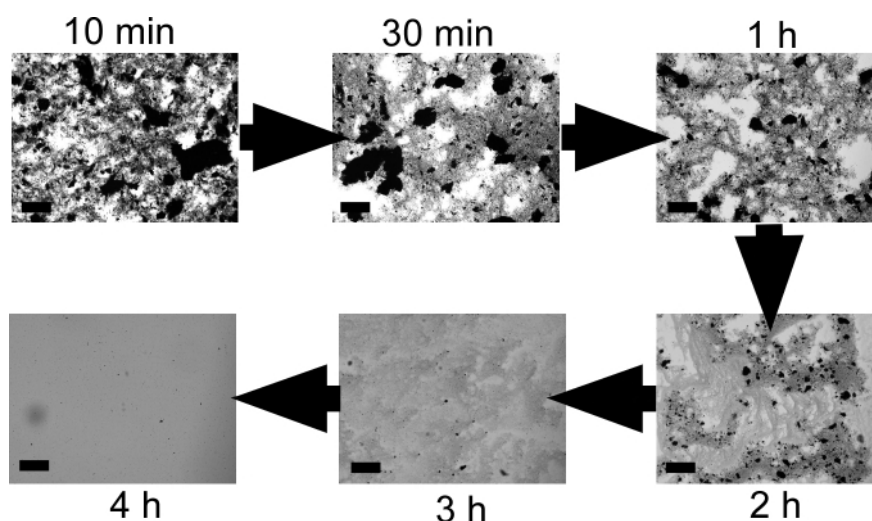


Fig. 4.1: Microscopic pictures of CNT-dispersion of 2.5 mg/mL HiPCO CNTs in 12.5 mg/mL aqueous SDBS solution with the Vial-Tweeter at 100% power and 0.5 s cycle (0.5 second sonication, 0.5 second pause, and so on). The same results can be achieved with tip sonication in the timescale of 30 minutes to 1 hour. Scale bar = 50 μm

Vial Tweeter

Advantages:

- Lower power, therefore less damage
- No contamination

Disadvantages

- No temperature control
- Long time (hours)
- Not up scalable

Tip Sonication

Advantages:

- Short time (30-60 minutes)
- Temperature control
- Up-scaling easier

Disadvantages

- High power, therefore probable CNT damage
- Sample contamination

The Vial Tweeter can score with a lower energy intake into the sample thus supposedly less CNT damage and no contamination with metal particles as with the use of a sonotrode. Yet the substantially longer treatment time of up to six hours, which may negate the lower energy advantage, and experimental difficulties due to lack of temperature control, let tip sonication seem as the better or at least easier choice as long as small metal impurities are tolerable. During Vial Tweeter treatment the samples heat up very quickly which can lead to bursting or melting of the Eppendorf vials calling for pauses in between sonication steps making the overall procedure even more time consuming. Of course this heating takes place also during tip sonication but it can easily be compensated for by immersing the sample in an ice bath. In addition to that the Vial Tweeter procedure is only available for small 1 – 1.5 mL samples, while the sonotrode treatment is easier to scale up.

So the choice of the right procedure is mainly dependent on experimental variables as long as certain energetic conditions are met. The mechanical force exercised on CNT aggregates must overcome a certain activation threshold in order to overcome the strong intertube interactions. Magnetic stirring is not sufficient to reach this goal (at least not in aqueous media, see chapter 4.2 for other media). From experiments with the vial tweeter it can be deduced that below an applied power of 7 W homogeneous over the sample the degree of debundling of CNT aggregates is negligible. This value is of course a very coarse approximation and can only serve as rule of thumb for devices that work in a similar fashion. If the criterion of activation energy is met the energy input has to go on sufficiently long as is needed to deliver the energy corresponding to creating the new surface that develops as CNT aggregates break. This means that there is a minimum treatment time set by the energy input of the chosen method and simply the amount of CNTs to disperse.

Quite logically more nanotubes take longer time to disperse. To disperse 2.5 mg HiPCO CNTs in one milliliter aqueous SDBS solution beyond optical resolution by tip sonication takes around 30 minutes, using the tip sonicator available in our lab, while dispersing 25 mg CNTs in 10 mL SDBS solution takes at least three hours. The relationship for up-scaling is not linear, i.e. 10 times the amount of CNTs does not mean tenfold increase in sonication time, because the energy input into the sample is also dependent on various other factors such as vial type and immersion depth of the sonotrode [115]. All things considered the method of choice for CNT dispersion used for most experiments in this thesis was tip sonication with the sample immersed in an ice or water bath for temperature control.

The second experimental step for lyotropic LC/CNT composite production is the transformation of the isotropic CNT dispersion into an LC phase by addition of more surfactant and subsequent homogenization. Only well homogenized samples without reaggregation of nanotubes show alignment of CNTs along the LC director, which can be directly verified by checking for the polarizer effect mentioned in chapter 2.3. The experiments concerning the optimal way of LC phase production were carried out using a standard mixture of a high quality dispersion of 2.5 mg/mL HiPCO CNTs in aqueous SDBS solution (mass ratio SDBS : CNTs = 5 : 1) which forms a nematic LC phase with addition of 28 wt% CTAB as secondary surfactant.

It was early on concluded that the goal of quick and reproducible homogenization cannot be achieved by adding the dry CTAB to the isotropic CNT dispersion because the CTAB in contact with the aqueous solution will form a thick, highly viscous mass, which will quickly clog the vial. This considerably impairs homogenization and the clog can only be removed by intrusive methods like stirring with a spatula, which due to the tendency of these composites to draw filaments is a very dirty and uncontrolled affair. It proved to be better to add the CNT dispersion to the dry surfactant. Upon adding the CNT dispersion to the dry CTAB slow and homogenous stirring should be started and continued for about an hour, even though the compound seems to be homogeneous by eye already after a couple of minutes.

Unfortunately this treatment is not yet enough to ensure high dispersion quality and thus alignment of the CNTs along the LC director. This is only achieved by another sonication step. The method of choice here is neither tip sonication nor Vial Tweeter treatment. Using the sonotrode does not work well on these samples because of their high viscosity. The cavitation zone that the sonotrode creates in the case of a very viscous and shear-thinning fluid is very small with no flow from the rest of the sample into it. The sonication is thus very inhomogeneous and ineffective and it eventually leads to evaporation of the water changing the mixture

composition. The evaporation of the water and the related very strong pressure increase in case of a closed vial is also the reason why the usage of the Vial Tweeter is no option. This option becomes even less attractive when considering the difficulties in transferring the composite mixture into Eppendorf vials, a step which would be required for using the Vial Tweeter.

Instead, traditional water bath sonication provides all the conditions needed. The sonication is fairly homogeneous throughout sample and the bath heats to a convenient degree: not as much as to cause large-scale water evaporation but enough to keep the samples from crystallizing. About three hours of bath sonication do the job as can be easily verified by sucking the composites into optically flat glass capillaries and looking for the polarizer effect.

An interesting alternative to the method described above is the use of freeze-drying as it allows for quite easy homogenization. Here one uses an isotropic CTAB solution that contains the right amount of CTAB plus an abundance of water. This solution gets mixed with the CNT dispersion just by pouring one into the other and turning the vial (closed) upside down a couple of times. The mixture is then immersed so rapidly into liquid nitrogen that it is vitrified (it “freezes” without crystallizing, i.e. it goes into a glassy state) and then the water is removed by vaccusuction so that it sublimates without entering the liquid phase. The remainder consists of a grey powder of homogeneously distributed SDBS-coated CNTs together with dry CTAB. Adding the right amount of water to this powder will yield a lyotropic LC/CNT composite. Unfortunately also with this method the bath sonication step is still necessary, as the CNTs will rapidly aggregate in the diluted mixture even if it is only seconds until it is vitrified. Moreover, the freeze-drying process takes a long time – one usually runs it over night – and since it does not remove the sonication step the normal procedure, as outlined above, seems the method of choice. Only for transporting preformed dry composite mixtures this method may hold some advantages, as a ready composite is sensitive to ageing via water evaporation and crystallization.

4.1.2. Substantial matters

In addition to the experimental procedures the choice of substances plays a major role and probably a much more fundamental role in a physical chemistry sense than the experimental details discussed above. Prior to this thesis the best-researched lyotropic LC/CNT mixture was the system based on SDBS for CNT stabilization and CTAB for LC formation [69,70,79,116]. In the present work we investigated possible alternatives to each of these surfactants. Specifically, we tested some of the most widely used surfactants as possible substitutes for SDBS, namely SDS, sodium cholate (SC) and sodium deoxy-cholate (SDC), which have been reported as good dispersion agents for CNTs [44,45]. The goal in substituting SDBS in the present recipe is the increase of CNT content and dispersion quality. Moreover, since SDBS is commercially available only as “technical grade”, i.e. with 80% purity, it renders the analysis of the results more difficult than in the case where all used substances have very high purity [117].

Regarding replacements of CTAB, the main goal is to get stable composites at room temperature since solutions of CTAB crystallize below the Krafft temperature of 25°C of this surfactant. Although the CTAB-composites are reasonably metastable, such that one can handle them for some time without particular precautions about temperature as long as they are in a bulk phase, they have to be stored at elevated temperatures for longer times, where they are slowly degrading due to water evaporation. To overcome this drawback two different alternative cationic surfactants were investigated: cetyl-ethyl-dimethyl-ammonium-bromide (CEDAB) and myristyl-trimethyl-ammonium-bromide (MTAB). The chemical structures of all surfactants discussed are depicted in Fig. 4.2.

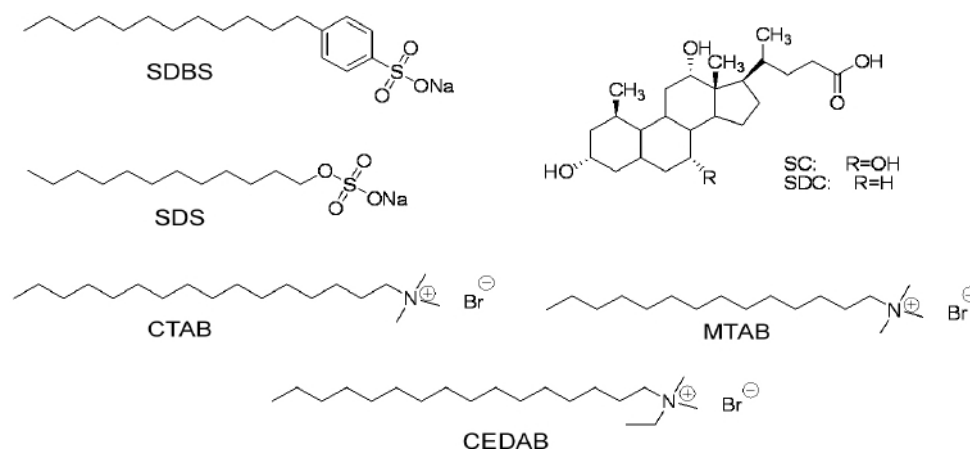


Fig. 4.2: Structures of surfactants used in this study, SDBS, SDS, SC/SDC, CTAB, MTAB, CEDAB

The sobering result of the investigation of SDS, SC and SDC was that no other surfactant than SDBS allowed a high concentration (up to 2.5 mg/mL) dispersion of HiPCO CNTs with aggregates below optical resolution at any surfactant concentration tested. The surfactant concentration was varied systematically from 2.5:1 up to 20:1 surfactant to CNT mass ratio. Too low surfactant concentrations were found not to be suitable while too high ones will not improve the results and eventually even give worse results. While too low concentration of the surfactant, especially at concentrations below the CMC [118], does not allow for effective coverage of the CNT surfaces, too high concentrations destabilize the dispersion via aggregation due to charge screening of the repulsive forces and possibly depletion attraction [119] (Fig. 4.3). A concentration of about 1 wt% (12.5 mg/mL) surfactant was chosen as standard procedure in agreement with literature data [44,118].

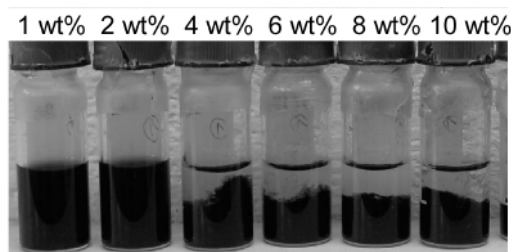


Fig. 4.3: Dispersion stability of 2.5 mg/mL HiPCO CNTs at varying SDBS concentration. Steady state after half a year of sedimentation.

The poor performance comes as no great surprise for SDS, since SDS lacks the benzene ring that is assumed to promote tube-surfactant interaction in the case of SDBS [114]. The wide usage of SDS to disperse CNTs is actually not due to its exceptional performance in CNT dispersion but probably rather because it is the single most commonly used surfactant in research facilities all over the world. For the SC and SDC however the explanation for our observations is not that easy. Most likely the disappointing performance can be deduced from the structural properties of these surfactants (Fig 4.4). Unlike most standard surfactants, which are composed of a polar head group and a non-polar tail, these two surfactants, which are derived from bile, have a steroidal structure. This gives them two sides with different polarity. In fact the non-polar side is larger than the polar one giving the molecule a bean-like structure with a convex non-polar side and a concave polar side. In solution such geometrical features get reflected in the micelle shape. While surfactants with SDBS-like structures, meaning large ionic head group and thin long non-polar tail, resulting in a packing parameter of around 1/3, form spherical micelles, SC and SDC form disklike micelles [120-123] which hints at a higher packing parameter, as far as this concept can be applied to this sort of surfactants.

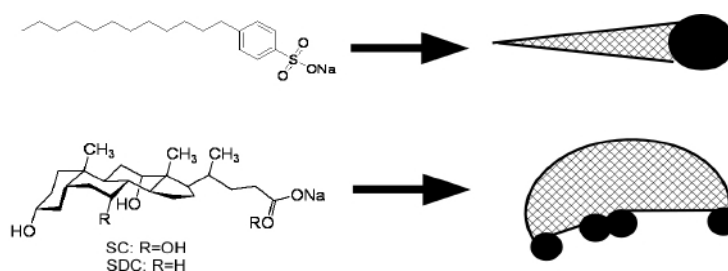


Fig. 4.4: Schematic depiction of the structure of SDBS and SDC/SC, polar moieties are indicated by black color, non-polar moieties are shaded.

This has an effect on the packing of surfactants around a nanotube. The shape of the SDBS micelles allow for a tight wrapping as the micelle structure can fit quite well with the curvature of the nanotube. A convex molecular structure like the one of the SC, on the other hand is incompatible with the similarly convex outer surface of the nanotubes, as this combination does not allow tight packing. The CNTs can be expected to cluster into aggregates so that the hydrophobic surface exposed to water is minimized. In fact, it was shown that CNTs dispersed in SC can organize themselves into highly aligned fibrils [124].

Additionally to these entropic effects related to the hydrophobic surfaces exposed to water also the enthalpic factors are to be considered. The interaction between the nanotubes and the SC/SDC can be considered as being mainly perpetrated by the methyl groups sticking out from the stiff steroid core so that only points of interaction are present rather than a large-scale area as with the flexible alkyl chain of SDBS which are known to strongly adsorb to the graphene-like structure of CNTs [125]. Also the benzene core of SDBS provides an anchor for π - π interactions and a polarizable entity, which promotes induced dipole-induced dipole interactions in the case of hemi-micelles formed on the CNT surface. In contrast to that stands the rigid σ -grid of the steroidal core of the SDC/SC, which is not very polarizable and inflexible when it comes to adjusting to the nanotube surface.

Finally, another factor that probably plays a role is the very nature of the stabilization of the colloidal suspension in general. The surfactants form a charged hull around the CNTs, which results in repulsive forces keeping the nanotubes separated. The magnitude of these repulsive forces depends on the surface charge present on the CNT-containing micelles. Although the SDBS molecule contains only one polar moiety instead of four/three in case of SC/SDC it nevertheless is a reasonable hypothesis that the formation of hemi-micelles on the nanotube surface – which seems to be the typical adsorption scheme for surfactants on CNTs [126,127] – leads to a higher surface charge in the case of SDBS than in case of SC/SDC due to the different micelle geometries. The potential difference in protonation due to different

acidic strengths of the corresponding acids can be neglected at these small concentrations (potentially the difference in acidity of the corresponding sulfonic acid and cholic acid could result in different degrees of protonation; see appendix for calculation). While SDBS is known to form micelles with an association number of around 30 molecules and a diameter of about 3 nm, SC forms micelles composed of only 3 - 4 molecules. For a hemi-micelle forming on a nanotube this means that a total of around 15 SDBS molecules cover roughly the same space on the nanotube surface as 2 SC molecules leading to a much higher surface charge and thus stronger electrostatic repulsion between adjacent nanotubes in dispersion (Fig. 4.5). In agreement with this deduction Sun et al. have measured a more negative zeta potential, the potential at the shear plane between the bulk liquid and a suspended particle, for CNT dispersions using SDBS than SC [118].

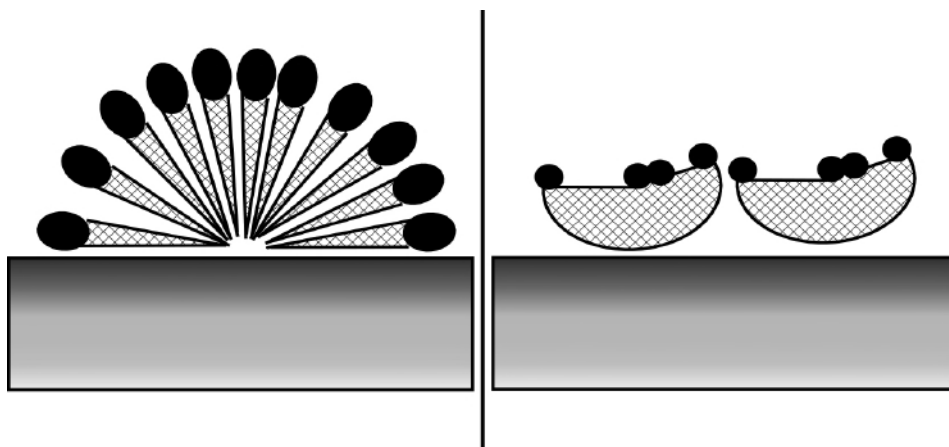


Fig. 4.5: Schematic depiction of the structure of SDBS and SDC/SC- hemimicelles, respectively, on a nanotube surface. Polar regions are indicated by black color, non-polar regions are shaded in the drawings representing surfactant molecules.

We should end this discussion of SC/SDC compared to SDBS by pointing out that other groups still claim very good results of CNT dispersion using these surfactants. It should be noted that none of these reports go to the high concentrations used here [44], or only reach their reported high CNT loadings before centrifugation [45].

For the replacement of CTAB for a substance that has a lower crystallization temperature the very similar structures of MTAB, which has a C_{14} chain instead of a C_{16} chain, and CEDAB, with one methyl group being replaced by an ethyl group, seem to be predestined. They show similar phase sequences in aqueous solution with alterations in concentration and most importantly in temperature (Fig. 4.6). In contrast to CTAB the other two both form stable LC phases at room temperature. However the concentrations of surfactant needed are higher than for CTAB with 32wt% for CEDAB and up to 40wt% for MTAB. Good liquid crystalline dispersions can be achieved with both surfactants although the higher amount of

surfactant can impair the homogenization process after adding the isotropic CNT-dispersion. This is especially the case for MTAB as it shows no intermediate nematic phase between the isotropic and the highly viscous hexagonal phase. Because of this it is recommendable to use CEDAB or CTAB as the most viable systems.

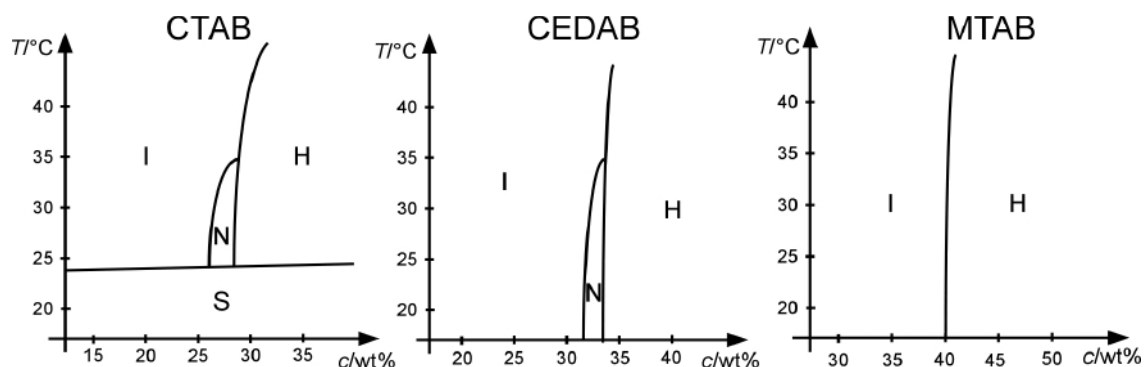


Fig. 4.6: Phase diagrams of CTAB, CEDAB and MTAB as established by POM and literature [128,129]

Another factor concerning the CNT dispersion quality is of course the type of nanotubes used. The type of nanotubes can have a great influence on the quality of the resulting dispersion [44]. In this study three different types of nanotubes were used. HiPCO SWCNTs, CoMoCat SWCNTs and MWCNTs. It turned out that only with the HiPCO tubes dispersion with aggregates below optical resolution was possible at the high concentrations desired. CoMoCat tubes and MWCNTs showed aggregates, albeit small, with any dispersion method and surfactant tested. These can be removed by centrifugation, yet this is not absolutely necessary, since in order to reach the polarizer effect they are in fact small and few enough to be tolerable. With any of the CNTs used sufficiently well dispersed samples can be produced so that an alignment of the CNTs in the LC phase can be visually confirmed by the polarizer effect (Fig. 4.7)

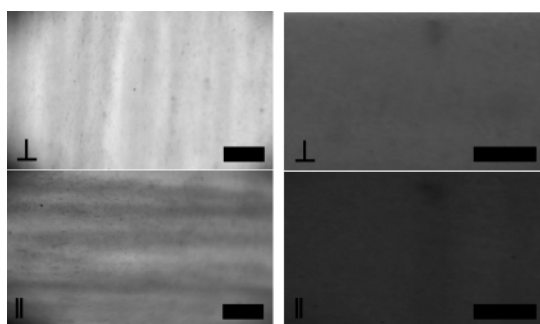


Fig. 4.7: Polarizer effect for samples containing 2.5 mg/mL HiPCO CNTs (left) and 10-30 nm thick MWCNTs (right). Scale bar = 50 μm .

The different performance with different types of nanotubes when it comes to the production of the initial isotropic dispersion can be explained by taking into account the differences in structure of the CNTs used. One difference that can be easily observed is the fact that HiPCO nanotubes are substantially less densely packed than all the other CNT samples as can be seen by them taking up much more space for the same mass and the dry CNT powder is “fluffier” than for CoMoCat and MWCNTs (this holds at least for the batches used for the studies in this thesis). Breaking up these loosely packed aggregates takes much less energy than breaking up the crystalline aggregates of the other CNT types.

The most important factors to consider are however most likely the length and the stiffness of the CNTs. As the energetic interaction between CNTs and surfactant should in first approximation be largely of the same magnitude for any of the different CNT types the entropic conditions ought to play a deciding role. According to the Flory-Huggins theory of polymer dissolution the mixing entropy of a polymer dispersed in a solvent is substantially smaller than for the case of a monomer solution, since the bound-together monomers in the case of the polymer solution have less possibilities of arrangement than if they were free. This effect even increases in importance when the polymer is long and stiff such as a CNT. The longer and stiffer the CNTs the less favored is the state of singular dispersion as the entropy of this state would be low [40]. Of the different CNT types used the HiPCO CNTs are the shortest with a length of hundreds of nanometers followed by CoMoCat CNTs with a length of about a micrometer and the MWCNTs with a length between 5 and 15 micrometers. When additionally considering the fact that MWCNTs are much more rigid than SWCNTs it can be easily understood that the MWCNTs should fare worst, as they in fact do. Finally, one cannot rule out that the lower curvature of an MWCNT outer surface compared to that of an SWCNT has an impact, possibly suggesting that different surfactants are optimum for S- and MWCNTs, respectively.

In conclusion of the results presented in this chapter a standard method for the production of high quality lyotropic LC/CNT composites can be deduced. The first step is the dispersion of HiPCO CNTs in an aqueous SDBS solution with a surfactant to CNT ratio of 5:1 using a tip sonicator until the CNT bundle size is below optical resolution. This dispersion is then added to the dry LC-forming surfactant, either CEDAB at 32wt% or CTAB at 28wt%, and the mixture is stirred for an hour, followed by sonication in an ultrasonic bath for of about 3 hours. By then a polarizer effect can be seen homogeneously throughout the sample if all stages of the preparation were successful.

4.2. Towards efficient dispersion of CNTs in thermotropic liquid crystals

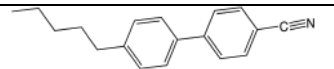
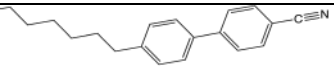
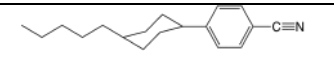
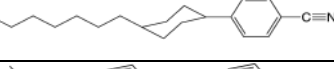
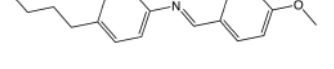
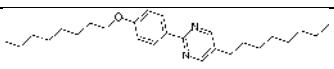
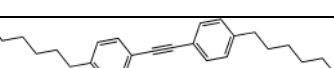

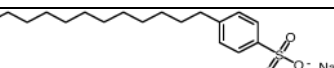
As mentioned in chapter 2.3 the idea behind putting CNTs into LCs is to provide a suitable medium for CNT dispersion alongside the transfer of the LC's inherent order to the CNTs. Standard media for CNT dispersions include most often aqueous surfactant solutions. But also organic solvents have been identified as useful alternatives, mainly NMP and its derivatives. Following a simple „*simila similibus solvuntur*“ (lat.: like dissolves like) approach thermotropic LCs seem to be predestined as solvents for carbon nanotubes, being aprotic, structurally relatively non-polar, yet highly polarizable and with the possibility of π - π stacking between their typical biphenyl core structure and the CNT-wall.

As with most topics on a closer look things get more complicated. On closer inspection the seemingly simple task of dispersing CNTs in a thermotropic LC proves to be a highly complex task, the success of which depends on various factors from dispersion method and conditions to the detailed structure of the employed LC. Thus far, although quite some effort was spent in the research of CNT/LC composites, a systematic investigation and identification of these factors was lacking and rendered CNT-dispersion to be a bit like alchemy depending on personal impressions and preferences. We systematically investigated factors such as dispersion method/procedure and LC-structure providing a first step towards efficient dispersion of CNTs in thermotropic LCs.

4.2.1. Results

We investigated a multitude of different thermotropic LCs as a host for CNTs (Tab. 4.1), systematically varying the structural properties of the LC host as well as optimizing dispersion procedures.

Tab. 4.1: Overview of the substances used as hosts in the work.

Code	Structure	Phase sequence [°C]	η [mPa s] [a]	μ [D] [b]	ϵ_r (N/I) [c]
5CB [d]		Cr. 23 N 35 Iso.	29.9@RT	6.3	11.6 / 7.0
7CB [d]		Cr. 30 N 42.8 Iso.	36.9@RT	6.3	10.0 / 6.1
PCH5 [d]		Cr. 31 N 55 Iso.	26@RT	5.9	3.7 / 3.5
PCH7 [d]		Cr. 30 (SmC _x 17) N 59 Iso.	29.4@RT	5.9	5.5 / 3.4
MBBA		Cr. 22 N 48 Iso.	39.6@RT	1.8 - 3.1 [e]	3.6 / 3.7
8OPhPy8		Cr. 28.5 SmC 55.5 SmA 62 N 68 Iso.	15@63°C	1.3	2.7 / 2.5
6T7		Cr. 20.5 (Sm 18.8) N 29.4 Iso.	23@RT	0.09	2.0 / 1.9
RO-TN-403/015S	Multi-component mixture (<i>n</i> CB, <i>n</i> OCB, <i>n</i> CT, <i>n</i> CPhPy, <i>n</i> PDP, 0.1 wt.-% cholesteryl nonanoate).	Cr. <0 N 81.5 Iso.	78.4@RT		5.5 / 4.6
E7	4-component mixture (5CB, 7CB, 8OCB and 5CT).	Cr. <-30 N 58 Iso.	45.5@RT		8.5 / 5.7
NMP		Cr. -23 Iso.	1.6@RT	3.89	- / 32
SDBS		Used in aqueous solution at a concentration of 2.5 wt.-%.			

[a] η = viscosity as measured in a standard cone rheometer (see Appendix). RT = room temperature. [b] μ = molecular dipole moment. [c] ϵ_r = relative dielectric permittivity at 10 kHz and $\pm 2.5^\circ\text{C}$ from the nematic (N) - isotropic (I) transition, in the N case measured along **n**. [d] These mesogens tend to organize into antiparallel dimers. [e] Several conformations have similar energy, the resulting μ ranging from 1.8D to 3.1D.

The first intriguing observation when dispersing CNTs in a thermotropic LC is that already simple stirring apparently dissolves the CNTs to a point that no aggregates are visible by eye and a homogeneous although coarse dispersion is yielded. This state is reached within minutes of gentle magnetic stirring and can be achieved independent of what LC is used with

the time needed being only correlated to the viscosity of the LC host (see Fig. 4.8). Although the dispersion is coarse the unprecedented ease in its production is interesting as it indicates beneficial CNT-mesogen interactions and since it allows an exceptionally gentle first step of CNT dispersion. Stirring slowly distributes CNTs into a large number of loose aggregates heavily infiltrated with LC as can be seen by microscopic inspection and centrifugation. Although the dispersions yielded by this method are not stable against centrifugation at all, the sediment becomes visibly larger with the stirring time reflecting the swelling of the initially compact CNT aggregates with LC molecules. In fact, already before stirring is initiated it is immediately apparent that the CNT powder swells as soon as it is brought into contact with the LC. For the RO-TN-403/015S thermotropic LC mixture, hereafter referred to as ROTN, the optimum time of stirring - the time after which no apparent increase in sediment could be found – was established as being around 24 h (Fig. 4.9).

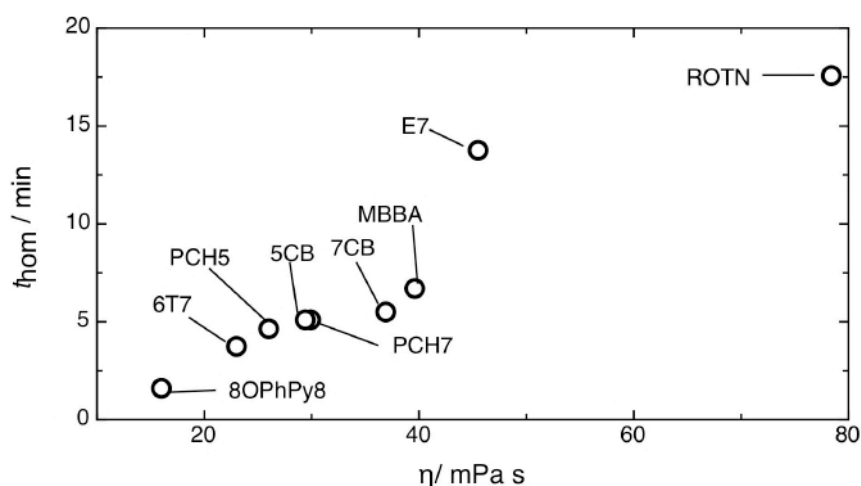


Fig. 4.8: Time t_{hom} until a homogenous dispersion is achieved (by eyesight) by stirring over the viscosity of the LC host.

This behavior stands in strong contrast to other solvents commonly used as a dispersion medium for CNTs such as THF, DMF or NMP. In none of these a visible reduction of particle size and apparent swelling and infiltration of solvent into the solid aggregates, hence dissolution, could be achieved through simple stirring of a few minutes and the solvent quickly cleared upon stopping the mechanical treatment. Thermotropic LC/CNT dispersions on the other hand, even though yielding a very coarse dispersion when treated this way, can be stable for days to weeks.

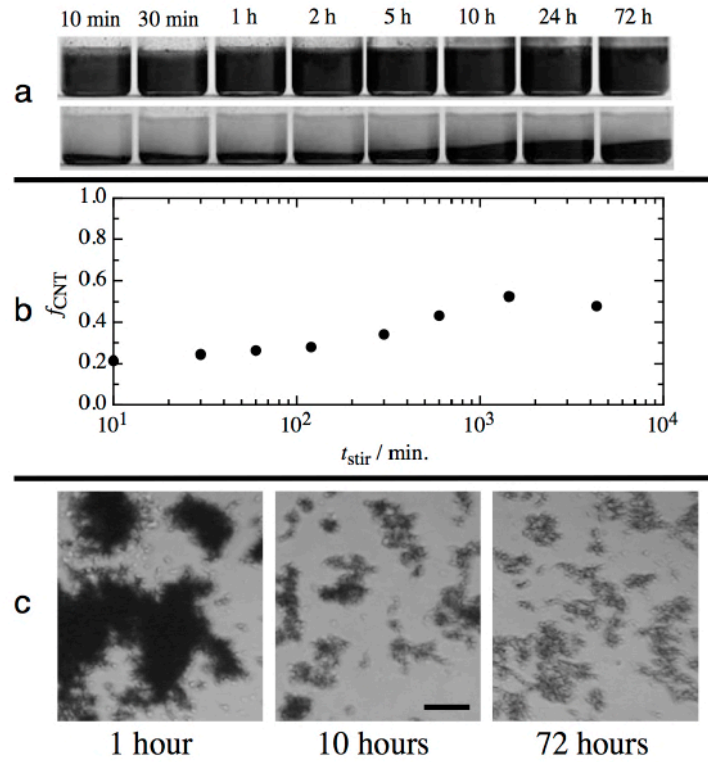


Fig. 4.9: (a) Pictures of CNT sediment after different stirring times (top and bottom rows are before and after centrifugation, respectively), (b) plot of the ratio of sediment to supernatant f_{CNT} over the stirring time and (c) microscopic pictures of the dispersion (sample between microscope slide and cover glass) taken directly after terminating stirring. Scale bar = 40 μm .

Although simple stirring does not provide a stable, high-quality dispersion it might be a possible gentle first-step of a more complex dispersion procedure. In order to investigate this possibility a series of experiments were conducted where stirred and unstirred samples were subjected to an additional sonication step of varying duration. Seven samples were produced with a nanotube content of 0.1 mg/mL HiPCO CNTs in the ROTN thermotropic LC mixture. Four of these samples were stirred for 24 h for maximum dispersion effect as shown above. Three of these samples were treated with a brief tip sonication in pulsed mode (0.5 s of sonication followed by a pause of 0.5 s) at 100% amplitude for 5, 10 and 15 minutes, respectively. The fourth sample acted as a reference. The rest of the samples were treated with ultrasound in the same fashion without prior stirring.

After preparation the samples looked macroscopically and (with the exception of the reference sample that was only stirred) also microscopically, identical. Centrifugation at 4000 g revealed the differences in dispersion quality (Fig. 4.10). In coherence with the expectations the sample that was only stirred quickly sedimented, being almost completely clear of CNTs in the supernatant after only 10 min of centrifugation. The best dispersion turned out to be the ones stirred followed by a brief sonication step. However the presence of aggregates above optical resolution in all the samples indicates that ROTN is not the best-suited host for CNTs.

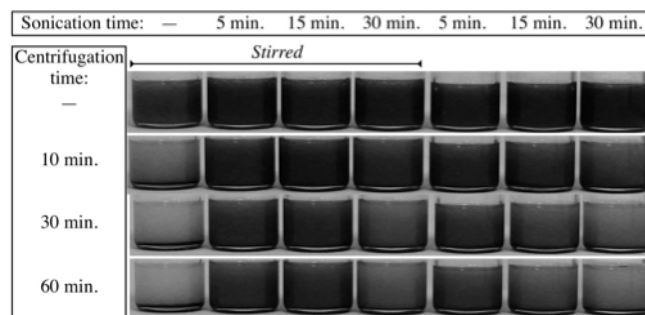


Fig. 4.10: Samples with 0.1mg SWCNTs / mL ROTN LC, prepared following different combinations of stirring and/or sonication. The top row shows the samples after the preparation phase, the following rows after stepwise increasing time of centrifugation.

Contrary to what one might assume at first grasp longer sonication does not necessarily yield a better dispersion. Both samples sonicated for 30 min are more prone to sedimentation than the more briefly sonicated ones. It is well known that colloid aggregation can be induced by shear flow, due to the increased chance of contact between particles. When preparing dispersion colloids there is thus a trade-off between the reduction of particle size achieved by mechanical processing and the increased risk of aggregation. From the stirring/sonication experiment it can be concluded that aggregation dominates after only a few minutes of sonication in ROTN.

The relative ease of CNT dispersion in thermotropic LCs suggests that the anisotropy of the LC is beneficial. In order to verify this hypothesis an experiment was conducted where samples of stir-dispersed CNTs in E7 were kept above, around and below the clearing point (Fig. 4.11). The fact that samples above the clearing point in the isotropic state show almost immediate aggregation serves as a confirmation of the importance of the anisotropy of the phase for the stability of CNT dispersions. Even if the initial dispersion was prepared by a more optimized tip sonication routine, aggregation can typically be seen after tens of minutes in the isotropic phase while samples below the clearing point show no signs of aggregation for days to weeks depending on the LC host. Note that the viscosity variation in the temperature range investigated is small and non-monotonic (see appendix) hence the reduced stability of isotropic samples is not just a result of viscosity reduction.

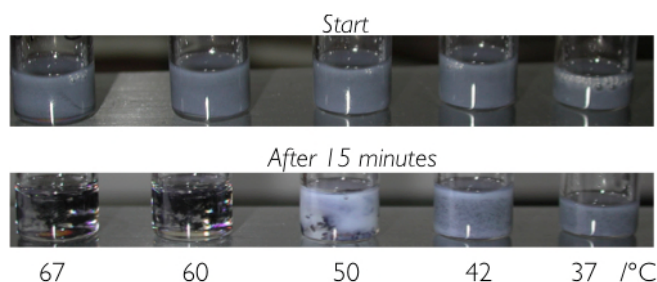


Fig. 4.11: Samples of stir-dispersed CNTs in E7 at different temperatures above, around and below the clearing point (58°C).

In correspondence with these results dispersions prepared above the clearing point show lower stability than dispersions prepared in the nematic phase. Keeping the LC host in the nematic phase during the preparation and storage of CNT-dispersions is highly advisable.

While the anisotropy of an LC host is beneficial for CNT dispersion there are still significant differences between different LCs. Experiments were carried out using similar procedures and CNT concentrations to gain further insights of how to choose an LC host for CNT dispersion. For testing the dissolution power of different LCs as well as the most common isotropic hosts for CNT dispersion – NMP and aqueous SDBS – and water as a bad-host reference the first 1.5 seconds of dispersion using a sonotrode were filmed with a high-speed video camera allowing us to measure how fast and to what extent the fluid turned opaque as a result of CNT aggregates being broken up (see Fig. 4.12). The LCs had to be heated to the isotropic phase since the turbidity of nematic samples obscures the view of the process. This experiment probes mainly the role of mixing enthalpy since the kinetic situation is similar for all solvents and entropic contributions can in a first approximation be neglected at this very first step of dispersion.

The experiment reveals major differences mainly between the aqueous hosts – water and aqueous SDBS – and all the LCs and NMP. A fast darkening as CNT aggregates are broken up can be seen for all the organic hosts while in water and SDBS solution the CNT grains are mainly whirled around with no significant reduction in aggregate size over the course of the experiment. Of the organic solvents all the LCs perform better than NMP, with the two LC mixtures, ROTN and E7, giving the best results, i.e. the darkest suspensions in minimum time.

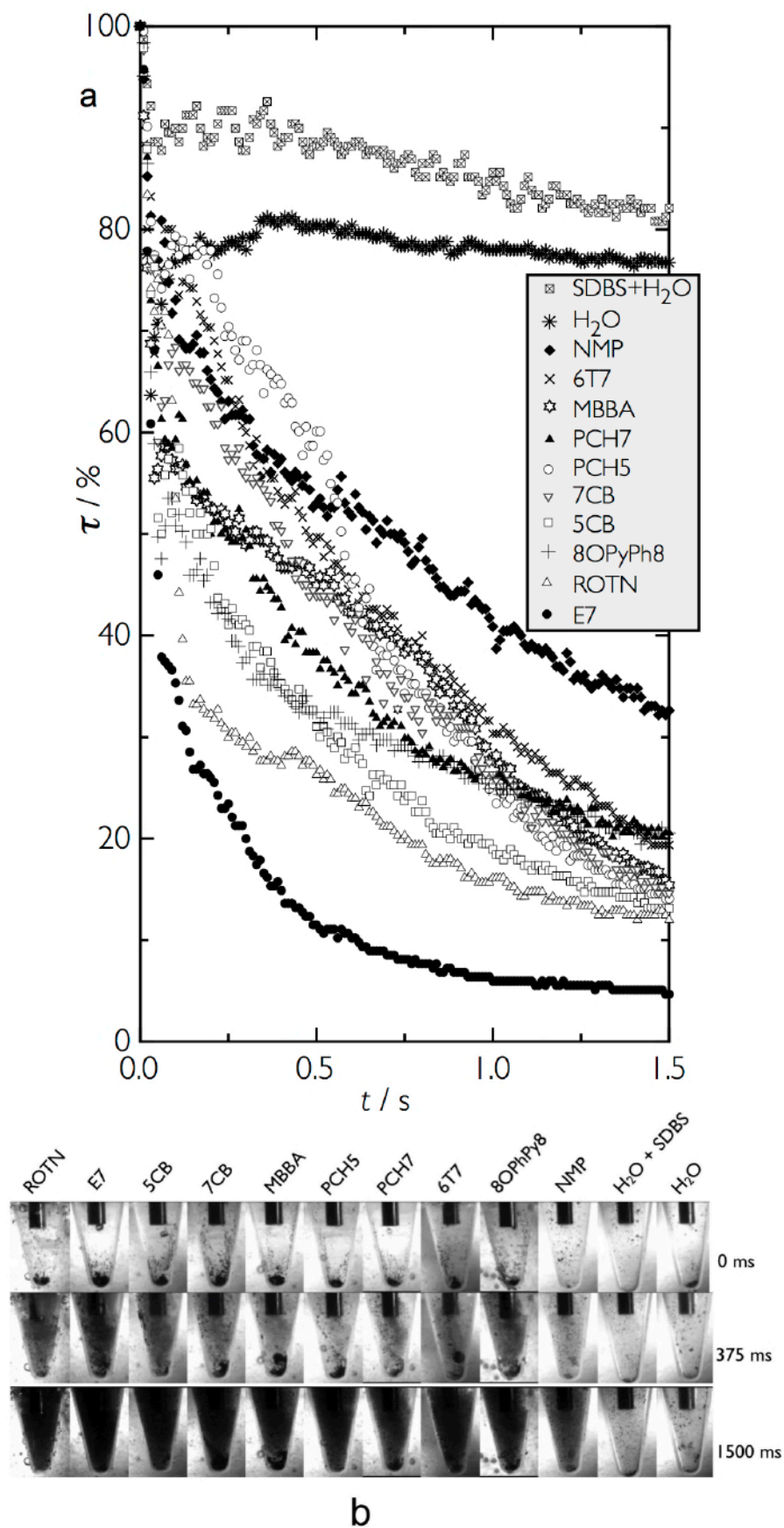


Fig. 4.12: (a) The first 1.5 s of sonotrode-mediated SWCNT dispersion in different LCs, expressed by the transparency τ as a function of sonication time t . (b) Representative still images from the video.

Further investigations were conducted testing the stability against centrifugation of CNTs dispersed in the LC hosts (except for 8OPhPy8 since its nematic phase is above the temperature range accessible with the centrifuge) and NMP using long-term sonication. Samples with 0.1 mg CNTs per mL solvent were sonicated for 30 minutes and then centrifuged at 4000g in several steps, the quality of the samples being regularly monitored (Fig. 4.13). The stability increases from 6T7 over 5CB, 7CB, PCH5, ROTN, PCH7 to E7 and MBBA. This sequence of the LCs shows no really obvious trend. No obvious correlation of the dispersion stability with the various structural properties of the LCs, such as dipole moment, permittivity, alkyl chain length, extended π -electron system or the presence of lone electron pairs can be identified easily.

The two LCs MBBA and E7 yield highly satisfactory suspensions, very similar to the dispersion in NMP. Their supernatants after 3 hours of centrifugation were investigated by optical microscopy, revealing that only few optically resolvable CNT aggregates were present. Those that were found were of low contrast and elongated along \mathbf{n} .

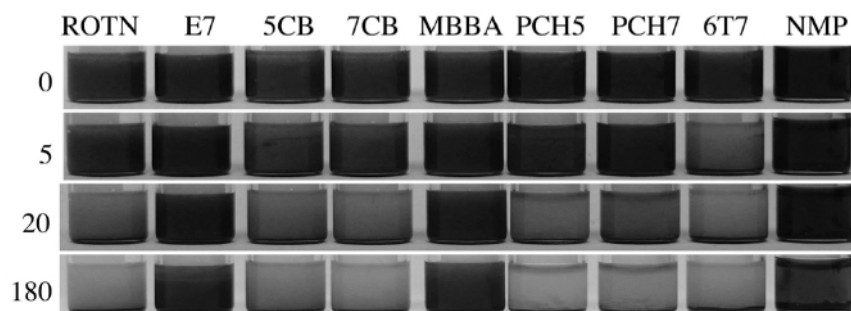


Fig. 4.13: 0.01 wt.-% SWCNT-in-LC samples, dispersed with sonotrode for 30 minutes (top row) and then centrifuged at 4000g for 5, 20 and 180 minutes, respectively.

To compare quantitatively the performance of the best LCs we performed optical absorption spectroscopy (see appendix) on the supernatants of E7, MBBA and NMP (as reference) after 3 hours of centrifugation, using the Beer-Lambert Law [130,131] to estimate the CNT concentration.

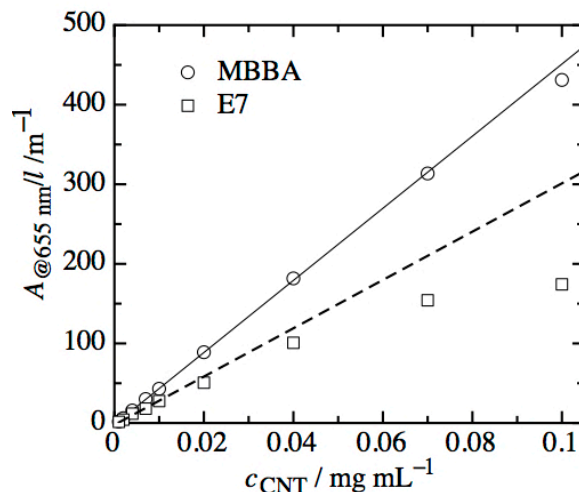


Fig. 4.14: Absorption at 655 nm divided by the sample length (1 cm) as a function of CNT concentration in samples of E7 and MBBA. The lines are best linear fits, yielding extinction coefficients $\alpha_{E7} \approx 3000 \text{ mL mg}^{-1}\text{m}^{-1}$ and $\alpha_{MBBA} \approx 4500 \text{ mL mg}^{-1}\text{m}^{-1}$.

Fitting linear functions to the low-concentration data points that follow linear behavior for each LC gave extinction coefficients $\alpha_{E7} \approx 3000 \text{ mL mg}^{-1}\text{m}^{-1}$ for E7 and $\alpha_{MBBA} \approx 4500 \text{ mL mg}^{-1}\text{m}^{-1}$ for MBBA (Fig. 4.14). For NMP we use the extinction coefficient published by Giordani et al. [43], $\alpha_{NMP} = 3264 \text{ mL mg}^{-1}\text{m}^{-1}$ at a wavelength of 660 nm. The resulting CNT concentrations in the three supernatants are summarized in Tab. 4.2. The two LCs turn out to be equally good and in fact better hosts than NMP, at least under these dispersion conditions. From these data we may estimate the maximum CNT content in E7 and MBBA to about 0.04 mg mL^{-1} .

Tab. 4.2: CNT concentration in the E7, MBBA and NMP supernatants in the experiment of Fig. 4.13 after 3 hours of centrifugation.

$C_{E7} / \text{mg mL}^{-1}$ ($\alpha_{E7} \approx 3000 \text{ mL mg}^{-1}\text{m}^{-1}$)	$C_{MBBA} / \text{mg mL}^{-1}$ ($\alpha_{MBBA} \approx 4500 \text{ mL mg}^{-1}\text{m}^{-1}$)	$C_{NMP} / \text{mg mL}^{-1}$ ($\alpha_{NMP} \approx 3264 \text{ mL mg}^{-1}\text{m}^{-1}$)
0.04	0.04	0.02

4.2.2. Discussion

The possible dissolution of a solute in a solvent is governed by the Gibbs free energy $\Delta_{\text{mix}}G$ [132] of the mixing process. For a thermodynamically stable solution $\Delta_{\text{mix}}G$ has to be negative, making the dissolution process exergonic, provided that any kinetic hindrance can be overcome. The Gibbs free energy $\Delta_{\text{mix}}G$ of mixing is connected with the change in enthalpy $\Delta_{\text{mix}}H$ and the change in entropy $\Delta_{\text{mix}}S$ of the mixing process

$$\Delta_{\text{mix}}G = \Delta_{\text{mix}}H - T\Delta_{\text{mix}}S \quad (4.1)$$

with T the temperature of the system.

The contributions to these factors specific to the case under discussion are as follows:

- i. *Enthalpic contributions*: CNT-CNT interactions and solvent-solvent interactions replaced by CNT-solvent interactions; CNT-induced elastic deformations of the nematic director field.
- ii. *Entropic contributions*: mixing entropy; adsorption of solvent molecules on CNTs.
- iii. *Kinetic contributions*: the velocity of CNT aggregation mainly depends on the affinity for aggregation and the CNT-CNT collision number. While the former is determined by (i) and (ii), the latter depends on the diffusion constant (anisotropic in LCs), the degree of orientational order, and the CNT aggregate size and morphology.

In the case of CNT dissolution in liquid crystals this leads to a complex interplay of the different contributions. The enthalpic contributions are largely due to the van der Waals interaction of CNTs with solvent molecules and interaction due to overlap of the molecular orbitals of solvent molecules with those of the CNT and the consequent possible charge transfer from the solvent molecules to the CNT or vice versa.

The van der Waals interaction [133] is composed of three basic interactions:

- The Keesom forces or dipole-dipole interactions [134]:

The Keesom forces describe the interaction between molecules with permanent dipoles. The potential energy E between two dipoles μ_1 and μ_2 is given by:

$$E = -\frac{1}{3kT(4\pi\epsilon)^2} \cdot \frac{\mu_1^2 \mu_2^2}{r^6} \quad (4.2)$$

with k the Boltzmann constant, T the temperature, ϵ the relative permittivity of the medium and r the distance between the dipole centers of mass.

- The Debye forces or dipole-induced dipole interactions [135]:

The Debye forces describe the interaction between a permanent dipole and an induced dipole. The potential energy E between a molecule with the permanent dipole μ and a non-polar molecule with the polarizability α amounts to:

$$E = -\frac{1}{(4\pi\epsilon)^2} \cdot \frac{\mu^2 \alpha}{r^6} \quad (4.3)$$

with ϵ the relative permittivity of the medium and r the interaction distance.

- The London forces or induced dipole-induced dipole interactions [136]:

The London forces describe the interaction between non-polar molecules due to induced dipoles caused by quantum fluctuations. The potential energy E between two molecules with the polarizabilities α_1 and α_2 amounts to:

$$E = -\frac{3}{2(4\pi\epsilon)^2} \cdot \frac{I_1 I_2}{r^6} \cdot \frac{\alpha_1 \alpha_2}{r^6} \quad (4.4)$$

with ϵ the relative permittivity of the medium, I_1, I_2 the ionization energies of the two molecules and r the intermolecular distance.

Note that none of the equations above takes into account the anisotropy of the LC phase and its physical properties and they are in principle only roughly valid for small molecules. Nevertheless they are still useful to discuss the key parameters that contribute to the Gibbs free energy of mixing $\Delta_{\text{mix}}G$. From the expressions above we can conclude that the interaction between CNTs and any molecules in general should be promoted by a large dipole moment μ and a large polarizability α of the molecules due to increased Debye and London forces. Both

these conclusions have already been verified in published studies [137,138]. Concerning LCs high dipole moment and high polarizability are often achieved by the commonly occurring polar groups and large systems of delocalized electrons in the structure of the LC molecule.

Connected to this, a factor frequently assumed to play a role involves the capability of π - π stacking interactions. The widespread classical belief is that π - π stacking arises due to overlap of the π -orbitals of the interacting molecules. However, contrary to this view π - π stacking interactions seem not to be a result of π -orbital overlap. Hunter et al. see them as arising from electrostatic interactions that result from variations in the charge distribution of aromatic molecules – the hydrogen atoms of a benzene ring carrying less charge than the carbon atoms. This results in a strongly patterned stacking interaction [139]. The most modern approach however is that the π - π stacking interactions are part of the London forces, particularly strong between aromatic molecules due to the high polarizability of the delocalized π -electron system and the possible close approach of the interacting molecules due to their plane structure [140]. The strongly patterned adsorption commonly linked to the maximizing of orbital overlap is in fact, quite contrary to the classical and still widely taught view, linked rather to a minimization of any possible overlap of occupied orbitals in order to avoid the Pauli repulsion between the filled orbitals.

Direct orbital interactions however play a role for the electron pair donicity or charge transfer (CT) interactions, both assumed to be key factors for the stability of CNT dispersions. From the third term of the Klopman-Salem Equation [141,142], here in a highly simplified form in order to extract the key point for this discussion (see Appendix for whole formula),

$$\Delta E = \frac{const.}{E_{HOMO} - E_{LUMO}} \quad (4.5)$$

we find that for the interaction energy of two molecules due to orbital overlap the main factor is the gap between the frontier orbitals, i.e. the highest occupied molecular orbital (HOMO) of the electron-donating molecule and the lowest unoccupied molecular orbital (LUMO) of the electron-accepting molecule. If the difference is small the interaction is maximized. The frontier orbitals of semiconducting nanotubes can be related to the first van Hove singularities in the valence and conduction bands, whereas those of metallic nanotubes correspond to the orbitals near the Fermi level.

The interaction of CNTs with free electron pairs on molecules is based on this interaction of a high HOMO, the free electron pair, with the LUMO of the CNT. Lone pairs with high energy are situated at atoms that are not too electronegative, so a lone pair at a nitrogen atom interacts more strongly than a lone pair at an oxygen atom. The electron pair donicity also

decreases with increasing s-orbital character of the lone pair, that is to say sp^3 - and sp^2 - hybridized lone pairs interact strongest.

As mentioned above this kind of orbital interaction plays only a minimal role in the interaction of small molecules with (unsubstituted) π -systems with CNTs, since their HOMO and LUMO lie deep within the valence and conduction bands of CNTs, respectively, so that the interaction in this case takes place mainly via the π - π stacking due to increased London forces [143]. CNTs typically have band gaps between 0.5 and 3 eV, giving rise to optical transitions in the near infrared and visible spectra [144]. This can be compared with the band gap of for instance benzene of 10.5 eV, giving it optical transitions in the UV range of the electromagnetic spectrum. Similar band gaps and transition regimes are found for most small aromatics including the typical mesogenic unit biphenyl. However, substituents to the π -system can alter the frontier orbital energies. Electron-donating groups raise the HOMO, while electron-accepting substituents lower the LUMO. In the vicinity of such adjusted molecules the CNTs can interact and act either as an electron donor or acceptor depending on the “needs” of the molecule in question. These interactions are often accompanied by a considerable charge transfer from the CNT to the molecule or vice versa, meaning that the newly formed frontier orbitals of the charge transfer complex are strongly localized on the different interacting species, the new HOMO being localized on the acceptor and the new LUMO being localized on the donor, respectively. The charge transfer gives rise to a dipole moment so that additional electrostatic forces appear between the CNT and the interaction partner molecule, making the CT interaction basically an electrostatic interaction. In contrast, the interaction of CNTs with lone pairs is only accompanied by a weak charge transfer and is mainly an orbital-controlled interaction [145,146].

The role of CT interactions for CNT dissolution can most strikingly be seen in the case of fullerenes, which can tentatively be considered the smallest nanotubes. Depending on the CT capabilities of the solvent fullerene solutions show different colors from pink to bluish violet. Carbon nanotubes are known to show CT interactions with nitroaromatics where the CNT acts as electron donor [148] and a strong CT complex was theoretically predicted for a mesogen containing a trifluoro-substituted phenyl ring [149]. The interaction of CNTs with a lone electron pair with only weak charge transfer is suggested to be the reason for the good dispersibility of CNTs in NMP [43] and in fact the varying strength of lone pair interactions depending on the electronic structure of the CNTs is the mechanism for many CNT separation methods [48,150,151].

We now move on to a consideration of the entropic contributions. Normally, for mixtures between small molecules, the entropy of mixing $\Delta_{\text{mix}}S$ would be positive, promoting dissolution. A mixed state always has a higher degree of disorder than a completely demixed system. However, the dissolution of CNTs is accompanied by a particularly low entropy of mixing $\Delta_{\text{mix}}S$, as can be understood following a reasoning related to the Flory-Huggins theory [152,153] for polymer solutions (suitably modified for taking the size and rigidity of CNTs into account) [42,154]. A polymer solution has lower entropy of mixing in comparison to a monomer solution since the bonding together of the monomers in the polymer reduces the degree of freedom in the monomer arrangement. This effect is even more pronounced for long, stiff “polymers” such as CNTs. Moreover, as much as strong enthalpic interactions between the CNT and the solvent would be favorable to compensate for the low solvation entropy, they come with an essential drawback, to some degree negating their usefulness for CNT-dissolution. The adsorption of a molecule on a CNT due to any of the interactions described above leads to a more or less pronounced fixation of said molecule on the CNT sidewall, effectively decreasing its degree of freedom of transversal movement and rotation. This effect grows during CNT dispersion with increasing CNT surface exposed to the adsorbing solvent making the mixing more and more unfavorable as more CNTs dissolve. This effect should be most pronounced for molecules capable of π - π stacking interactions [155] and adsorption of alkyl chains [156], which are both known to adsorb very strongly and with specific ordered patterns to graphitic structures [125,157]. In the first case it is the maximization of attractive and minimization of repulsive interactions arising from offset aromatic stacking, in the latter case it is the geometrical fit of the hydrogen atoms of the alkyl chains with the centers of the graphene hexagonal rings that ensures a regular adsorption pattern. Both these interactions promote favorable enthalpic interactions while at the same time reducing the entropy of the system. Interaction with lone pairs also causes a certain fixation of the molecule to the CNT wall but since there is only one strong bonding point the loss in configurational entropy is less pronounced [43]. In the case of CT complexes the fixation depends strongly on the magnitude of the charge transfer. Strong ordered adsorption is known for charge transfer between suitably substituted phenyl rings [148,149]

Summarizing the above, we thus find an analogy with the LC phase itself for CNT dispersion. The liquid crystalline state exists due to a balancing of order-promoting and order-disrupting interactions of the mesogens. Similarly the question of CNT dissolution appears to be a question of balancing the enthalpic and entropic contributions to the mixing process.

In addition to the enthalpic and entropic factors every dispersion and sedimentation process is controlled also by kinetic effects. One of the most important in the case of LC hosts is the anisotropic viscosity. Aggregation of adjacent CNTs aligned along \mathbf{n} is less likely than in case of an isotropic solvent because the viscosity is much higher for movement perpendicular to \mathbf{n} than for movement along the director. Likewise, orientational fluctuations, which increase the chance of inter-tube contact substantially, are counteracted by the rotational viscosity for reorientation about axes perpendicular to \mathbf{n} . This reduces the CNT-CNT collision number, kinetically stabilizing the suspension. Apart from viscosity, the diffusion of a CNT or aggregate is governed by its frictional coefficient f , proportional to the cross section in the direction of diffusion. With D the diffusion coefficient and k the Boltzmann constant we have $D \propto kT/f$. Because of the extreme anisometry of CNTs, f is exceptionally dependent on the orientation with respect to the diffusion direction. With nanotubes that are well dispersed and aligned along \mathbf{n} this yields orders of magnitude greater diffusion parallel to \mathbf{n} than perpendicular since the effective CNT cross section is much greater for the latter direction, again counteracting aggregation. Obviously, this kinetic stabilization relies entirely on the nematic order of the host, the transfer of this order onto the CNT guests, and on the CNTs being well dispersed rather than in aggregates with close to isotropic cross section. It thus disappears for a poor dispersion and/or for a sample heated to the isotropic phase, in line with our experimental observations.

Considering the factors outlined above the performance of the liquid crystals in the various dispersion experiments appears not as random as it may seem at first glance. The surprisingly easy, albeit coarse, dispersion of CNTs in the thermotropic LCs achievable by gentle stirring and the visible swelling of the CNT aggregates hint at largely favorable enthalpic interactions. At this coarse state of dispersion they are not significantly counteracted by the entropy loss connected to the LC adsorption onto the CNTs. The kinetic factors of aggregate distribution throughout the LC phase and LC intrusion into CNT bundles are the velocity determining steps, hence the viscosity dependence. Since the stirring experiments revealed no pronounced swelling for NMP or DMF, it can be deduced that the elastic forces that, contrary to any isotropic phases, exist inside an LC phase, promote the disassembly of disordered CNT aggregates by adding up to the shear forces during the stirring process. This promotes an easy coarse dispersion even though in a non-agitated sample they are expected to expel large CNT-aggregates from the nematic phase, thereby minimizing the deformations of the director field as seen by the instability upon standing of the so-produced coarse dispersions.

The favorable interactions between CNTs and LCs are further confirmed by the high-speed camera tip sonication experiments. Here any beneficial influence of the anisotropy of the nematic LC phase is excluded since the experiments were conducted with the LC heated to the isotropic state. The experiments probe mainly the enthalpic contributions with only small entropic contributions expected to play a role towards the end of the experiments when, at least for the non-aqueous hosts, a considerable debundling of the CNT aggregates took place. All the LCs perform largely similar to, and in fact even better than NMP, solidifying the evidence for favorable CNT/LC interactions. The outstanding early-stage performance of both LC mixtures, studied (they fare quite differently in the long term sonication experiments) can be tentatively explained as a result of multiple different mesogens that can all adsorb on the CNT walls counteracting large-scale ordered adsorption of molecules from the solvent, thus minimizing the loss of entropy compared to unimolecular solvents. The adsorption of LC molecules onto the CNT sidewall introduces a positional and orientational order that is not present in the isotropic phase. Scanning tunneling microscopy (STM) investigations of LCs on highly ordered pyrolytic graphite (HOPG) demonstrated that mesogens can adsorb strongly on a graphitic surface, even forming 2D crystals [158]. Interestingly, the adsorption was driven not by aromatic interactions but by the tight geometrical fit of the hydrogens of the alkyl chains on the graphitic lattice. Similar strong ordered adsorption is known for the interaction between polycyclic aromatic hydrocarbons [155] and CNTs and was theoretically predicted for LC molecules [149,159]. This behavior would constitute a severe entropy decrease but likely gets to some extent suppressed by the presence of differently structured mesogens, resulting into a smaller entropy loss upon adsorption and thereby explaining the relative better performance of ROTN and E7. It seems a reasonable hypothesis that all the LCs express more favorable enthalpic interactions with CNTs, i.e. more negative mixing enthalpy, with CNTs than NMP, which is hypothesized to show a mixing enthalpy close to zero [40].

Extending the argument above to nematic phases, the fact that an LC in its nematic phase is itself ordered should make the solvation entropy penalty less pronounced. While the adsorption of mesogens onto CNTs gives rise to a positional order that is not present in a nematic phase, orientational order is the natural state; hence entropy loss due to adsorption-induced alignment is negligible. Keeping the solvent in its nematic phase thus minimizes the solvation entropy penalty; a conjecture that fits well with our experimental observations that CNT sedimentation is promoted by heating a suspension into the isotropic state. This is further supported by a Japanese study on LC wetting of HOPG [160], revealing that LCs generally wet HOPG in the nematic but not in the isotropic phase. Directly related is the observation of

Coleman et al. that in order to minimize the surface energy of the solvent, this should be matched to that of the CNTs. In a first approximation this corresponds to a solvent surface tension $\gamma \approx 40 \text{ mN m}^{-1}$ [42,154]. While γ in LCs is more complex due to the phase anisotropy, literature data for 5CB indicate an effective surface tension of $\gamma \approx 35 \text{ mN m}^{-1}$ [161], quite close to the desired value.

In the isotropic phase, however, there is no general beneficial effect of reduced solvation entropy penalty. Only the two LC mixtures exhibit a reduction due to the inhibited ordered adsorption of the structurally different LC mixture components, distinguishing them from the other isotropic LC materials, even prompting the good performance of ROTN which overall shows not to be an ideal LC host.

In the experiment testing the CNT dispersion stability upon centrifugation a substantial variation is revealed between the LCs, only in case of E7 and MBBA matching that of NMP. It thus seems that, while the thermodynamic situation is favorable with any LC host at the very beginning, this may change later in the dispersion process depending on the chemical details of the LC. Following the considerations above we suggest that the lack of stability of CNT dispersions in all the LCs but E7 and MBBA may be explained largely in terms of the configurational entropy decrease of solvent molecules as they adsorb during sonication, possibly strongly and in an ordered fashion, on the rapidly expanding area of exposed CNT surface. This solvation entropy penalty can increase the Gibbs Free Energy of mixing $\Delta_{\text{mix}}G$ substantially, the more so the better the CNTs are dispersed since their available surface area increases with dispersion quality. NMP, in contrast, is thought not to adsorb in an ordered fashion on CNTs [43].

Tab. 4.3: Influences of the structural features of LCs on the enthalpy of interaction with CNTs and promotion (+) or counteraction (-) of ordered adsorption onto the CNT sidewall from general considerations of the physical chemistry, literature and the experimental results outlined in the previous subchapter. See text for details.

Structural feature	Enthalpy reduction	Ordered adsorption
permanent dipole	(+)	(+)
π -System		
planar	+++	++
twisted	++	-
saturated ring system	+	--
alkyl chain	+	+
lone electron pair	+++	(-)
CT complex	+++	(+)

In order to understand the varying performance of the different LCs the different structural properties and how they influence the enthalpy of the CNT/LC interactions and the ordered adsorption of a LC molecule have to be considered (Tab. 4.3).

Among the LCs investigated in our study 6T7 was clearly the poorest CNT solvent. It displayed only intermediate performance in the early stage sonication experiment (Fig. 4.12) and in the post-sonication centrifugation test (Fig. 4.13) it performed by far the worst. Obviously, an extended aromatic core such as the tolane in 6T7 does not on its own make a mesogen a good CNT solvent. 6T7 was synthesized in particular to promote π - π stacking interactions. The tolane core of 6T7 allows a planar conformation and thus a complete conjugation of the π -electron system thereby maximizing the polarizability of the molecule and maximizing the London and Debye forces between the LC and the CNT. However, it can be reasoned that the promoted π - π stacking leads to a considerable fixation of the molecule onto the CNT sidewall, even more so as it also possesses two rather long alkyl chains causing a great loss in configurational entropy. Overall it seems that the beneficial enthalpic interaction gets completely negated by the strong adsorption, making 6T7 the poorest choice for CNT dispersion.

The two next better LCs 5CB and 7CB both also possess a polarizable π -electron system, however the hydrogen atoms on the two adjacent phenyl rings force the molecule into a twisted conformation, counteracting ordered adsorption. Furthermore both LCs possess a rather high dipole moment promoting the Debye forces between the LC and CNT. Also a possible charge transfer interaction involving the cyano-substituted phenyl ring can be postulated due to the cyano group being an electron acceptor. Even a lone electron pair is part of the structure. In order to understand why these LCs are still not particularly good CNT dispersion hosts one has to consider different factors. While indeed the high dipole moment should promote the Debye forces it furthermore promotes the Keesom forces between the LC molecules. The relatively strong interaction between the permanent dipoles is reflected in the fact that these cyanobiphenyls tend to organize themselves into antiparallel dimers. When such a dimer comes into contact with a CNT the effective interaction is thus closer to the much weaker London forces since the permanent molecular dipoles compensate each other within the mesogen dimer. In a similar way that protic solvents expel the non-hydrogen-bonding CNTs, solvent molecules with high permanent dipoles prefer “to stay among themselves”. This hypothesis gets an even stronger basis when considering that the best performing pure LC, MBBA, only shows a medium dipole moment and it is known that the dispersive London forces play the major role in its phase organization [162]. Taking into account that 6T7 with its poor performance exhibits a very weak dipole moment it seems a reasonable assumption

that increasing the mesogen dipole moment leads to a trade-off situation where LC/CNT interactions are strengthened as well as LC/LC interactions. It can be assumed that a medium dipole moment is a structural feature promoting CNT-dissolution. For the possible electron-pair donor capabilities it should be said that due to the preferred orientation of the LC molecules along the tube axis [159], especially in a nematic phase, the cyano electron pair simply is not accessible for interaction. Furthermore, its donor capability would be limited due to its *sp*-character.

Turning to the two next best pure LC hosts, PCH5 and PCH7, with the preceding considerations in mind, the counteracting of an ordered adsorption due to the cyclohexane ring can readily be identified as a key component for their better performance. The longer-chain homologue performed distinctly better among the two. This difference indicates that additional to π - π -stacking interaction the adsorption of the alkyl chain onto the CNT surface plays a role in the mesogen-nanotube interaction, improving the dispersion stability for the longer-chain homologue. In contrast, however, the two cyanobiphenyl homologues 5- and 7CB showed almost no difference, the longer-chain homologues possibly being slightly worse. Although more homologues would need to be investigated to draw clear-cut conclusions, the apparently different chain length dependence between the *n*CB and PCH*n* series may be related to the different linkages between core and tail. The sp^3 link between tail and cyclohexane in PCH*n* extends the chain along the core axis, whereas the sp^2 link between tail and phenyl ring in *n*CB prevents a collinear tail extension along the core (see Tab. 4.1), a geometrical difference that must influence the interaction with the CNT surface. Moreover, the different linkages lead to greater tail flexibility in *n*CB than in PCH*n*, rendering the entropic cost of strong tail adsorption to a CNT surface (expected in particular for longer chains) more severe for the former mesogen series.

The very best pure host liquid in terms of CNT dispersion stability upon centrifugation (Fig. 4.13) is MBBA. When considering what distinguishes this LC from all the others already a quick look with the naked eye at an MBBA sample reveals a striking difference: while all other LCs are uncolored, MBBA is yellow. This reflects different electronic properties as compared to the other LCs used, giving rise to $n\pi^*$ and $\pi\pi^*$ optical transitions [163]. Furthermore we may identify the polar C=N bond at the center of the core with its lone electron pair as a possible key element. The lone electron pair at the nitrogen atom very likely constitutes the HOMO of the MBBA molecule. Unlike for the cyano groups of the other LCs the sp^2 electron pair of MBBA may be accessible for interaction with the CNTs even when the LC molecule is oriented along the tube axis. Furthermore Schiff's bases in general and the

benzylidenaniline core structure of MBBA are very well known to form CT-complexes with electron-accepting partners [164-166]. As already mentioned above, MBBA possesses a medium dipole moment promoting dipole-induced dipole interactions with the CNT all the while its phase organization still relies on the dispersive London forces between the molecules [162] making a possible expulsion of the CNTs due to strong Keesom forces improbable. In reality, what at first sight may look like an extended π -system is disrupted by a twisted conformation [163], inhibiting a strongly ordered adsorption due to π - π stacking. Following these considerations and interpreting the experimental results it can be concluded that, among all the tested pure LC substances, MBBA possesses by far the best balance of enthalpic and entropic contribution to the Gibbs free energy of mixing.

With E7 the fact that this is a four-component mixture gives an entropic benefit since different mixture components can adsorb onto one and the same CNT, counteracting 2D crystal formation and thus reducing the solvation entropy. The importance of the multiple constituents is further highlighted by the fact that the two main constituents of E7, 5CB (51 wt.-%) and 7CB (25 wt.-%), both performed rather poorly when used each on its own as CNT host. On the other hand, also ROTN is a mixture, yet the dispersion stability of CNTs upon centrifugation is substantially worse. Possibly the presence of a chiral dopant in ROTN, not present in any of the other LCs studied, may play a role for this result.

Summarizing the results of this discussion we can conclude that the main factor for good dispersion of CNTs in a thermotropic LC is the favorable enthalpic interaction coupled with the avoidance of a too great entropy penalty due to loss of configurational freedom caused by strong ordered adsorption of the LC molecules on the CNTs. Several structural features can be identified that promote this or that minimize the negative consequences:

- the LC phase in general
- non-planarity of the molecule
- interaction via **one** lone electron pair
- mixtures

A counteracting structural feature should accompany any adsorption-promoting one, e.g. a saturated cyclohexane ring should compensate the π - π stacking of a phenyl ring. An optimized dispersion technique of combined stirring and sonication steps while keeping the sample in the nematic phase is advisable.

4.3. Filament formation in carbon nanotube-doped lyotropic liquid crystals

As mentioned before composites of lyotropic LCs and CNTs are interesting for aligning carbon nanotubes. The liquid crystalline matrix transfers its order to CNTs dispersed in it, an outcome that can be readily confirmed by the polarizer effect shown by these composites if they are uniformly aligned by shear-flow. Yet these composites also show drastically altered and improved viscoelastic properties as long thin filaments can be drawn from them (Fig. 4.15). In these filaments the nanotubes are well aligned along the filament and have been shown to exhibit an order parameter of up to $S = 0.7$ [70]. This filament-forming behavior is of basic physicochemical interest and if understood the flexibility of filament drawing and deposition could be used in applications providing well-aligned CNTs on any substrate and any continuous deposition pattern imaginable.

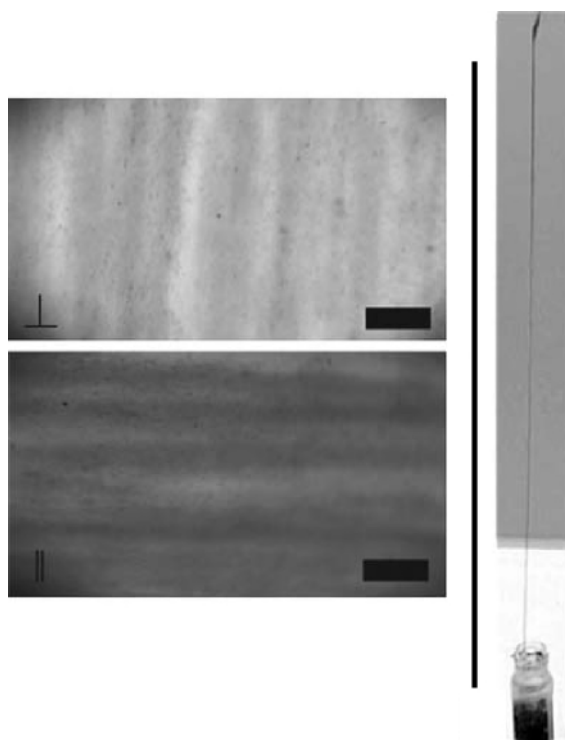


Fig. 4.15: Polarizer effect of a sample containing 2.5 mg/mL HiPCO nanotubes, scale bar = 100 μm (left,) and filament drawn out of the bulk sample (right) [167].

4.3.1. Understanding the filament formation process

This chapter explores the properties of the composites formed by CNTs in lyotropic LCs, mainly focusing on the viscoelastic behavior and the tendency towards filament formation shown by these composites (Fig. 4.15). Most experiments shown here were conducted using aqueous CTAB-solutions as LC host phase for the SDBS-dispersed CNTs. The composites were produced as outlined in chapter 4.1 by mixing an isotropic dispersion of CNTs in aqueous SDBS-solution with the amount of CTAB to form the desired LC host phase followed by a sonication step until the polarizer effect could be seen.

The first fundamental observation in researching these composites is that without CNTs the pure LC phase shows no tendency of forming filaments whatsoever. The same is true for composites of the same CTAB-based LC phase with SDBS-stabilized C_{60} fullerenes instead of CNTs. For lyotropic LC/CNT composites to form filaments the CNTs furthermore have to be present above a critical concentration threshold c_T and in good more or less individual dispersion. This threshold was established for HiPCO-CNTs to be between 0.5 mg/mL and 1 mg/mL. While the threshold was not quantitatively measured for other CNT types it was shown that all different types of CNTs available for this study induced filament-formation in the lyotropic LC at the standard concentration of 2.5 mg/mL, regardless of the different lengths, diameters or whether they were multi- or single-walled. Below the threshold of 0.5 mg/mL the HiPCO-composites did not form filaments while in the lower part of the established range short (centimeters), unstable filaments can be formed. Above 1 mg/mL it becomes possible to easily draw long filaments at a speed on the order of 1m/s which will eventually break when the drawing stops or when not enough composite material remains on the drawing device, i.e. a metal spatula or Pasteur pipette, to support an ever growing filament.

As with the polarizer effect the dispersion quality plays a crucial role for the filament drawing process. Although the quality of the dispersion does not have to be as high as for seeing the composite acting as linear polarizer, a too coarse dispersion prohibits the filament formation. Despite the fact that filaments can be drawn from these mixtures even if the quality of the dispersion is somewhat inferior to that needed for the polarizer effect, all the samples were sonicated to such a state of better dispersion quality in order to ensure homogenous properties all over the samples.

Another imperative for filaments is found to be the liquid crystallinity of the host phase. Filaments cannot be drawn from the composite when the CTAB concentration is far below the threshold for rendering the host phase nematic. Only close to the isotropic/nematic threshold

concentration it was possible to draw filaments from samples, which were macroscopically isotropic in the bulk. However, it is well known, and was also confirmed by POM in this study, that mixtures close to the appearance of a steady-state nematic phase can undergo a shear-induced transition to the long-range ordered state [168] so that the filaments drawn out of these composite most certainly were nematic. At higher CTAB concentrations, corresponding to the development of a hexagonal phase, homogenization of the samples proved to be difficult due to the large amount of dry substance involved and the high viscosity of the resulting crude mixture. It was shown by X-ray scattering that composites with up to 32 wt%, thus deep in the hexagonal phase of the pure CTAB/water system, are still nematic when SDBS-stabilized CNTs of the quality used in this study were added [169]. While one could be tempted to attribute this effect to the nanotubes disturbing the hexagonal ordering this phase shift can also be seen by only adding the low amount of SDBS present in the composites to the pure phase. It is thus not necessarily caused primarily by the CNTs.

Despite the heavy loading with CNTs the mixture still flows, albeit slowly, and reacts to gravity within seconds if for example the vial containing it is turned upside down. A detailed analysis of the rheological properties of these compounds reveals that the CNT loading has a distinct impact on the shear viscosity of the system (Fig 4.16). The pure liquid crystal phase shows an expected shear thinning transition [170] from a high shear viscosity regime to a low shear viscosity regime at a critical shear rate of about 1 s^{-1} which can be explained by the alignment of the director \mathbf{n} of the nematic phase along the shear flow and the resulting lesser interaction and entanglement of the wormlike micelles. By adding only a small amount of CNTs of 0.05 mg/mL the transition behavior disappears and the data now falls solely in the low viscosity regime with a slightly higher viscosity than the pure sample only at shear rates around 100 s^{-1} . A further doubling of the CNT concentration leads to a generally decreased viscosity at all shear rates but the highest, without any transition behavior. Further increasing the CNT concentration to 0.25 mg/mL again increases the shear viscosity to the values of the 0.05 mg/mL sample, still with no transition behavior identifiable.

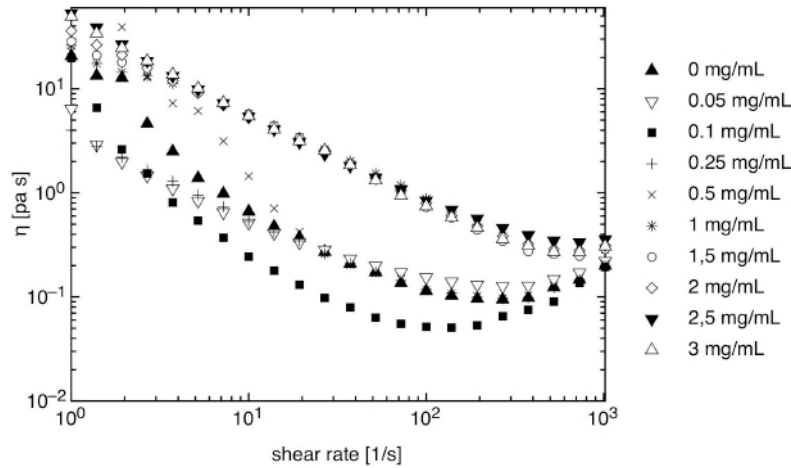


Fig. 4.16: Shear viscosity of HiPCO CNT/LC composites with aqueous CTAB as host phase as a function of shear rate and CNT concentration.

The behavior changes when the CNT concentration reaches 0.5 mg/mL, the concentration at which the first signs of filament forming behavior can be observed. Here a clear cross-over from a high viscosity regime at low shear rates to a system with low shear viscosity can be found at a critical shear rate of about 10 s^{-1} . Further increase of CNT content above the critical threshold for the filament formation yields a viscosity dependence that is basically identical at all investigated higher concentrations (up to 2.5 mg/mL) and only at very low shear rates a slight concentration dependence can be found showing higher viscosity for higher CNT content. A transition behavior cannot be found in these above c_T samples which all fall in the high viscosity regime regardless of shear rate. Moreover, whereas a minimum was found at shear rates around 100 s^{-1} at all lower concentrations there is a monotonic decrease in viscosity up to about 1000 s^{-1} for $c \geq 1 \text{ mg/mL}$.

Obviously, the threshold seen at c_T for filament drawing corresponds to a transition to a new type of behavior in terms of the rheological properties. As mentioned before filaments can be drawn from composites indifferently of CNT type, a behavior that is also reflected in the shear viscosity data. The viscosity curves show little to no difference upon varying the CNT type (Fig. 4.17).

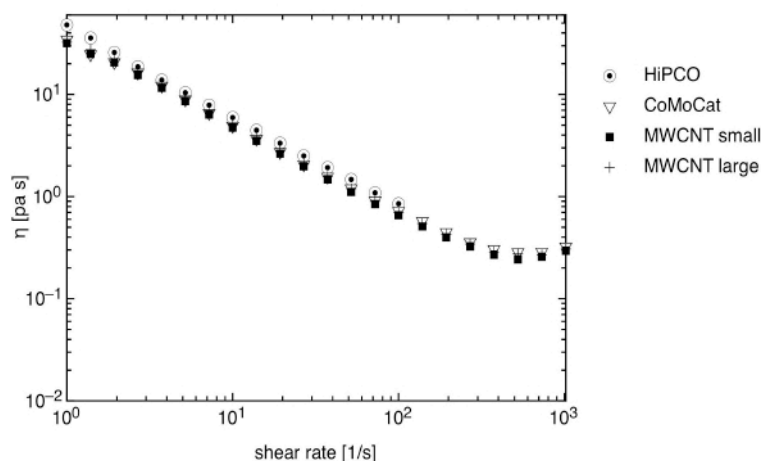


Fig. 4.17: Shear viscosity of HiPCO CNT/LC composites with aqueous CTAB as host phase as a function of shear rate and CNT concentration (top) and shear viscosity of CNT/LC composite as a function of shear rate and CNT-type (bottom). The concentration of the host phase is in all cases 28 wt% CTAB.

Interestingly this uniformity of shear viscosity is also shown upon varying the concentration of the host phase (Fig. 4.18). Even though no filaments can be drawn from mixtures with a content of 20 wt% of CTAB loaded with 2.5 mg/mL HiPCO, a mixture that is well in the isotropic phase and where obviously no polarizer effect can be seen, the shear viscosity is almost identical to that of a 30 wt% CTAB sample which is loaded with CNTs at the same concentration. It is important to realize that this CTAB concentration, in the pure system, would show a hexagonal phase, with diverging viscosity, as shown in Fig. 4.18.

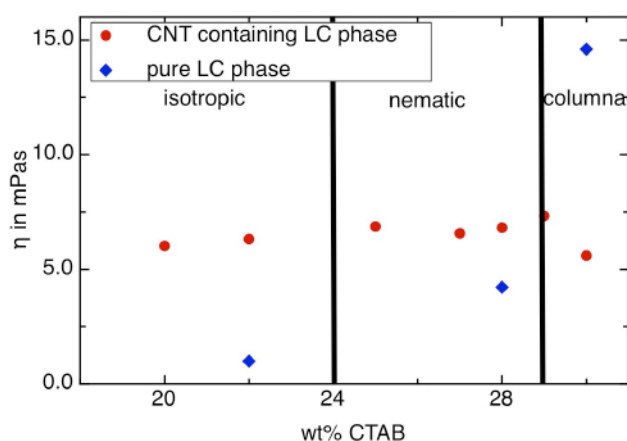


Fig. 4.18: Shear viscosity of 2.5 mg/mL HiPCO-CNTs containing compounds and CNT free phases at a shear rate of 10 s^{-1} . The phase notation refers to the CNT-free system.

The entirety of the observations described above suggests that if elongational flow is applied to a lyotropic liquid crystalline phase with sufficient content of well-dispersed CNTs an extended linear structure is formed that can support a filament drawn out of such a composite. This can be understood by considering it as a case of supramolecular polymerization

[171,172]. If long and stiff rod micelles are subjected to elongational or shear stress they orient along the flow. A theoretical treatment of this situation suggests that if the micelles are sufficiently long and stiff the promotion of orientational order through the stress results in a further linear growth of the micelles, which in turn causes an even higher orientational order. A positive feedback loop arises, that, under the right conditions leads to a divergence of the rod length and a very high degree of orientational order [171].

In the system of a composite of CNTs in a lyotropic LC the „monomers“ of this supramolecular polymerization are the rodlike micelles of the LC host phase, in our case CTAB micelles whose growth in length and fusion with neighboring micelles is the mechanism of the polymerization [172]. The CNTs are needed to give the micelles a sufficient length and stiffness, a situation, which has been, confirmed through cryo electron microscopy investigations by Regev and co-workers [173,174] for CTAB micelles in the vicinity of carbon nanotubes. The role of the nematic host phase is to provide a quadrupolar ordering field that was recognized by van der Schoot as a key factor in the divergence of the effective chain length [171].

An alternative explanation of a depletion attraction driven linear aggregation of the CNTs in the anisotropic LC phase [92,93] can be ruled out by the fact that similarly produced composites of C₆₀-fullerene in a CTAB-host phase do not show filament forming behavior. As the anisotropic depletion attraction does not require anisometric particles but only an anisotropic phase [175] one should expect C₆₀-containing composites to show a similar behavior as the CNT-composites if the depletion attraction were the primary cause. However it is likely a secondary factor as will be shown below.

The distinct threshold on the viscoelastic properties seen for the filament formation and in the shear viscosity investigations suggests that this phenomenon can be described as a percolation transition, i.e. the establishment of macroscopic connectivity when the nanotube concentration reaches a certain minimum value. Turner and Gates [172] explicitly identify the supramolecular polymerization resulting from the micelle growth and fusion as a form of gelation, a phenomenon that can be classified as an example of percolation. In our case the percolation threshold is between 0.5 and 1 mg/mL CNT concentration, which translates into volume fractions of 0.0004 to 0.0007 (calculated with an average CNT density of 1.35 g/cm³).

This percolation threshold is exceptionally low compared to gelation effects of CNTs in isotropic solution – CNTs form physical gels at concentrations above a rigidity percolation threshold of around 0.0026 of volume fraction [176] – and it is even one magnitude below examples of electrical percolation [91]. An explanation for this lies in the details of the percolation mechanism and the „monomers“ of the supramolecular polymerization and their inter-

actions with each other. The interplay of micelles, and CNTs being in an anisotropic phase under shear or elongational flow renders this percolation phenomenon significantly more complex than the situations where CNTs suspended in isotropic liquid hosts, as will now be explained.

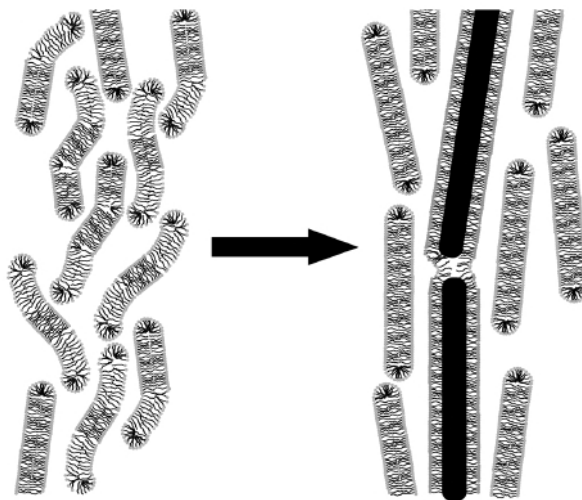


Fig. 4.19: Schematic depiction of the stiffening of lyotropic LC micelles by the addition of CNTs

The addition of the nanotubes to the lyotropic phase does not cause large-scale gelation but only causes a stiffening of the micelles in the direct vicinity of the CNT (Fig. 4.19). At low concentrations this causes a decrease in micelle entanglements and a promotion of the phase's shear-alignment behavior leading to an even lower shear viscosity than that of the pure LC phase. Under shear the CNT-stiffened micelles align and grow in length by fusing with other surrounding micelles. However this can only develop into a supramolecular polymerization mechanism when the phase is sufficiently loaded with CNTs. Only if both fusing micelles contain or are in the vicinity of a CNT the growing micelles retain sufficient rigidity for increasing the orientational order and thus setting in motion the above mentioned feedback loop (fusing micelles diverge in length, leading to increased orientational order, and so on). At too low CNT concentrations CNT-stiffened micelles may fuse with a micelle that contains no CNT, thereby reducing the rigidity of the fused associate and thus breaking the feedback loop. Only if the nanotubes are present at such a high concentration that they can link into an essentially quasi-infinite linear chain, i.e. sufficient to ensure macroscopic connectivity, can they provide the required micelle stiffening throughout the length divergence process. The minimum concentration for the chains to reach arbitrary lengths defines the percolation threshold for the filament formation.

While the viscosity behavior under shear flow may give hints as to when a certain compound also shows filament-forming behavior, the right viscoelastic behavior cannot be the

only criterion, since CNT-containing isotropic mixtures that do not form filaments nor exhibit a polarizer effect show shear viscosity behavior that is largely similar to that of the CNT-containing LC-phases. It seems that the data that can be assessed by shear viscosity measurements under increasing CNT-loading is mainly due to interactions between CNT-containing micelles, which dominate the compound's behavior through a promotion of shear-thinning due to micelle stiffening, accompanied by a general increase of viscosity into the high-viscosity regime by the simple addition of solid particles to the system. For such behavior there only need to be micelles and CNTs at high enough concentration, and these components are also present in isotropic phases. For the polarizer effect and the filament formation additional predicaments have to be met. In the most part these predicaments are about the occurrence of a quadrupolar ordering field, which causes the feedback loop of the supramolecular polymerization. The vital components of this field are the liquid crystallinity of the system promoted by ordering effects of the CNTs on the one hand and the elongational flow in the filament drawing process on the other hand, which has a higher ordering effect on the phase and its components than simple shear flow. Both effects work together to provide a sufficiently high ordering field to enable the filament extraction.

The ordering effect that the CNTs exhibit on the phase or more precisely the surrounding micelles can also be verified by considering that, as mentioned above, the pure LC-phase with the small addition of SDBS that is also present in the CNT-containing compounds effectively suppresses the occurrence of a hexagonal phase well above 30 wt% of CTAB. Yet in former studies it was shown that CNT/LC-composites of this composition indeed show a hexagonal phase [70]. The difference of these studies is only in the seemingly small detail of the CNT purity, which was as high as 99% in the older works while it is only 85% in the current study. The small additional amount of CNTs in the former studies and the absence of impurities apparently resulted in the effective stabilization of an ordered hexagonal phase even though it should be suppressed in the catanionic mixture of the host phase.

The exceptionally low percolation threshold of this phenomenon is intriguing. In general CNTs should show the lowest percolation threshold in a completely unaligned state [90,93]. Yet this is different in the case of “sticky” tubes [92]. If the nanotubes attract each other the percolation threshold can be strongly affected. Depletion attraction forces leads to a “stickiness” of the CNTs that strongly reduces the percolation threshold. Moreover this effect gets promoted by the anisotropic phase, which also renders depletion attraction forces anisotropic leading to a promoted self-assembly into chains of the CNTs. Along with the polymerization

mechanism based on increasing orientational order of fusing micelles the low percolation threshold can thus be understood.

Macroscopically the described polymerization mechanism results in a strong increase of the elongational viscosity allowing the extraction of filaments of the composite, meaning that with applied elongational stress the composite behaves more as an elastic solid than a liquid, which is its state at low shear/elongational stress. This also explains the breaking of the filaments as soon as the drawing stops as the relatively solid filament becomes liquid again. It can be considered as an analogue to a coil-stretch transition known from polymer solutions. At low stresses dissolved polymers typically have a coiled conformation. If they are subjected to shear or elongational flow the coil disentangles and the polymer chain is stretched out thereby reducing the shear viscosity of the system. However, while the shear viscosity decreases upon stretching the elongational viscosity shows a steep increase, because the stress is along the stretched polymer chain [177]. This results in filamentous behavior, which is possible at very low polymer concentrations [178].

In our case the coils are replaced by the CNT/micelle “monomers” that when subjected to elongational flow form a stretched out chain and hence increase the elongational viscosity of the compound to such magnitudes that make filament extraction possible. The highly increased elongational viscosity stems from the fact that one is practically pulling at a CNT chain, albeit connected by weak links. The mechanical strength of the CNTs to some extent gets transferred to the lyotropic LC in which they are dispersed.

4.3.2. Application of LC/CNT-filaments

The filaments formed by lyotropic LC/CNT composites have a considerable application potential as they make it possible to transfer aligned CNTs on any given substrate in any imaginable continuous deposition pattern. Should this property be able to be made compatible with modern industrial production techniques it might hold a new approach in the application of CNTs. In order to explore these possibilities some deposition procedures were investigated. A “writing” device was developed that allows the controlled and continuous dispensing of a lyotropic LC/CNT composite using a microfluidic device [116]. The compound was pumped out of a supply vial by the use of pressurized air through a tube system with a tapered capillary attached at the end. Using this device it was possible to write thin lines of LC/CNT composite on substrates of our choice (Fig. 4.20 left).

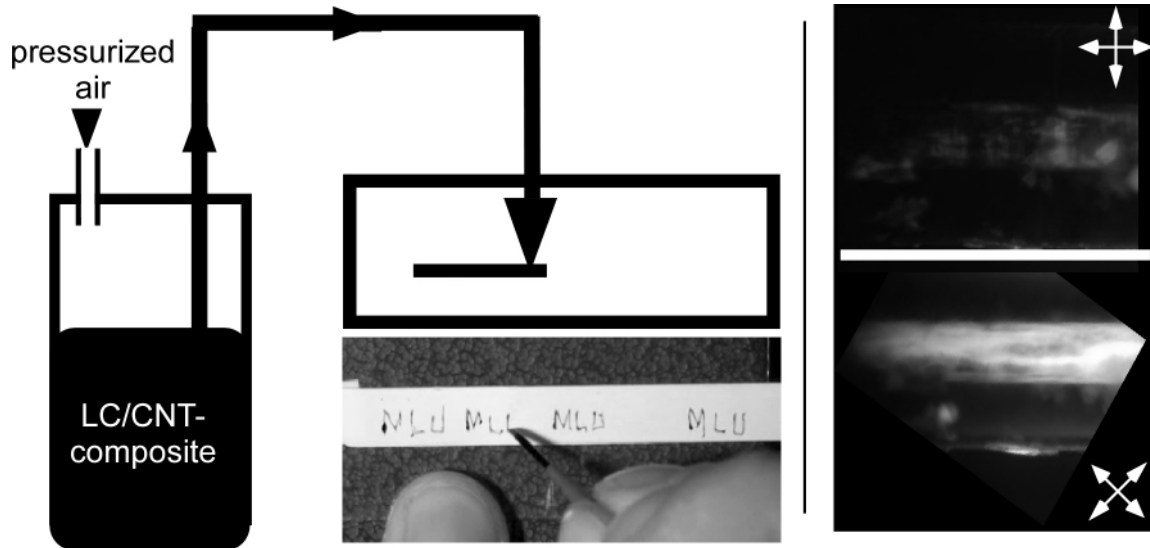


Fig. 4.20: Schematic depiction of the writing device and picture of the writing of the letters MLU (Martin-Luther-University) on Teflon tape (left), microscopic image of flow aligned LC in capillary of writing device (right, white arrows indicate orientations of polarizers).

While being pumped through the tube system the LC/CNT-composite fluid gets aligned along the flow direction as verified by POM (Fig. 4.20 right) and to some extent it retains this alignment after deposition. The compound gets aligned along the flowing direction in the capillary, yet upon dispensing it is immobilized on the substrate surface. The speed of writing is important in order to apply an elongational stress to the written lines, which improves the alignment since only upon application of elongational stress the filaments with highly aligned CNTs form. In general longer lines drawn faster show better alignment than short lines drawn slowly since in the latter case the elongational stress is less pronounced.

Another factor is the substrate used and the subsequent washing step, needed in order to dissolve the LC matrix since in possible applications the CNTs are generally desired without surfactant. This washing step is in fact the most crucial step since the CNTs are very easily washed away. For this matter glass substrates are the least effective. The CNTs are not sufficiently fixed to the polar glass surface and they are easily washed away, destroying any deposited structure. Teflon band proved more effective than glass even though it is famous for its non-stickiness. The reason for this seems to be the small dent in the substrate surface produced when the capillary pen presses on it, hence the composite gets partially embedded into the teflon. However, the most effective substrate investigated was double-sided scotch tape. This could hold most of the CNT-material even after a 16 hour washing step of carefully submerging the samples into a water bath.

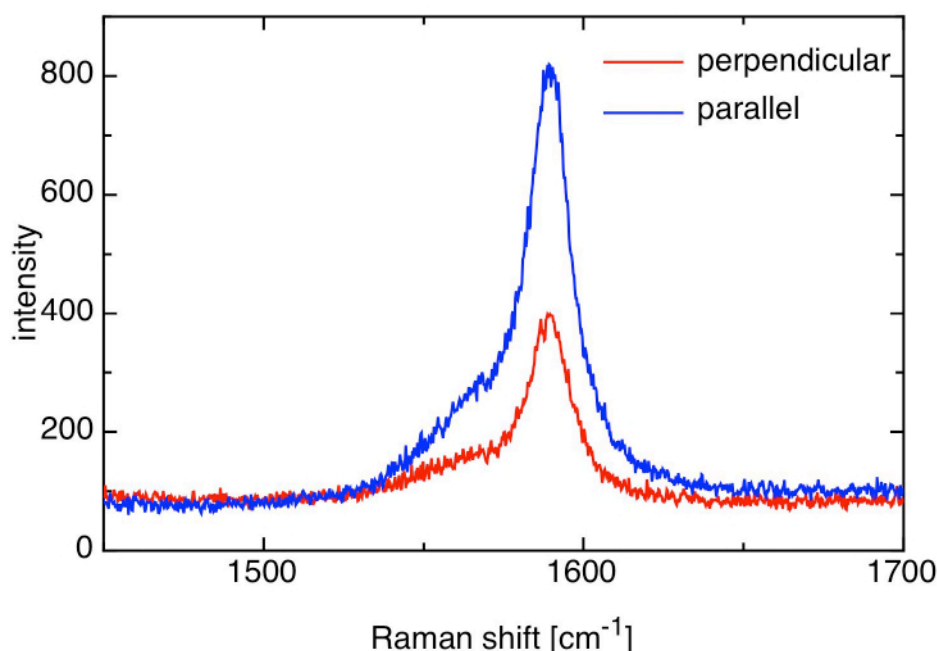


Fig. 4.21: Spectra of the G-Band of the CNTs with the polarization of the incident light being perpendicular and parallel, respectively, to the written CNT-lines, confirming the CNT alignment in the written CNT-lines. The ratio of the peak-areas is 1:2 which translates into an order parameter of about $S=0.25$.

The written CNTs gained by this method prove to retain some alignment, although the alignment as verified by Raman spectroscopy is not very good with a maximum order parameter on the order of $S = 0.25$ being achieved at some points of a sample (Fig. 4.21). Other parts showed almost no alignment.

In order to improve and further develop the dispensing technique a commercial programmable glue dispenser was used to deposit LC/CNT composites on substrates (Fig. 4.22 left). In accordance with the issue of the writing speed in the aforementioned manual method the

simple continuous pumping of a composite onto a substrate is not suitable to produce aligned CNTs as only a thick unaligned blob of LC/CNT composite is achieved. Controlled filament deposition can however be achieved by tuning the process. The dispenser works in the way that it can be programmed to dispense at certain points of the substrate for a certain time. For this it moves to the preprogrammed point and lowers the dispensing needle to the substrate and dispenses the compound for the programmed time. After that it retracts from the surface and moves to the next point.

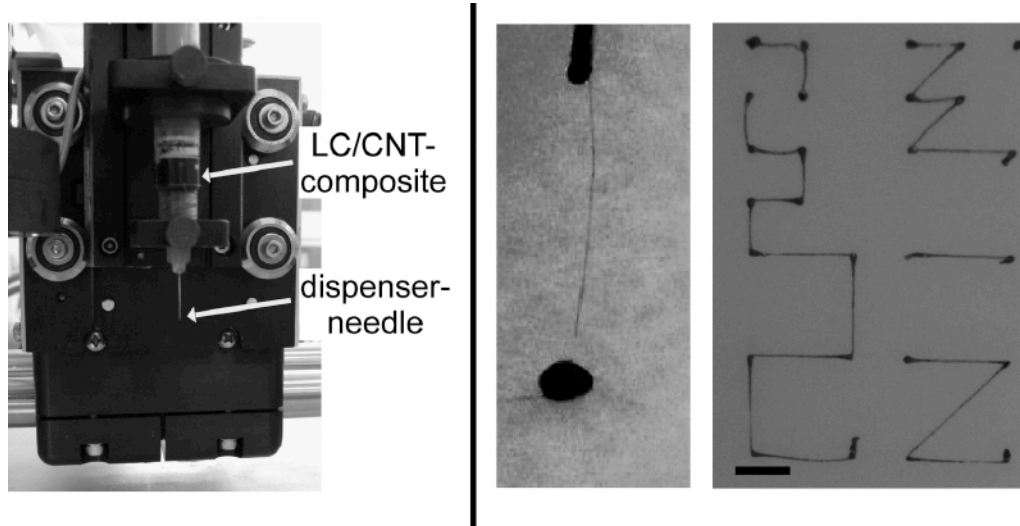


Fig. 4.22: Photo of the glue dispensing system (left), filament drawn from dispensed lyotropic LC/CNT droplet as the dispenser needle detracts from the surface (middle) and pattern of deposited LC/CNT composite filaments, scale bar: 5 mm (right)

After having dispensed a droplet of filament-forming LC/CNT mixture on the substrate, when the needles retracts, a filament is formed that is deposited on the substrate as the needle moves to the next point (Fig. 4.22 right). By using this mechanism it is possible to deposit filaments in structures of straight lines with widths on the order of tens of microns and easily several centimeters in length on any given substrate. The CNTs in such filaments have previously been shown to exhibit an order parameter up to $S = 0.6$ [70]. However as with the first writing technique the consequent washing step still needs to be improved since also many of the deposited CNTs are removed in the washing procedure.

A different approach to using the filaments that avoids the problematic washing step is to polymerize the system instead. First attempts of thermal polymerization of a LC/CNT composite from HiPCO-CNTs and CTAB following a procedure developed by Islam *et. al* [179] however did not produce satisfying results as the polymerization proved to be inhomogeneous and unspecific. The reason for this can probably be found in the different compositions of the compounds as Islam *et al.* did not follow a cationic approach and had a lower CNT concentration (0.1 mg/mL in contrast to 2.5 mg/mL). Even more than the different compositions the

lack of a good homogenization procedure obviously plays a role in the failure of this experiment. Since the polymerization is triggered by heat the composite has to be preformed before all the components needed to start a polymerization such as initiator and crosslinker, are added, since the production of the composites includes crucial steps, which must be performed at elevated temperatures. This however severely impairs the homogenous distribution of those components in the compound leading to inhomogeneous results.

A more promising procedure might be a UV-light initiated polymerization following published procedures [180-182]. This allows the selective triggering of the polymerization and the relatively unhindered production of homogenous compounds with all crucial components in good distribution. However, such polymerizations are greatly inhibited by the presence of oxygen [183]. First preliminary tests without nanotubes with the use of degassed water, polymerizable acrylate-modified CTAB, 1,6-hexanediol dimethacrylate as crosslinker and Irgacure 2958 as initiator, and with the dry mixtures carefully flushed with argon show promising results as a homogenous gel is formed. More research should be devoted to this topic in the future.

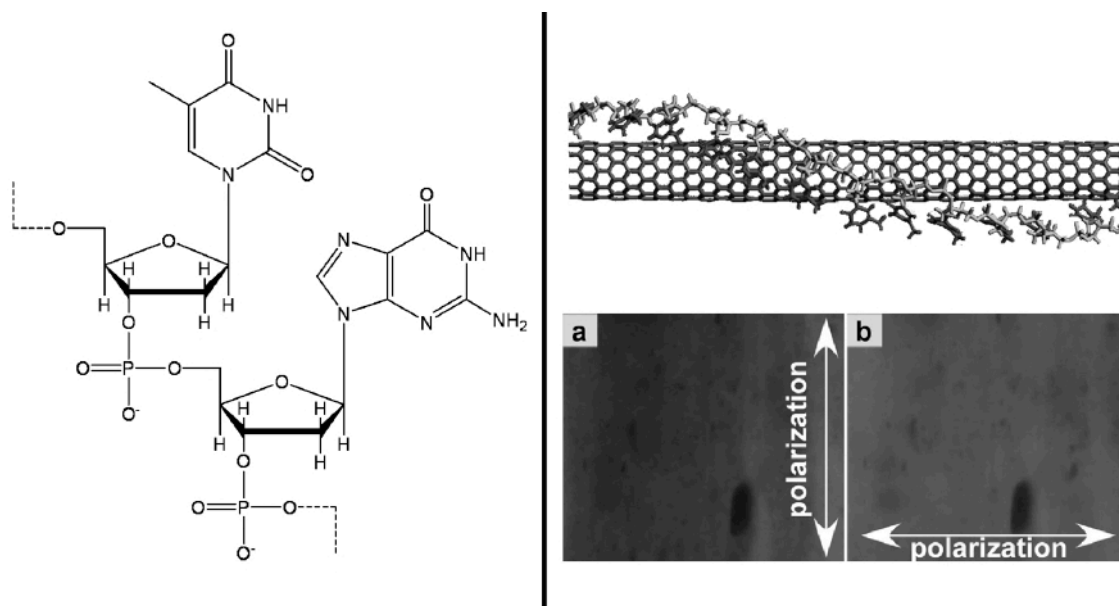


Fig. 4.23: Structure of d(GT)₁₀ single stranded DNA (left), scheme of DNA wrapping a CNT [39] and polarizer effect of an LC/CNT-composite produced with DNA as surfactant (2.5mg/mL HiPCO in 28 wt% CTAB) (right).

Especially interesting is the combination of the here discussed techniques with CNTs dispersed using DNA (Fig. 4.23 left) as a surfactant [184] since DNA holds the potential for separating CNTs in their different chiralities by chromatography [39]. As a proof of concept we produced a LC/CNT composite using single-stranded d(GT)₁₀-DNA as anionic CNT-stabilizer and CTAB as cationic LC-forming surfactant [116]. Even though the DNA compo-

sites proved to be of lower quality than the usual composites with SDBS, meaning more bundles and a polarizer effect with lower contrast, both the polarizer effect and the filament forming behavior could be seen in these compounds (Fig. 4.23 right). Combined with CNT fractionation techniques this holds the potential for application of unichiral, well dispersed and aligned CNTs thereby solving all the problems with CNT application outlined before.

4.4. CNT percolation in thermotropic LCs

In the field of CNT composites the percolation threshold of the CNTs, i.e. the minimum concentration at which the CNTs form a continuous network, is of much importance. This threshold defines the minimum concentration at which CNTs can render a material they are brought into conductive or give it a mechanical enhancement (note that the percolation threshold varies depending on which property is observed; electrical and mechanical percolation threshold are not the same). However, if the CNTs are brought into a thermotropic LC in order to enhance its display properties percolation of the CNTs and thus increased conductivity of the resulting compound have to be avoided.

In order to investigate the percolation characteristics of CNTs in thermotropic LCs the electrical conductivity σ of LC/CNT composites was measured in dependence of the HiPCO SWCNT concentration in E7 using a dielectric bridge and sample cells with well-defined electrode area and separation. Different original alignments of the LC were tested, planar and homeotropic, respectively and a frequency and DC-bias sweep were performed on each sample which was filled into standard LC cells composed of two glass slides coated with square indium tin oxide (ITO) electrodes. The electrodes are covered with an orientation layer for planar or homeotropic LC alignment.

In the absence of a DC-bias field no true percolation can be seen in the conductivity data (Fig. 4.24 top). All the samples show a similar behavior and only the sample with the highest CNT concentration shows a discernable difference, as the increase of the conductivity normally associated with the capacitor character of the cell occurs already at lower frequencies than in any of the other samples. This highest concentrated sample is probably very close to percolation, with CNT clusters present. The aggregates in the cell can act as an array of capacitors hence increasing the AC conductivity already at lower concentrations than for the other samples.

However, upon the application of a DC-bias of about 0.5 V/ μ m or greater a distinct percolation threshold can be observed for all sample categories at a CNT concentration between 3.6 and 9.4 μ g/mL (Fig. 4.24 bottom). For all sample categories the conductivity of samples above the percolation threshold concentration increases continuously with increasing DC-bias voltage, the slope being the greatest at low voltages but with no sign of saturation even at the maximum DC-bias applied during the experiment, 1.5 V/ μ m (Fig 4.25).

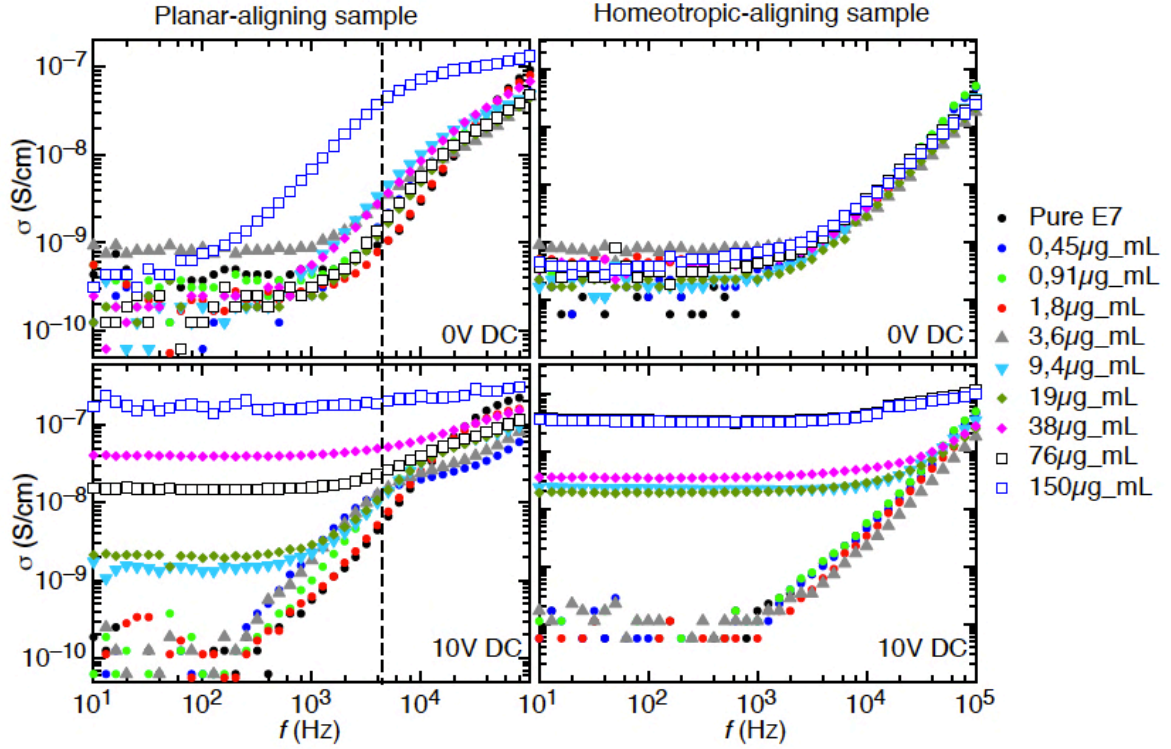


Fig. 4.24: Frequency dependence of the conductivity of thermotropic LC/CNT composites with varying CNT content in E7 in different aligning LC cells at different DC- bias in the nematic phase (cell thickness 10 μm).

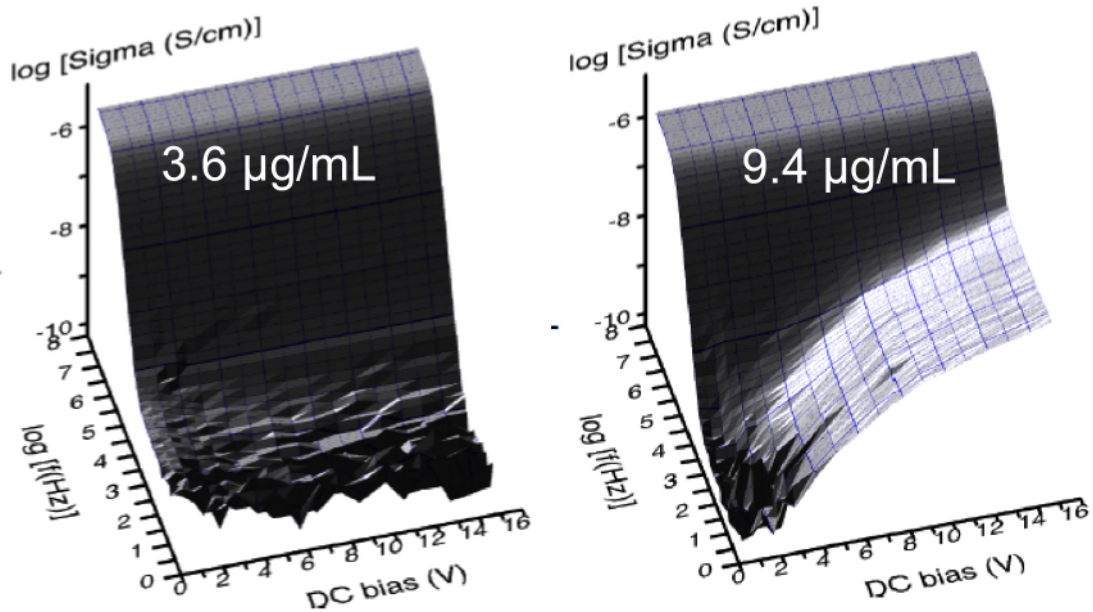


Fig. 4.25: Conductivity characteristic of LC/CNT composites below the percolation threshold (3.6 $\mu\text{g/mL}$ HiPCO CNTs in E7, left) and above the percolation threshold (9.4 $\mu\text{g/mL}$ HiPCO CNTs in E7, right), both in planar aligning cells.

From the diagrams one may get the impression that there is a voltage threshold for percolation to take place but it could be that the effect is essentially threshold-free, only at low voltages the induced conductivity is still much lower than the intrinsic conductivity of the sample, such that the contribution from the percolation network cannot be seen (Fig. 4.26).

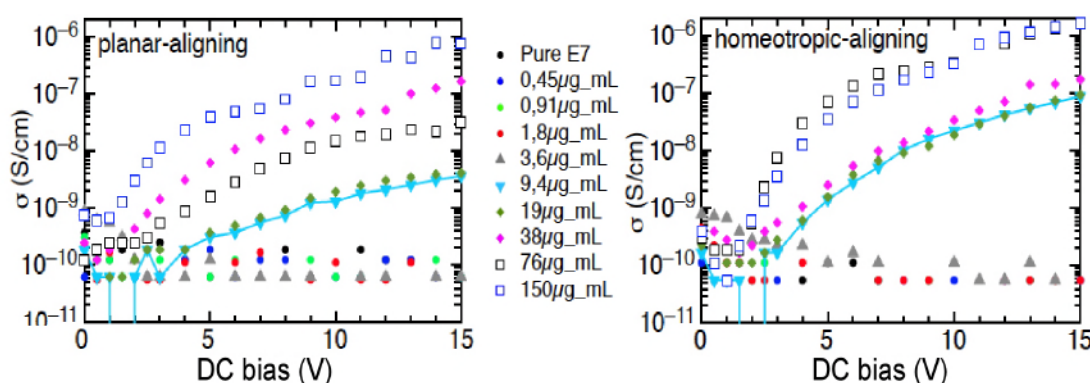


Fig. 4.26: Dependency of the conductivity on the DC-bias at a frequency of 100 Hz.

A dynamic percolation apparently process takes place under the influence of an electric field. In the electric field the CNTs are polarized, align along the field and attract each other to form a linear continuous network connecting the electrodes [185] (Fig. 4.27). With higher voltage the mutual attraction of the CNTs increases creating more and more stable conductive pathways as the counteracting Brownian motion gets more and more suppressed therefore increasing the overall conductivity of the sample.

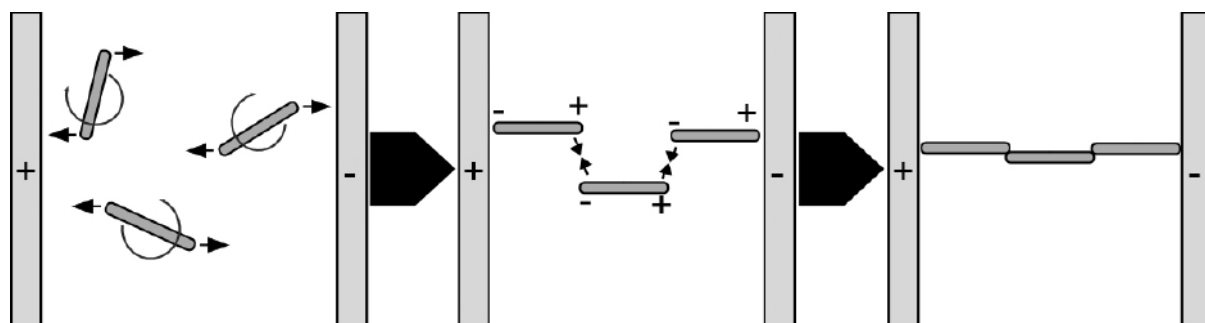


Fig. 4.27: Schematic depiction of the dynamic self-assembly of a continuous CNT network in the presence of an electric field. First the CNTs orient along the field, attract each other due to field-induced polarization and ultimately form a continuous conductive path through the cell.

There may also be a contribution to the voltage dependence of the conductivity from the fact that only 1/3 of the nanotubes in the used HiPCO SWCNT sample are intrinsically metallic, the rest being semiconducting. In order for a semiconducting tube to contribute to a percolation network it must be subjected to a voltage above its threshold voltage along the nanotube. With the natural variety of tube types in the sample used, not only do 2/3 of the tubes require a voltage to start conducting, but the threshold voltage of these tubes also varies from tube to tube. Thus, as the voltage is increased a greater and greater fraction of the tubes in the sample become conducting, contributing to the electric percolation network and thus increasing the conductivity.

The percolation threshold lies in between 3.6 $\mu\text{g/mL}$ and 9.4 $\mu\text{g/mL}$ for all the sample categories, irrespective of the original orientation. One might assume that the anisotropic nature of the LC works as a template for an emerging network, thereby influencing the percolation threshold. However, the percolation threshold stays the same even for samples heated into the isotropic state, indicating that the LC phase plays only a secondary role in the assembly of the network (Fig 4.28). One may contemplate that the presence of the CNTs and their tendency to align along the field may promote the long-range order and thus shift the phase transition temperature upwards, such that the sample under field application is in fact nematic after all. A future experiment in a sample cell with in-plane electrodes could test for this possibility.

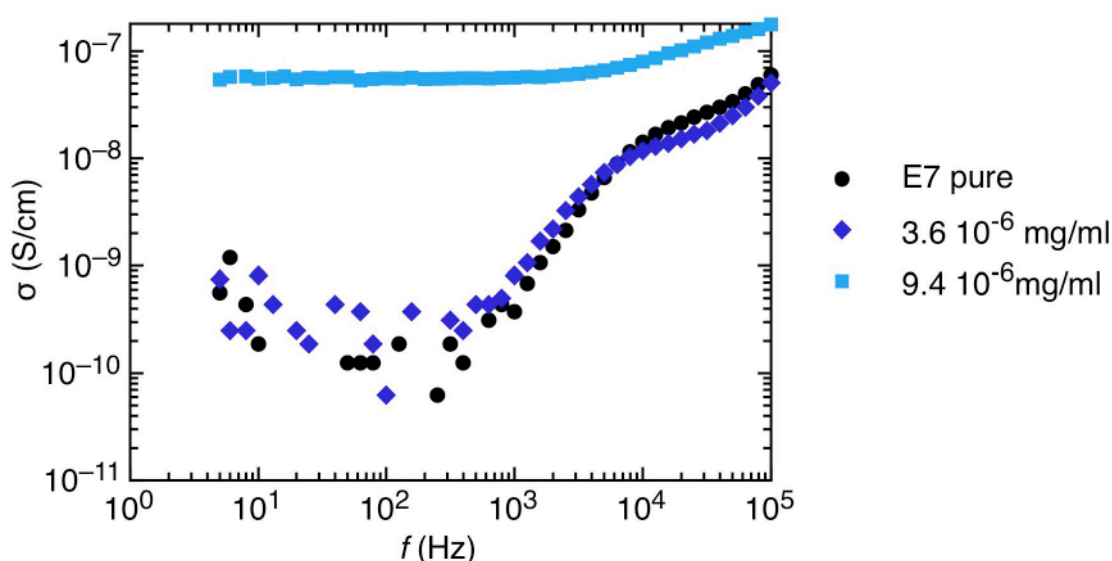


Fig. 4.28: Conductivity measurements of samples in the isotropic phase (at 70 °C, in cells with planar aligning orientation layer) at 10 V DC bias reveal the same percolation threshold as in the nematic phase.

For the samples close to the percolation threshold the field-induced conductivity values are distinctly higher for the initially homeotropic sample (about an order of magnitude difference at 10V at 9.4 $\mu\text{g/mL}$) but the difference gets smaller with increasing nanotube concentration, being negligible at about 50 $\mu\text{g/mL}$ or more. One might tenuously interpret this as showing that the orientational ordering imposed by the LC host onto the CNT guests is important for the conductivity of the network, increasing it for an initially homeotropic aligned host in contrast to decreasing it for initially planar alignment. This seems reasonable, considering that even above the Frederiks threshold – the voltage above which the LC aligns itself along the electric field (about 2 V for E7), the principle of any LCD – the director actually never switches close to the surfaces. A persistent planar alignment at the surfaces might pose a hindrance to the network formation and the forming of a conductive path.

However, while the qualitative behavior is similar and reproducible for any original LC alignment and also in the isotropic phase, a quantitative interpretation of the conductivity data should be taken with care, since aggregation in the sample (especially when heated in the isotropic phase), insecurities with contacting the cells and a general “individuality” of the cells renders interpretations beyond the percolation threshold highly unconfident.

The percolation threshold we obtained for this field induced percolation case is qualitatively similar but quantitatively almost an order of magnitude lower compared to published data concerning the dynamic field-induced percolation of HiPCO SWCNTs in chloroform [94]. In fact Lima et al. report a percolation threshold of 25 $\mu\text{g/mL}$ with continuous sonication during the measurement to keep the CNTs in good dispersion, as a large-scale aggregation would severely disturb the formation of a continuous linear network. In light of this the LC mixture E7 furthermore proves its exceptional properties as a CNT host system, at least when not heated in the isotropic phase as reproducibility is poor as soon as samples were once heated into the isotropic. A more successful way of obtaining quantitatively reproducible data might be to dilute the LC host with a small amount of an isotropic solvent with good CNT dispersion capacity, e.g. NMP, such that the phase becomes isotropic at room temperature. This would also rule out any potential memory effect that might be present in the experiments carried out on LC samples heated to the isotropic phase; the slower rotational dynamics of the long CNTs might lead to a situation where CNT networks aligned by the LC at room temperature persist after heating to the isotropic state, possibly stabilized by CNT aggregation taking place with retained alignment.

In conclusion, the ability of a suitable thermotropic LC host to disperse CNTs allows a very low dynamic percolation threshold between 3.6 and 9.4 $\mu\text{g/mL}$. The dynamic percolation process itself is driven by the external field and while the LC alignment might play a role for the absolute value of the conductivity, for the principle of the matter it seems to play a secondary role, seeing that the percolation threshold is the same in the isotropic phase.

4.5. CNTs and fullerenes in chiral thermotropic LCs

The nanotube doping of chiral nematic liquid crystals follows the two general approaches for LC/CNT composites, aiming at the alignment of the CNTs by the LC or/and the tuning of the LC properties by CNT doping. In the case of chiral thermotropics this means CNTs could be aligned in periodic arrangements such as the short-pitch helical conformation of cholesteric phases or the complex structure of the blue phases, the latter potentially interesting for the production of metamaterials, i.e. artificial materials with unusual properties such as a negative refractive index. An example of the second approach is the influence on the phase behavior of the LC, where a particular interest lies in the stabilization of the blue phase. The potential of using these phases for display applications is very attractive, but it is difficult to realize due to the small natural temperature range of blue phases.

In order to investigate the influence of CNT-doping on chiral thermotropic LCs and vice versa, a mixture of 46 wt% cholesteryl nonanoate, 44 wt% cholesteryl oleyl carbonate and 10 wt% cholesteryl benzoate [186,187] was doped with 0.01 wt% of different types of carbon nanotubes. In addition, samples were prepared that were doped with C₆₀ fullerenes or with graphite powder as reference. We can regard C₆₀ as being the “smallest possible nanotube” and it can thus be seen as the extreme case of short CNTs. The first very apparent observation when doping cholesteric LCs with carbon particles is the enhanced brilliance of the selective reflection colors of bulk samples (Fig. 4.29), albeit less pronounced for the fullerene-doped samples due to the brownish color of C₆₀. CNT doping with amounts as small as 0.01 wt% causes a significant reduction of light scattering of the sample as the particles effectively absorb any transmitted light, such that the appearance of a doped LC sample is dominated by the selective reflection light, the color of which depends on the pitch of the cholesteric helix. Normally in the application of cholesteric LCs in for example temperature sensors the LCs is placed on a black background to minimize stray light and improve the brilliance of the colors. By doping the LCs with CNTs this background is incorporated in the LC, improving the result.

Interestingly the doping not only enhances the brilliance of the color but also changes the wavelength of selective reflection and therefore the pitch of the cholesteric helix at a given temperature (Fig. 4.29). The alteration of the pitch differs greatly between the different carbon species as can be seen by the different colors of the selective reflection at a given temperature (Fig. 4.30).

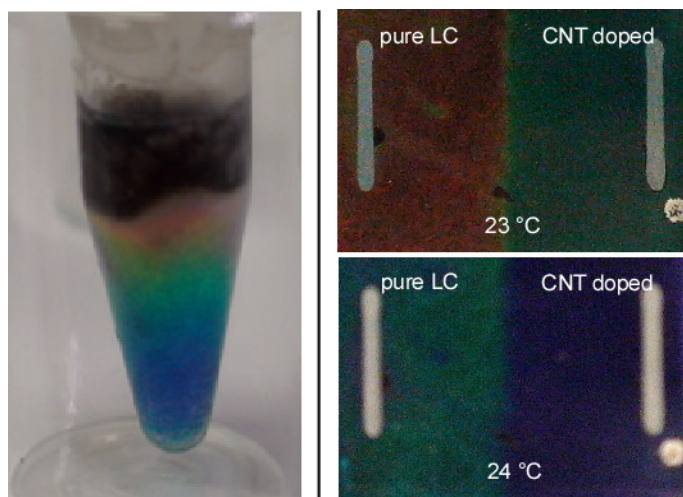


Fig. 4.29: Bulk sample of HiPCO SWCNT-doped cholesteric LC (cholesteryl ester mixture) showing selective reflection over the full visible color spectrum due to heating by hand warmth at the bottom of the vial (left) and contact sample of pure cholesteric LC (cholesteryl ester mixture) and a sample doped with 0.02 wt% CNTs at two different temperatures (right).

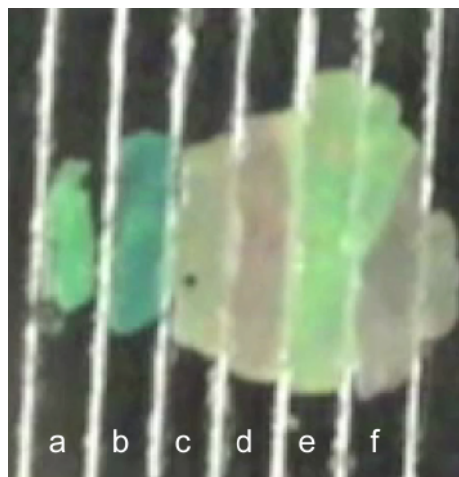


Fig. 4.30: Mixture of 46 wt% cholesteryl nonanoate, 44 wt% cholesteryl oleyl carbonate and 10 wt% cholesteryl benzoate (f) doped with 0.01 wt% of HiPCO SWCNTs (a), CoMoCat SWCNTs (b), MWCNTs (c), graphite (d) and C₆₀ (e) at 26°C.

Further investigation of the HiPCO and C₆₀-doped samples shows that the pitch or more accurately the wavelength of selective reflection λ_r (the helix pitch is obtained by dividing by the average refractive index, typically about 1.5) of the cholesteryl ester mixture decreased with the addition of either CNTs or C₆₀ at a certain temperature. In fact, the whole pitch-temperature dependence gets shifted to lower temperatures (Fig. 4.31). This behavior is more significant for C₆₀ as dopant than for the CNTs. It can be reasoned that this is due to the higher number of particles added for C₆₀ compared to the same mass of CNTs. If a hyperbolic function is fitted to the experimental data for the pitch vs. temperature behavior obtained with a sample series doped with varying amounts of HiPCO or C₆₀ we can obtain a temperature T_{NA} for a virtual N*/SmA* transition for the mixtures. As explained in chapter 2.1.1 the lay-

ered molecular arrangement of the SmA* phase is not compatible with the director helix, hence the pitch typically tends to infinity upon cooling towards an N*/SmA* transition. This virtual transition temperature turns out to be lowered by a shift ΔT_{NA} that is roughly proportional to the concentration of additive. Twice the amount of CNTs/C₆₀ doubles the reduction of the virtual N*/SmA* transition.

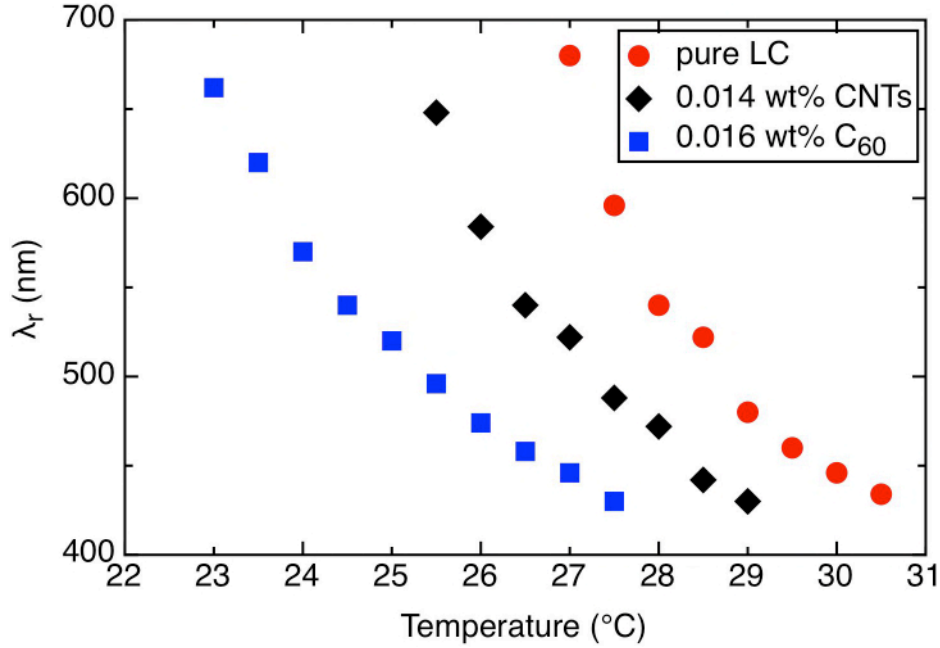


Fig. 4.31: Dependency of the wavelength of selective reflection λ_r on the temperature for the pure cholesteric mixture and for mixtures doped with HiPCO CNTs and C₆₀, respectively.

The shift of the pitch dependency is accompanied by a reduction of the melting temperature, that is also proportional to the concentration of additive, albeit smaller than the shift of the virtual N*/SmA* transition. Empirically we found the relation to be roughly:

$$\Delta T_{fus} \pm 0.1 \approx 0.38 \Delta T_{NA} \quad (4.6)$$

The proportionality between the concentration of dopant and the reduction of transition temperatures hint that the effects are of a colligative nature. Using an average melting enthalpy $\Delta_{fus}H$ calculated from the melting enthalpies of the three mesogenic mixture components:

$$\Delta_{fus}H = \sum_i x_i \cdot \Delta_{fus}H_i = 26.08 \text{ kJ/mol} \quad (4.7)$$

The reduction of the melting point ΔT_{fus} can be theoretically calculated using the known law:

$$\Delta T = \frac{RT_{fus}^0{}^2}{\Delta_{fus}H} m \quad (4.8)$$

where R is the universal gas constant, T_{fus}^0 the melting point of the pure LC mixture, $\Delta_{\text{fus}}H$ the melting enthalpy of the pure LC mixture, M the average molar mass of the LC mixture and m the molality of the dopant (mol carbon particle per g LC). The calculated values are smaller than the experimental data for both the melting point and the virtual N*/SmA* transition for C₆₀ doped LC mixtures (Fig. 4.32) which can most likely be explained by the fact that the theory of melting point reduction as outlined above is only valid for true solutions.

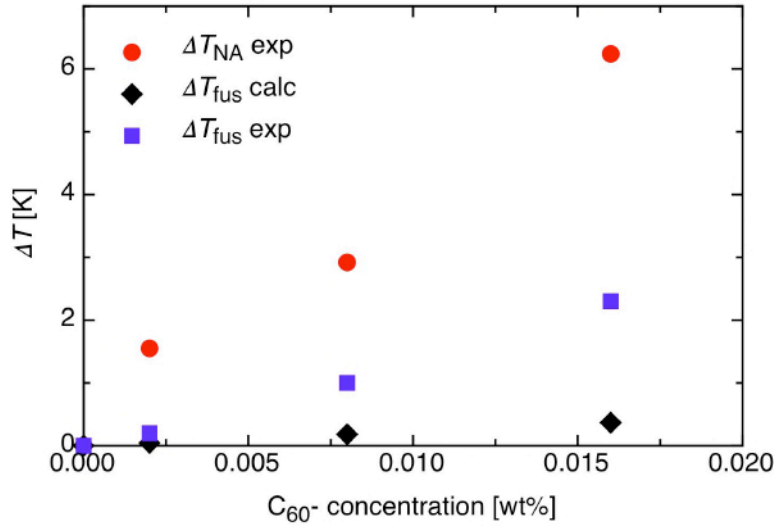


Fig. 4.32: Experimental and calculated data for reduction of the melting point and the virtual N*/SmA* transition in dependence of the concentration of C₆₀.

Similar results have been found by Lisetski et al. [188] for different cholesteryl ester mixtures but there exists also differing data for nanoparticle doping of cholesteric liquid crystals with platinum particles [189]. Here the nanoparticles deposit in ribbons according to the cholesteric pitch and the pitch actually increases with the doping, so the exact opposite behavior is shown. Lisetski et al. have identified the occurrence of a SmA* phase below the cholesteric phase as a key component for the pitch behavior that is seen for carbon nanoparticle doping. Although our mixture shows no smectic phases two of the pure components do. The decreasing pitch of the cholesteric helix upon CNT doping is reflected by a decrease in the T_{NA} transition temperature – both real and virtual, apparently. From this it can be conjectured that the CNTs or fullerenes disturb the translational order of a potential SmA* phase (or crystalline phase for that matter), thereby lowering its thermal stability and tightening the cholesteric pitch as a secondary effect.

More than the decreased stability of the SmA* or crystalline phase the actual stability of the dispersion in the cholesteric phase might play a role. Normally, insoluble impurities would separate from a liquid host phase leaving the bulk phase unaffected, therefore not influencing the melting point. However if the phase separation is not possible an impurity-

driven effect that systematically reduces the melting point of the host material even without dissolution can be observed [190]. In the case of the cholesteryl ester mixtures the high viscosity may kinetically trap the system in a state of good dispersion so that the formation of two practically non-interacting phases is not possible and an interface-driven reduction of the melting temperature can take place and be measured. In fact, we could not find any significant change in pitch or transition temperatures with other cholesteric mixtures such as the commercial room temperature nematic mixture ROTN doped with cholesteryl nonanoate or the chiral dopant CB15 which proved not to form stable suspensions and were much less viscous than the cholesteryl ester mixtures. The mechanism of this melting point reduction is somewhat different from the standard theory as there is an additional interfacial energy influencing the system, which probably explains the discrepancies between the theoretically predicted and experimental reductions of the melting point.

In general the additional order in form of the director helix present in the cholesteric phase seems to have adverse effects on CNT dispersion stability. In an experiment with dispersions of HiPCO CNTs in ROTN doped with different amounts of cholesteryl nonanoate – more chiral dopant equals shorter pitch of the cholesteric helix – it was found that with decreasing pitch also the stability of the dispersion was decreasing (Fig. 4.33), even though the cholesteryl nonanoate in a reference experiment with a toluene and pentane mixture proved to have a stabilizing effect on the CNT-dispersion, preventing fast aggregation and sedimentation. Also the increased viscosity of stronger doped cholesterics would normally be considered a stabilizing factor due to inhibited aggregation. Yet the disturbance that the CNTs pose for the cholesteric phase apparently outweighs the stabilizing effects.

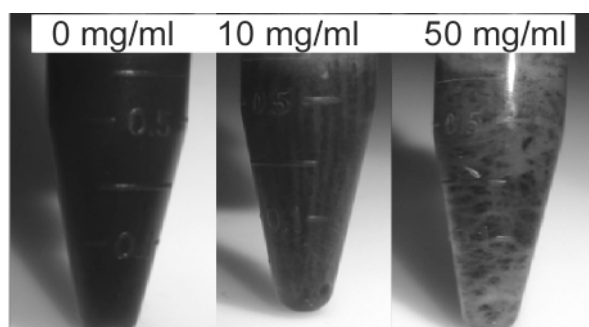


Fig. 4.33: Dispersions of 0.1 mg CNTs in 1 ml ROTN doped with different amounts of cholesteryl nonanoate, (indicated at the top of each image), in no case enough to induce selective reflection, after 2 days of standing.

This effect can be observed very well during phase transitions from the isotropic phase into the cholesteric phase as small CNT aggregates form the centers of defects disturbing the build-up of an otherwise continuous director field. These aggregates will move along defect

lines and literally be pushed together by the elastic forces of the anisotropic phase [175,191]. The CNTs get expelled by the LC host in a similar fashion to what is observed for homeotropically aligning spherical particles in nematic phases [192], although even more pronounced due to the additional degree of order in the cholesteric phase.

Interestingly a similar effect can be seen in the opposite case, a transition from the cholesteric to the isotropic phase. A CNT or CNT aggregate that “has found its place” in a homogeneous cholesteric phase, meaning that it is well incorporated in the phase with strongly adsorbed LC molecules on its side wall which are part of a continuous director field, will stay as long as possible in the cholesteric phase as the isotropic phase forms upon reaching the transition temperature. This anchoring in the cholesteric phase will cause aggregation as the nanotubes get concentrated in the increasingly small remainders of the cholesteric phase. Flow processes during the phase transition even produce enough force to let CNT aggregates flow through cholesteric channels, being pushed together (Fig. 4.34) in an analogous but contrary fashion to the aggregation happening at the reverse transition from isotropic to cholesteric [193]. This anchoring effect can also be seen by the fact that the phase transition occurs the latest in the vicinity of CNT aggregates, letting them show a significant “after-glow” between crossed polarizers when the rest of the LC is already completely isotropic, also known for nematic LCs [194]. In fact, all the described mechanisms are also valid for simple nematic samples and corroborate the results presented in chapter 4.2.1 regarding the poor stability of CNT dispersions around the transition temperature.

Unfortunately this poses many problems for one of the most desirable applications of nanoparticle doping of cholesteric LCs, the stabilization of the structurally highly complex blue phases BP* to extend their temperature range beyond the usual few degrees Celsius or less, thus making them accessible for display applications. The principle of this approach is that the nanoparticles in general and the nanotubes in particular should occupy the defect sites or defect lines, respectively, thereby stabilizing the whole phase by counteracting a possible phase transition. This approach was already used to stabilize blue phases by employing polymerizable substances, which were mixed with the LC and tended to concentrate at the defect sites [195]. Upon polymerization the blue phase may be sufficiently stable for prototype display application [196]. Similar reports exist for nanoparticle doping of blue phases [197].

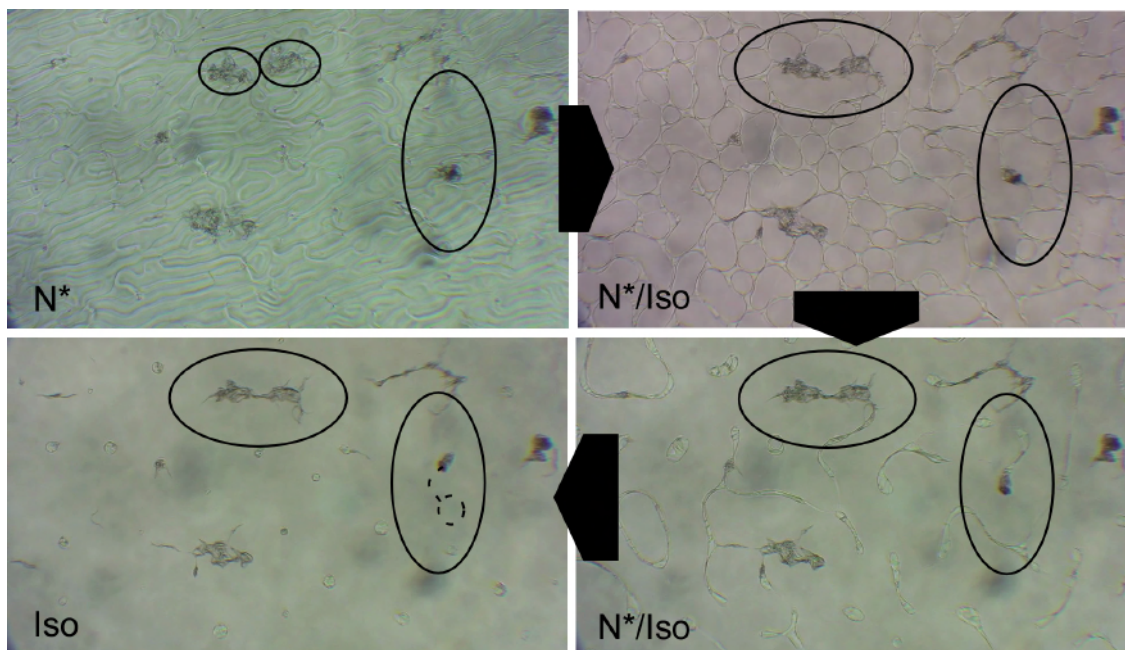


Fig. 4.34: CNTs dispersed in an N^* phase (top left) as it undergoes a transition (right) towards the isotropic phase (bottom left). CNT aggregates are compressed as they stay in the cholesteric phase, moving towards each other eventually uniting (dashed line illustrates route of CNT aggregate in cholesteric “channel” during phase transition).

In our case however we did not achieve any changes in the phase sequence of ROTN doped with a sufficient amount of CB15 to obtain blue phases, neither with HiPCO SWCNTs nor with C_{60} . Considering the dispersion destabilizing effects of a cholesteric phase and that ROTN proved not to be the best choice for CNT dispersion (see chapter 4.2) it is a reasonable assumption that the yielded state of dispersion in the BP^* -showing composites was simply too coarse to really affect the phase behavior. Thus the CNTs get expelled by the LC phase and the interaction between the two substances is limited to surface effects at the boundary between liquid crystal and CNT aggregate.

In conclusion, here, as within the whole field of LC/CNT composites, the stability and quality of the dispersion is the main factor on which the impact of CNT doping on LCs depends. As shown the kinetic trapping of a system might be a tool for overcoming these shortcomings and the employment of specifically designed liquid crystal compounds is of high interest in order to exploit the unique properties of such composites.

5. Conclusions and Outlook

The work presented here touched upon many aspects of the field of LC/CNT composites. The unique challenges of the production of said composites have been detailed in chapters 4.1 and 4.2. We have seen the peculiar requirements of the seemingly simple task of dispersing CNTs in LCs, both lyotropic and thermotropic, concerning the detailed procedure and the structural properties of the used substances. For both types of LCs the investigations allowed to devise recommended procedures for the reliable production of LC/CNT composites. In the case of lyotropic LCs a two step procedure of CNT dispersion in an isotropic surfactant solution using strong tip sonication followed by a rather low power bath sonication after adding the dispersion to the LC phase forming compound was found to give best results concerning dispersion quality and CNT content. For thermotropic LCs a combination of gentle stirring and sonication, without leaving the nematic phase, proved to yield the highest quality dispersions.

The detailed structural properties of the used substances proved to be of much importance for the resulting composites. The quality and CNT content of dispersions in isotropic surfactant solutions for the production of lyotropic LC/CNT composites seems to be mainly influenced by the packing of the surfactant molecules around the nanotube and the resulting surface charge. SDBS proved to be the most efficient of the tested surfactants and our procedure allowed concentrations up to 2.5 mg/mL, much higher than most of the published data.

The dispersion of CNTs in thermotropic LCs turned out to be a truly unique challenge as a „*simila similibus solvuntur*“ (lat.: like dissolves like) approach fails to give justice to the complexity of the different influences that govern the dispersion process. A careful balancing of the entropic and enthalpic factors of CNT/LC interaction is the key to success, as a strong adsorption due to beneficial enthalpic conditions leads to a decrease in entropy, negating the enthalpic advantage. In addition to the anisotropic LC phase itself several structural features of the LC molecules were identified to promote high quality CNT dispersion. Results in the same concentration range as one of the best solvents for CNTs, NMP, were achieved and a guideline for the choice of LC could be deduced.

Composites produced using the refined methods developed from the investigations and the informed choice of substances showed unique properties and prove the potential of self-assembly for application. Exceptionally low percolation thresholds were achieved for the filament forming behavior of lyotropic composites and the electrical conductivity in case of thermotropic LCs. The formation of filaments from lyotropic LC/CNT composites is an impressive example of the power of self assembly as a supramolecular polymerization is caused by the combined forces of the anisotropy of the LC phase, the presence of micelles, the stiffening of these micelles by CNTs, the linkage of these micelles by anisotropic depletion attraction and elongational stress. In case of the thermotropic LCs the percolation is made possible by the attractive forces arising as a result of CNT polarization upon application of a DC field, the LC probably acting mainly as a very good solvent, effectively individualizing CNTs.

The potential application of LC/CNT composites was shown by the possible controlled deposition of the lyotropic LC/CNT composite filaments and the influence of CNT doping on the properties of cholesteric LCs. In both cases it is apparent that the good dispersion of the CNTs is a mandatory prerequisite for the effects seen, thus further highlighting the importance of the basic research concerning dispersion quality, both procedure and substance-wise.

Hence the work presented is an important step in the reliable application of CNT composites. Yet in research every step is followed by another. Aspirations for future work on these subjects should endeavor to shed further light into the basic workings of the dispersion process, finding even better host systems for the CNTs and trying to solidify the evidence for the postulates deduced from the data presented here. The possibility of polymerization should be further investigated for both lyotropic and thermotropic systems as it would provide the means for an electron microscopic visualization of the microstructure of the composites.

Great potential lies in the possible compatibility of the deposition of aligned CNTs on substrates using the filament forming process of lyotropic LC/CNT composites. It should be tried to make this compatible with commercially used dispensing systems and methods such as printing or electrospinning.

And lastly concerning the often-shunned magic of self-assembly one can conclude by citing Robert A. Heinlein:

“One man’s “magic” is another man’s engineering.” [198]

6. Bibliography

- [1] Reinitzer, F.: "Beiträge zur Kennniss des Cholesterins", *Monatshefte für Chemie*, 9, 421-441, **1888**.
- [2] Kelker, H. & Scheurle, B.: "A Liquid-crystalline (Nematic) Phase with a Particular Low Solidification Point", *Angew Chem Int Edit*, 8, 884-&, **1969**.
- [3] Helfrich, W. & Schadt, M.: "Lichtsteuerzelle", CH532261 (A), Switzerland, **1970**.
- [4] Iijima, S.: "Helical Microtubules of Graphitic Carbon", *Nature*, 354, 56-58, **1991**.
- [5] Dhar, S., Liu, Z., Thomale, J., Dai, H. & Lippard, S. J.: "Targeted single-wall carbon nanotube-mediated Pt(IV) prodrug delivery using folate as a homing device.", *J Am Chem Soc*, 130, 11467-11476, **2008**.
- [6] Faraji, A. H. & Wipf, P.: "Nanoparticles in cellular drug delivery.", *Bioorg Med Chem*, 17, 2950-2962, **2009**.
- [7] [Anon: "Carbon nanotubes: New weapons against cancer", *Expert Rev Anticanc*, 7, 1335-1335, **2007**.
- [8] Bianco, A.: "Potential usefulness of carbon nanotubes for cancer therapy", *M S-med Sci*, 25, 125-127, **2009**.
- [9] Ji, S. R. et al.: "Carbon nanotubes in cancer diagnosis and therapy", *Bba-rev Cancer*, 1806, 29-35, **2010**.
- [10] Poland, C. A. et al.: "Carbon nanotubes introduced into the abdominal cavity of mice show asbestos-like pathogenicity in a pilot study.", *Nat Nanotechnol*, 3, 423-428, **2008**.
- [11] Yamashita, K. et al.: "Cancer hazard of carbon nanotubes: Size/shape-dependent induction of DNA damage and inflammation", *Cytokine*, 48, 55-55, **2009**.
- [12] Firme, C. P. & Bandaru, P. R.: "Toxicity issues in the application of carbon nanotubes to biological systems", *Nanomed-nanotechnol*, 6, 245-256, **2010**.
- [13] Edwards, B. C.: "Design and deployment of a space elevator", *Acta Astronaut*, 47, 735-744, **2000**.
- [14] Aravind, P. K.: "The physics of the space elevator", *Am J Phys*, 75, 125-130, **2007**.

- [15] Rao, C. N., Sood, A. K., Subrahmanyam, K. S. & Govindaraj, A.: "Graphene: the new two-dimensional nanomaterial.", *Angew Chem Int Ed Engl*, 48, 7752-7777, **2009**.
- [16] Rinzler, A. G.: "Materials processing - Sorting out carbon nanotube electronics", *Nat Nanotechnol*, 1, 17-18, **2006**.
- [17] Clarke, A. C.: Profiles of the future : an inquiry into the limits of the possible / by Arthur C. Clarke, London : The Scientific Book Club, **1962**.
- [18] Lehmann, O.: Flüssige Kristalle, Verlag Engelmann, Leipzig, **1904**.
- [19] Maier, W. & Saupe, A.: "Eine einfache molekulare Theorie des nematischen kristallinflüssigen Zustandes", *Z Naturforsch Pt A*, 13, 564-566, **1958**.
- [20] Bragg, W. H. A. W. L. B.: X Rays and Crystal Structure, G. Bell and Sons Ltd, **1915**.
- [21] Stegemeyer, H., Blumel, T., Hiltrop, K., Onusseit, H. & PORSCH, F.: "Thermodynamic, Structural and Morphological-Studies on Liquid-Crystalline Blue Phases", *Liq Cryst*, 1, 3-28, **1986**.
- [22] Stegemeyer, H.: Lyotrope Flüssigkristalle. Grundlagen - Entwicklung - Anwendung, Steinkopff Verlag, **1999**.
- [23] Dörfler, H.-D.: Grenzflächen und kolloid-disperse Systeme. Physik und Chemie, Springer, Berlin, **2002**.
- [24] Israelachvili, J. N., Mitchell, D. J. & Ninham, B. W.: "Theory of Self-Assembly of Hydrocarbon Amphiphiles into Micelles and Bilayers", *J Chem Soc Farad T 2*, 72, 1525-1568, **1976**.
- [25] Osawa, E.: *Kagaku*, 25: 854, **1970**.
- [26] Kroto, H. W., Heath, J. R., O'Brien, S. C., Curl, R. F. & S, a., RE: "C-60 - Buckminsterfullerene", *Nature*, 318, 162-163, **1985**.
- [27] Wang, X. et al.: "Fabrication of ultralong and electrically uniform single-walled carbon nanotubes on clean substrates.", *Nano Lett*, 9, 3137-3141, **2009**.
- [28] Saito, R., Dresselhaus, G. & Dresselhaus, M. S.: Physical Properties of Carbon Nanotubes, World Scientific Publishing Company, **1998**.
- [29] Adams, T. A.: Physical Properties of Carbon nanotubes, <http://www.pa.msu.edu/cmp/csc/ntproperties/main.html#intro>,
- [30] Terranova, M. L., Sessa, V. & Rossi, M.: "The World of Carbon Nanotubes: An Overview of CVD Growth Methodologies.", *Chemical Vapor Deposition*, 12, 315-325, **2006**.
- [31] Guo, T., Nikolaev, P., Thess, A., Colbert, D. T. & Smalley, R. E.: "Catalytic growth of single-walled nanotubes by laser vaporization", *Chem Phys Lett*, 243, 49-54, **1995**.

- [32] Ando, Y. & Zhao, X. L.: "Synthesis of carbon nanotubes by arc-discharge method", *New Diam Front C Tec*, 16(3), 123-137, **2006**.
- [33] Balasubramanian, K. & Burghard, M.: "Nanocylinders with highly potential utility - Functionalized carbon nanotubes", *Chem Unserer Zeit*, 39, 16-25, **2005**.
- [34] van Hove, L.: "The Occurrence of Singularities in the elastic Frequency Distribution of a Crystal", *Phys Rev*, 89, 1189-1193, **1953**.
- [35] Fermi, E.: "Zur Quantelung des idealen einatomigen Gases", *Zeitschrift für Physik*, 26, 902-912, **1926**.
- [36] Charlier, J. C.: "Defects in carbon nanotubes", *Accounts Chem Res*, 35, 1063-1069, **2002**.
- [37] Arnold, M. S., Green, A. A., Hulvat, J. F., Stupp, S. I. & Hersam, M. C.: "Sorting carbon nanotubes by electronic structure using density differentiation", *Nat Nanotechnol*, 1, 60-65, **2006**.
- [38] Green, A. A. & Hersam, M. C.: "Ultracentrifugation of single-walled nanotubes", *Mater Today*, 10, 59-60, **2007**.
- [39] Zheng, M. et al.: "DNA-assisted dispersion and separation of carbon nanotubes.", *Nat Mater*, 2, 338-342, **2003**.
- [40] Bergin, S. D. et al.: "Towards Solutions of Single-Walled Carbon Nanotubes in Common Solvents", *Advanced Materials*, 20, 1876-1881, **2008**.
- [41] Bergin, S. D. et al.: "Exfoliation in ecstasy: liquid crystal formation and concentration-dependent debundling observed for single-wall nanotubes dispersed in the liquid drug gamma-butyrolactone", *Nanotechnology*, 18, 455705, **2007**.
- [42] Bergin, S. D. et al.: "Multicomponent solubility parameters for single-walled carbon nanotube-solvent mixtures.", *ACS Nano*, 3, 2340-2350, **2009**.
- [43] Giordani, S. et al.: "Debundling of single-walled nanotubes by dilution: Observation of large populations of individual nanotubes in amide solvent dispersions", *J Phys Chem B*, 110, 15708-15718, **2006**.
- [44] Blanch, A. J., Lenehan, C. E. & Quinton, J. S.: "Optimizing surfactant concentrations for dispersion of single-walled carbon nanotubes in aqueous solution.", *J Phys Chem B*, 114, 9805-9811, **2010**.
- [45] Wenseleers, W. et al.: "Efficient Isolation and Solubilization of Pristine Single-Walled Nanotubes in Bile Salt Micelles", *Adv Funct Mater*, 14, 1105-1111, **2004**.
- [46] Engel, M. et al.: "Thin Film Nanotube Transistors Based on Self-Assembled, Aligned, Semiconducting Carbon Nanotube Arrays", *Acs Nano*, 2, 2445-2452, **2008**.

- [47] Kim, S., Xuan, Y., Ye, P. D., Mohammadi, S. & Lee, S. W.: "Single-walled carbon nanotube transistors fabricated by advanced alignment techniques utilizing CVD growth and dielectrophoresis", *Solid-State Electronics*, 52, 1260-1263, **2008**.
- [48] LeMieux, M. C. et al.: "Self-sorted, aligned nanotube networks for thin-film transistors.", *Science*, 321, 101-104, **2008**.
- [49] Krupke, R., Hennrich, F., von, L., H & Kappes, M. M.: "Separation of metallic from semiconducting single-walled carbon nanotubes", *Science*, 301, 344-347, **2003**.
- [50] Casavant, M. J., Walters, D. A., Schmidt, J. J. & Smalley, R. E.: "Neat macroscopic membranes of aligned carbon nanotubes", *Journal of Applied Physics*, 93, 2153, **2003**.
- [51] Fischer, J. E. et al.: "Magnetically aligned single wall carbon nanotube films: Preferred orientation and anisotropic transport properties", *J Appl Phys*, 93, 2157-2163, **2003**.
- [52] Fry, D. et al.: "Anisotropy of sheared carbon-nanotube suspensions", *Phys Rev Lett*, 95, ARTN 038304, **2005**.
- [53] Wang, H. et al.: "Shear-SANS study of single-walled carbon nanotube suspensions", *Chem Phys Lett*, 416, 182-186, **2005**.
- [54] Gerdes, S., Ondarcuhu, T., Cholet, S. & Joachim, C.: "Combing a carbon nanotube on a flat metal-insulator-metal nanojunction", *Europhys Lett*, 48, 292-298, **1999**.
- [55] Kim, D. H., Koo, J. Y. & Kim, J. J.: "Electrostatic displacement of multiwalled carbon nanotubes by scanning a voltage-applied tip of an atomic force microscope", *The European Physical Journal Applied Physics*, 28, 301-304, **2004**.
- [56] Liu, H., Chiashi, S., Ishiguro, M. & Homma, Y.: "Manipulation of single-walled carbon nanotubes with a tweezers tip", *Nanotechnology*, 19, ARTN 445716, **2008**.
- [57] Dittmer, S., Svensson, J. & Campbell, E. E. B.: "Electric field aligned growth of single-walled carbon nanotubes", *Curr Appl Phys*, 4, 595-598, **2004**.
- [58] Ismach, A. & Joselevich, E.: "Orthogonal self-assembly of carbon nanotube crossbar architectures by simultaneous graphoepitaxy and field-directed growth", *Nano Lett*, 6, 1706-1710, **2006**.
- [59] Yao, Y. G. et al.: "Temperature-mediated growth of single-walled carbon-nanotube intramolecular junctions", *Nat Mater*, 6, 283-286, **2007**.
- [60] Hata, K. et al.: "Water-assisted highly efficient synthesis of impurity-free single-walled carbon nanotubes", *Science*, 306, 1362-1364, **2004**.
- [61] Huang, S. M., Dai, L. M. & Mau, A. W. H.: "Patterned growth and contact transfer of well-aligned carbon nanotube films", *J Phys Chem B*, 103, 4223-4227, **1999**.

-
- [62] Maruyama, S., Einarsson, E., Murakami, Y. & Edamura, T.: "Growth process of vertically aligned single-walled carbon nanotubes", *Chem Phys Lett*, 403, 320-323, **2005**.
- [63] De Volder, M. et al.: "Diverse 3D Microarchitectures Made by Capillary Forming of Carbon Nanotubes.", *Adv Mater*, 22, 4384-4389, **2010**.
- [64] Barnes, T. M. et al.: "Carbon nanotube network electrodes enabling efficient organic solar cells without a hole transport layer", *Appl Phys Lett*, 96, ARTN 243309, **2010**.
- [65] Li, J., Cassell, A. M. & Dai, H. J.: "Carbon nanotubes as AFM tips: Measuring DNA molecules at the liquid/solid interface", *Surf Interface Anal*, 28, 8-11, **1999**.
- [66] Kuwahara, S. et al.: "Fabrication and characterization of high-resolution AFM tips with high-quality double-wall carbon nanotubes", *Chem Phys Lett*, 429, 581-585, **2006**.
- [67] Wang, R., Xu, H. M., Li, D. & Liang, J.: "Growth of single-walled carbon nanotubes on the given locations for AFM tips", *Acta Phys-chim Sin*, 23, 565-568, **2007**.
- [68] Dierking, I., Scalia, G. & Morales, P.: "Liquid crystal-carbon nanotube dispersions", *J Appl Phys*, 97, 044309, **2005**.
- [69] Lagerwall, J. et al.: "Nanotube alignment using lyotropic liquid crystals", *Adv Mater*, 19, 359-364, **2007**.
- [70] Scalia, G. et al.: "Spontaneous macroscopic carbon nanotube alignment via colloidal suspension in hexagonal columnar lyotropic liquid crystals", *Soft Matter*, 4, 570-576, **2008**.
- [71] Dierking, I., Scalia, G., Morales, P. & LeClere, D.: "Aligning and reorienting carbon nanotubes with nematic liquid crystals", *Adv Mater*, 16, 865-869, **2004**.
- [72] Kuhnast, M., Tschierske, C. & Lagerwall, J.: "Tailor-designed polyphilic promoters for stabilizing dispersions of carbon nanotubes in liquid crystals.", *Chem Commun (Camb)*, 46, 6989-6991, **2010**.
- [73] Baik, I. S. et al.: "Electrical-field effect on carbon nanotubes in a twisted nematic liquid crystal cell", *Appl Phys Lett*, 87, 263110, **2005**.
- [74] Chen, H. Y. & Lee, W.: "Suppression of field screening in nematic liquid crystals by carbon nanotubes", *Appl Phys Lett*, 88, 222105, **2006**.
- [75] Chen, H. Y., Lee, W. & Clark, N. A.: "Faster electro-optical response characteristics of a carbon-nanotube-nematic suspension", *Appl Phys Lett*, 90, 033510, **2007**.
- [76] Jeon, S. Y. et al.: "Effects of carbon nanotubes on electro-optical characteristics of liquid crystal cell driven by in-plane field", *Appl Phys Lett*, 90, 121901, **2007**.
- [77] Lee, C. W. & Shih, W. P.: "Quantification of ion trapping effect of carbon nanomaterials in liquid crystals", *Materials Letters*, 64, 466-468, **2010**.

- [78] Lee, W., Wang, C. Y. & Shih, Y. C.: "Effects of carbon nanosolids on the electro-optical properties of a twisted nematic liquid-crystal host", *Appl Phys Lett*, 85, 513-515, **2004**.
- [79] Lagerwall, J. P. F. & Scalia, G.: "Carbon nanotubes in liquid crystals", *J Mater Chem*, 18, 2890-2898, **2008**.
- [80] Essam, J. W.: "Percolation Theory", *Rep Prog Phys*, 43, 833-912, **1980**.
- [81] Grimmet, G.: Percolation, Springer-Verlag GmbH, **1989**.
- [82] Shante, V. K. S. & Kirkpatrick, S.: "Introduction to Percolation Theory", *Adv Phys*, 20, 325-&, **1971**.
- [83] Stauffer, D. & Aharony, A.: Introduction To Percolation Theory, CRC Press, **1994**.
- [84] Dalton, N. W., Domb, C. & Sykes, M. F.: "Dependence of Critical Concentration of Dilute Ferromagnet on Range of Interaction", *P Phys Soc Lond*, 83, 496-&, **1964**.
- [85] Domb, C. & Dalton, N. W.: "Crystal Statistics with long-range Forces.I. equivalent Neighbour Model", *P Phys Soc Lond*, 89, 859-&, **1966**.
- [86] Parker, S. F., Williams, K. P. J., Meehan, P., Adams, M. A. & Tomkinson, J.: "Analysis of Carbon Black-filled Polymers by Vibrational Spectroscopy", *Appl Spectrosc*, 48, 669-673, **1994**.
- [87] Nogales, A. et al.: "Low percolation threshold in nanocomposites based on oxidized single wall carbon nanotubes and poly(butylene terephthalate)", *Macromolecules*, 37, 7669-7672, **2004**.
- [88] Martin, C. A. et al.: "Formation of percolating networks in multi-wall carbon-nanotube-epoxy composites", *Composites Science and Technology*, 64, 2309-2316, **2004**.
- [89] Grujicic, M., Cao, G. & Roy, W. N.: "A computational analysis of the percolation threshold and the electrical conductivity of carbon nanotubes filled polymeric materials", *J Mater Sci*, 39, 4441-4449, **2004**.
- [90] Kyrylyuk, A. V. & van der Schoot, P.: "Continuum percolation of carbon nanotubes in polymeric and colloidal media (vol 105, pg 8221, 2008)", *P Natl Acad Sci Usa*, 105, 11451-11451, **2008**.
- [91] Du, F. M., Fischer, J. E. & Winey, K. I.: "Effect of nanotube alignment on percolation conductivity in carbon nanotube/polymer composites", *Phys Rev B*, 72, ARTN 121404, **2005**.
- [92] Vigolo, B., Coulon, C., Maugey, M., Zakri, C. & Poulin, P.: "An experimental approach to the percolation of sticky nanotubes", *Science*, 309, 920-923, **2005**.

- [93] Zakri, C. & Poulin, P.: "Phase behavior of nanotube suspensions: from attraction induced percolation to liquid crystalline phases", *Journal of Materials Chemistry*, 16, 4095-4098, **2006**.
- [94] Lima, M. D., Andrade, M. J., Skákalová, V., Bergmann, C. P. & Roth, S.: "Dynamic percolation of carbon nanotubes in liquid medium", *Journal of Materials Chemistry*, 17, 4846-4853, **2007**.
- [95] Park, C. et al.: "Aligned single-wall carbon nanotube polymer composites using an electric field", *Journal of Polymer Science Part B Polymer Physics*, 44, 1751, **2006**.
- [96] Asakura, S. & Oosawa, F.: "Interaction between Particles suspended in Solutions of Macromolecules", *J Polym Sci*, 33, 183-192, **1958**.
- [97] Yodh, A. G. et al.: "Entropically driven self-assembly and interaction in suspension (vol 359, pg 921, 2001)", *Philos T Roy Soc A*, 359, 2629-2629, **2001**.
- [98] Marenduzzo, D., Finan, K. & Cook, P. R.: "The depletion attraction: an underappreciated force driving cellular organization.", *J Cell Biol*, 175, 681-686, **2006**.
- [99] van der Schoot, P.: "Depletion interactions in lyotropic nematics", *J Chem Phys*, 112, 9132, **2000**.
- [100] Bleisteiner, B.: "Raman- und PL-Spektroskopie an Kohlenstoffnanoröhrchen", *Nachrichten aus der Chemie*, 55, 430-432, **2007**.
- [101] Jorio, A. et al.: "Characterizing carbon nanotube samples with resonance Raman scattering", *New J Phys*, 5, 139.1-139.17, **2003**.
- [102] Maultzsch, J., Telg, H., Reich, S. & Thomsen, C.: "Radial breathing mode of single-walled carbon nanotubes: Optical transition energies and chiral-index assignment", *Phys Rev B*, 72, ARTN 205438, **2005**.
- [103] Wepasnick, K. A., Smith, B. A., Bitter, J. L. & Howard Fairbrother, D.: "Chemical and structural characterization of carbon nanotube surfaces.", *Anal Bioanal Chem*, 396, 1003-1014, **2010**.
- [104] Duesberg, G. S., Loa, I., Burghard, M., Syassen, K. & Roth, S.: "Polarized Raman spectroscopy on isolated single-wall carbon nanotubes", *Phys Rev Lett*, 85, 5436-5439, **2000**.
- [105] Demus, D., Goodby, J. W., Gray, G. W., Spiess, H. W. & Vill, V.: 4 Volume Set, *Handbook of Liquid Crystals*, Wiley-VCH, **1998**.
- [106] Technologies, A.: *The Impedance Measurement Handbook*, www.agilent.com, **2009**.

- [107] Cheng, X., McCoy, J. H., Israelachvili, J. N. & Cohen, I.: "Imaging the microscopic structure of shear thinning and thickening colloidal suspensions.", *Science*, 333, 1276-1279, **2011**.
- [108] Barnes, H. A.: Handbook of Elementary Rheology, University of Wales, Institute of Non-Newtonian Fluid Mechanics, **2000**.
- [109] Oswald, P. & Pieranski, P.: Liquid Crystals: Concepts and Physical Properties Illustrated by Experiments, Two Volume Set (Liquid Crystals Book Series), CRC Press, **2006**.
- [110] Michel-Levy, A. & Lacroix, A.: Les Mineraux des Roches, Librairie Polytechnique, Paris, **1888**.
- [111] Hilding, J., Grulke, E. A., Zhang, Z. G. & Lockwood, F.: "Dispersion of carbon nanotubes in liquids", *J Disper Sci Technol*, 24, 1-41, **2003**.
- [112] Lucas, A. et al.: "Kinetics of Nanotube and Microfiber Scission under Sonication", *J Phys Chem C*, 113, 20599-20605, **2009**.
- [113] Priya, B. R. & Byrne, H. J.: "Investigation of sodium dodecyl benzene sulfonate assisted dispersion and debundling of single-wall carbon nanotubes", *J Phys Chem C*, 112, 332-337, **2008**.
- [114] Islam, M. F., Rojas, E., Bergey, D. M., Johnson, A. T. & Yodh, A. G.: "High weight fraction surfactant solubilization of single-wall carbon nanotubes in water", *Nano Lett*, 3, 269-273, **2003**.
- [115] Taurozzi, J. S., Hackley, V. A. & Wiesner, M. R.: "Preparation of nanoparticle dispersions from powdered Material using ultrasonic disruption", *CEINT/NIST Protocol*, **2010**.
- [116] Schymura, S., Enz, E., Roth, S., Scalia, G. & Lagerwall, J. P. F.: "Macroscopic-scale carbon nanotube alignment via self-assembly in lyotropic liquid crystals", *Synthetic Met*, 159, 2177-2179, **2009**.
- [117] Danov, K. D., Kralchevska, S. D., Kralchevsky, P. A., Broze, G. & Mehreteab, A.: "Effect of nonionic admixtures on the adsorption of ionic surfactants at fluid interfaces. 2. Sodium dodecylbenzene and dodecylbenzene", *Langmuir*, 19, 5019-5030, **2003**.
- [118] Sun, Z. et al.: "Quantitative Evaluation of Surfactant-stabilized Single-walled Carbon Nanotubes: Dispersion Quality and Its Correlation with Zeta Potential", *J Phys Chem C*, 112, 10692-10699, **2008**.
- [119] Vigolo, B. et al.: "Macroscopic Fibers and Ribbons of Oriented Carbon Nanotubes", *Science*, 290, 1331-1334, **2000**.

- [120] Amenitsch, H., Edlund, H., Khan, A., Marques, E. F. & La, M., C: "Bile salts form lyotropic liquid crystals", *Colloid Surface A*, 213, 79-92-PII S0927-7757(02)00360-6, **2003**.
- [121] Kawamura, H. et al.: "Spin label studies of bile salt micelles", *J Phys Chem*, 93, 3321-3326, **1989**.
- [122] Marques, E. F., Edlund, H., La Mesa, C. & Khan, A.: "Liquid crystals and phase equilibria binary bile salt-water systems", *Langmuir*, 16, 5178-5186, **2000**.
- [123] Zakrzewska, J. et al.: "Investigations of aggregation behavior of bile salts by small-angle X-ray scattering", *J Phys Chem*, 94, 5078-5081, **1990**.
- [124] Hobbie, E. K. et al.: "Self-assembly of ordered nanowires in biological suspensions of single-wall carbon nanotubes.", *ACS Nano*, 3, 189-196, **2009**.
- [125] Groszek, A. J.: "Selektive Adsorption at Graphite/Hydrocarbon Interfaces", *Proc R Soc Lon Ser-a*, 314, 473-&, **1970**.
- [126] Angelikopoulos, P. & Bock, H.: "Directed self-assembly of surfactants in carbon nanotube materials.", *J Phys Chem B*, 112, 13793-13801, **2008**.
- [127] Angelikopoulos, P. et al.: "Dispersing Individual Single-Wall Carbon Nanotubes in Aqueous Surfactant Solutions below the cmc", *J Phys Chem C*, 114, 2-9, **2010**.
- [128] G, H. & H, H.: "Lyotropic nematic phases of double chain surfactants", *Progr Colloid Polym Sci*, 76, 123-131, **1988**.
- [129] Varade, D., Aramaki, K. & Stubenrauch, C.: "Phase diagrams of water-alkyltrimethylammonium bromide systems", *Colloids and Surfaces A: Physicochemical and Engineering Aspects*, 315, 205-209, **2008**.
- [130] Lambert, J. H.: *Photometria sive de mensura et gradibus luminis, colorum et umbrae*, Eberhardt Klett, Augsburg ("Augusta Vindelicorum"), **1760**.
- [131] Beer, A.: "Bestimmung der Absorption des rothen Lichts in farbigen Flüssigkeiten", *Annalen der Physik und Chemie*, 86, 78-88, **1852**.
- [132] Gibbs, J. W.: "On the Equilibrium of Heterogenous Substances", *Transactions of the Connecticut Academy of Arts and Sciences*, 3, 198, **1875**.
- [133] van der Waals, J. D.: "Over de Continuïteit van den Gas- en Vloeistofoestand", Universiteit Leiden, **1873**.
- [134] Keesom, W. H.: "Die van der Waalsschen Kohäsionskräfte", *Physikalische Zeitschrift*, 22, 129-141, **1921**.
- [135] Debye, P.: "Die van der Waalschen Kohäsionskräfte", *Physikalische Zeitschrift*, 21, 178-187, **1920**.

- [136] Eisenschitz, R. & London, F.: "Über das Verhältnis der van der Waalsschenkräfte zu den homoopolaren Bindungskräften", *Zeitschrift für Physik*, 60, 491, **1930**.
- [137] Cheng, Q., Debnath, S., Gegan, E. & Byrne, H. J.: "Effect of Solvent Solubility Parameters on the Dispersion of Single-Walled Carbon Nanotubes", *J Phys Chem C*, 112, 20154-20158, **2008**.
- [138] Rajesh, C., Majumder, C., Mizuseki, H. & Kawazoe, Y.: "A theoretical study on the interaction of aromatic amino acids with graphene and single walled carbon nanotube.", *J Chem Phys*, 130, 124911, **2009**.
- [139] Hunter, C. A. & Sanders, J. K. M.: "The nature of pi-pi interactions", *J Am Chem Soc*, 112, 5525-5534, **1990**.
- [140] Grimme, S.: "Do special noncovalent pi-pi stacking interactions really exist?", *Angew Chem Int Ed Engl*, 47, 3430-3434, **2008**.
- [141] Klopman, G.: "Chemical Reactivity and Concept of Charge- and Frontier-controlled Reactions", *J Am Chem Soc*, 90, 223-&, **1968**.
- [142] Salem, L.: "Intermolecular Orbital Theory of Interaction between Conjugated Systems.I. General Theory", *J Am Chem Soc*, 90, 543-&, **1968**.
- [143] Woods, L. M., B descu, C. & Reinecke, T. L.: "Adsorption of simple benzene derivatives on carbon nanotubes", *Physical Review B*, 75, 155415, **2007**.
- [144] Kataura, H. et al.: "Optical properties of single-wall carbon nanotubes", *Synthetic Met*, 103, 2555-2558, **1999**.
- [145] Kong, J. & Dai, H.: "Full and Modulated Chemical Gating of Individual Carbon Nanotubes by Organic Amine Compounds", *J Phys Chem B*, 105, 2890-2893, **2001**.
- [146] Backes, C. & Hirsch, A. in *Chemistry of Nanocarbons* (eds Akasaka, T., Wudl, F. & Nagase, S.) 526 (John Wiley & Sons, Ltd, 2010).
- [147] Catalan, J., Saiz, J. L., Laynez, J. L., Jagerovic, N. & Elguero, J.: "The Colors of C-60 Solutions", *Angew Chem Int Edit*, 34, 105-107, **1995**.
- [148] Chen, W., Duan, L. & Zhu, D.: "Adsorption of Polar and Nonpolar Organic Chemicals to Carbon Nanotubes", *Environ Sci Technol*, 41, 8295-8300, **2007**.
- [149] Park, K. A., Lee, S. M., Lee, S. H. & Lee, Y. H.: "Anchoring a liquid crystal molecule on a single-walled carbon nanotube", *J Phys Chem C*, 111, 1620-1624, **2007**.
- [150] Hong, G. et al.: "Separation of metallic and semiconducting single-walled carbon nanotube arrays by "scotch tape".", *Angew Chem Int Ed Engl*, 50, 6819-6823, **2011**.
- [151] Maeda, Y. et al.: "Large-scale separation of metallic and semiconducting single-walled carbon nanotubes", *J Am Chem Soc*, 127, 10287-10290, **2005**.

- [152] Flory, P. J.: "Thermodynamics of High Polymer Solutions", *J Chem Phys*, 9, 660-661, **1941**.
- [153] Huggins, M. L.: "Solutions of Long Chain Compounds", *J Chem Phys*, 9, 440, **1941**.
- [154] Coleman, J. N.: "Liquid-Phase Exfoliation of Nanotubes and Graphene", *Adv Funct Mater*, 19, 3680-3695, **2009**.
- [155] Gotovac, S. et al.: "Effect of nanoscale curvature of single-walled carbon nanotubes on adsorption of polycyclic aromatic hydrocarbons.", *Nano Lett*, 7, 583-587, **2007**.
- [156] Bhinde, T., Clarke, S. M., Phillips, T. K., Arnold, T. & Parker, J. E.: "Crystalline structures of alkylamide monolayers adsorbed on the surface of graphite.", *Langmuir*, 26, 8201-8206, **2010**.
- [157] Fisher, A. J. & Blochl, P. E.: "Adsorption and Scanning-Tunneling-Microscope Imaging of Benzene on Graphite and MoS₂", *Phys Rev Lett*, 70, 3263-3266, **1993**.
- [158] Walba, D. M., Stevens, F., Parks, D. C., Clark, N. A. & Wand, M. D.: "Near-atomic resolution imaging of ferroelectric liquid-crystal molecules on graphite by stm", *Science*, 267, 1144-1147, **1995**.
- [159] Dawid, A. & Gwizdala, W.: "Dynamical and structural properties of 4-cyano-4-n-pentylbiphenyl (5CB) molecules adsorbed on carbon nanotubes of different chiralities: Computer simulation", *Journal of Non-Crystalline Solids*, 355, 1302-1306, **2009**.
- [160] Sano, M. & Kunitake, T.: "Influence of Phase and Chain-Length of Liquid-Crystals on Wetting Phenomena of Graphite", *Langmuir*, 8, 320-323, **1992**.
- [161] Tarakhan, L. M.: "Determination of the surface tension of 5CB liquid crystal by the pendant drop method", *Ukr J Phys*, 51, 22-26, **2006**.
- [162] Baran, J. W. & Les, A.: "Interaction energy between some nematogenic molecules", *Mol Cryst Liq Cryst*, 54, 273-288, **1979**.
- [163] Mizuno, M. & Shinoda, T.: "Internal-Rotation of N-(para-Metoxybenzylidene) -para-normal-Butylaniline (MBBA) and Benzylidene-Aniline (BA)", *Mol Cryst Liq Cryst*, 69, 103-119, **1981**.
- [164] Neumann, W. P.: "Matallorganische Molekülverbindungen.,2. Das Problem der Farbe aluminiumorganischer Molekülverbindungen", *Liebigs Ann Chem*, 667, 12-+, **1963**.
- [165] Gaber, M., Elmorsi, M. A. & Abdelghafar, M.: "Ionisation-Potentials and Electron-Affinities of Organic-Molecules from electronic Charge-Transfer Spectra", *J Chem Soc Pakistan*, 10, 125-129, **1988**.

- [166] Gaber, M., Mohamed, G. B. & Abdelghafar, M.: "On the Formation of 1-2 (Donor-Acceptor) CT-Complexes between Hydroxy Aromatic Schiff-Base Donors and Nitrobenzenes Acceptors", *J Chem Soc Pakistan*, 9, 423-429, **1987**.
- [167] Schymura, S., Dölle, S., Yamamoto, J. & Lagerwall, J.: "Filament formation in carbon nanotube-doped lyotropic liquid crystals", *Soft Matter*, 7, 2663, **2011**.
- [168] Cappelaere, E., Cressely, R. & Decruppe, J. P.: "Linear and Nonlinear Rheological Behavior of Salt-Free Aqueous CTAB Solutions", *Colloid Surface A*, 104, 353-374, **1995**.
- [169] Schörg, F.: "Lyotrope Flüssigkristallphasen für die geordnete Dispersion von Kohlenstoffnanoröhrchen: Präparation und Struktur", Universität Stuttgart, Diplomarbeit, **2009**.
- [170] Coppola, L., Gianferri, R., Nicotera, I., Oliviero, C. & Ranieri, G. A.: "Structural changes in CTAB/H₂O mixtures using a rheological approach", *Phys Chem Chem Phys*, 6, 2364-2372, **2004**.
- [171] van der Schoot, P.: *Supramolecular Polymers*, Second Edition, CRC Press, **2005**.
- [172] Turner, M. S. & Cates, M. E.: "Flow-induced phase-transitions in rod-like micelles", *J Phys-condens Mat*, 4, 3719-3741, **1992**.
- [173] Nativ-Roth, E., Regev, O. & Yerushalmi-Rozen, R.: "Shear-induced ordering of micellar arrays in the presence of single-walled carbon nanotubes", *Chem Commun*, 2037-2039, **2008**.
- [174] Nativ-Roth, E., Yerushalmi-Rozen, R. & Regev, O.: "Phase behavior and shear alignment in SWNT-surfactant dispersions", *Small*, 4, 1459-1467, **2008**.
- [175] van der Schoot, P.: "Self-assembly of globular particles in a nematic dispersion of colloidal rods", *J Chem Phys*, 117, 3537-3540, **2002**.
- [176] Hough, L. A., Islam, M. F., Janmey, P. A. & Yodh, A. G.: "Viscoelasticity of single wall carbon nanotube suspensions", *Physical review letters*, 93, 168102, **2004**.
- [177] Lodge, A. S.: *Elastic liquids;: An introductory vector treatment of finite-strain polymer rheology*, Academic Press, **1964**.
- [178] Amarouchene, Y., Bonn, D., Meunier, J. & Kellay, H.: "Inhibition of the finite-time singularity during droplet fission of a polymeric fluid", *Phys Rev Lett*, 86, 3558-3561, **2001**.
- [179] Islam, M. F. et al.: "Nematic nanotube gels", *Phys Rev Lett*, 92, 088303, **2004**.
- [180] Sievens-Figueroa, L. & Guymon, C. A.: "Cross-Linking of Reactive Lyotropic Liquid Crystals for Nanostructure Retention", *Chemistry of Materials*, 21, 1060-1068, **2009**.

- [181] Lester, C. L., Smith, S. M., Colson, C. D. & Guymon, C. A.: "Physical properties of hydrogels synthesized from lyotropic liquid crystalline templates", *Chem Mater*, 15, 3376-3384, **2003**.
- [182] Lester, C. L., Smith, S. M., Jarrett, W. L. & Guymon, C. A.: "Effects of monomer organization on the photopolymerization kinetics of acrylamide in lyotropic liquid crystalline phases", *Langmuir*, 19, 9466-9472, **2003**.
- [183] O'Brien, A. K. & Bowman, C. N.: "Impact of oxygen on photopolymerization kinetics and polymer structure", *Macromolecules*, 39, 2501-2506, **2006**.
- [184] Zheng, M. et al.: "Structure-based carbon nanotube sorting by sequence-dependent DNA assembly", *Science*, 302, 1545-1548, **2003**.
- [185] Monti, M., Natali, M., Torre, L. & Kenny, J. M.: "The alignment of single walled carbon nanotubes in an epoxy resin by applying a DC electric field", *Carbon*, 50, 2453-2464, **2012**.
- [186] Brown, G. H. & Wolken, J. J. 165-167 (Academic Press, New York, 1979).
- [187] Elser, W. & Ennulat, R. D.: *Adv. Liq. Cryst.*, 2, **1976**.
- [188] Lisetski, L. N., Minenko, S. S., Zhukov, A. V., Shtifanyuk, P. P. & Lebovka, N. I.: "Dispersions of Carbon Nanotubes in Cholesteric Liquid Crystals", *Molecular Crystals and Liquid Crystals*, 510, 43-50, **2009**.
- [189] M. Mitov, Portet, C., C. Bourgerette, Snoeck, E. & Verelst, M.: "Long-range structuring of nanoparticles by mimicry of a cholesteric liquid crystal", *nature materials*, 1, **2002**.
- [190] Hock, C. et al.: "Melting-Point Depression by Insoluble Impurities: A Finite Size Effect", *Phys Rev Lett*, 101, 023401, **2008**.
- [191] Loudet, J. C.: "Colloidal inclusions in liquid crystals: Phase separation mechanisms and some dynamical aspects", *Liquid Crystals Today*, 14, 1-14, **2005**.
- [192] Petrov, P. G. & Terentjev, E. M.: "Formation of Cellular Solid in Liquid Crystal Colloids", *Langmuir*, 17, 2942-2949, **2001**.
- [193] Meeker, S. P., Poon, W. C. K., Crain, J. & Terentjev, E. M.: "Colloid-liquid-crystal composites: An unusual soft solid", *Phys Rev E*, 61, R6083-R6086, **2000**.
- [194] Scalia, G. et al.: "Effect of phenyl rings in liquid crystal molecules on SWCNTs studied by Raman spectroscopy", *Phys Status Solidi B*, 243, 3238-3241, **2006**.
- [195] Kikuchi, H., Yokota, M., Hisakado, Y., Yang, H. & Kajiyama, T.: "Polymer-stabilized liquid crystal blue phases", *Nat Mater*, 1, 64-68, **2002**.

- [196] Ge, Z., Gauza, S., Jiao, M., Xianyu, H. & Wu, S.-T.: "Electro-optics of polymer-stabilized blue phase liquid crystal displays", *Appl Phys Lett*, 94, 101104, **2009**.
- [197] Yoshida, H. et al.: "Nanoparticle-Stabilized Cholesteric Blue Phases", *Appl Phys Express*, 2, ARTN 121501, **2009**.
- [198] Heinlein, R. A.: Time enough for love, the lives of Lazarus Long; a novel, Putnam, New York, **1973**.
- [199] Gibson, H. W. & Pochan, J. M.: "Effect of Cholesteryl Alkanoate Structure on Liquid-Crystal Transition Thermodynamics - Pure and in Binary Mixtures", *J Phys Chem-us*, 77, 837-845, **1973**.
- [200] Gray, G. W. & Hannant, M.: "Crystalline State and the Mesophases of Cholesteryl Oleyl Carbonate", *Mol Cryst Liq Cryst*, 53, 263-270, **1979**.
- [201] Chickos, J. S., Nichols, G. & Ruelle, P.: "The estimation of melting points and fusion enthalpies using experimental solubilities, estimated total phase change entropies, and mobile order and disorder theory", *J Chem Inf Comp Sci*, 42, 368-374, **2002**.
- [202] Gray, G. W. & McDonnell, D. G.: "Synthesis and Liquid-Crystal Properties of chiral Alkyl-Cyano-Biphenyls (and Alkyl-Cyano-p-Terphenyls) and of some related chiral Compounds derived from Biphenyl", *Mol Cryst Liq Cryst*, 37, 189-211, **1976**.
- [203] Lindmann, B. & Wennerstrom, H.: Topics in current chemistry: Micelles, Springer-Verlag, Berlin ; New York, **1980**.
- [204] Hait, S. K., Majhi, P. R., Blume, A. & Moulik, S. P.: "A critical assessment of micellization of sodium dodecyl benzene sulfonate (SDBS) and its interaction with poly(vinyl pyrrolidone) and hydrophobically modified polymers, JR 400 and LM 200", *J Phys Chem B*, 107, 3650-3658, **2003**.
- [205] Cheng, D. C. H. & Gulari, E.: "Micellation and Intermicellar Interactions in Aqueous Sodium Dodecyl Benzene Sulfonate Solutions", *J Colloid Interf Sci*, 90, 410-423, **1982**.
- [206] Linke, D.: "Detergents: An Overview", *Method Enzymol*, 463, 603-617, **2009**.
- [207] Hao, L., Lu, R. H., Leaist, D. G. & Poulin, P. R.: "Aggregation number of aqueous sodium cholate micelles from mutual diffusion measurements", *J Solution Chem*, 26, 113-125, **1997**.
- [208] Eichkorn, K., Weigend, F., Treutler, O. & Ahlrichs, R.: "Auxiliary basis sets for main row atoms and transition metals and their use to approximate Coulomb potentials", *Theor Chem Acc*, 97, 119-124, **1997**.

- [209] Eichkorn, K., Treutler, O., Ohm, H., Haser, M. & Ahlrichs, R.: "Auxiliary Basis-Sets to approximate Coulomb Potentials", *Chem Phys Lett*, 240, 283-289, **1995**.
- [210] Becke, A. D.: "Density-functional exchange-energy approximation with correct asymptotic-behavior", *Phys Rev A*, 38, 3098-3100, **1988**.
- [211] Weigend, F.: "Accurate Coulomb-fitting basis sets for H to Rn", *Phys Chem Chem Phys*, 8, 1057-1065, **2006**.
- [212] Weigend, F. & Ahlrichs, R.: "Balanced basis sets of split valence, triple zeta valence and quadruple zeta valence quality for H to Rn: Design and assessment of accuracy", *Phys Chem Chem Phys*, 7, 3297-3305, **2005**.
- [213] Guldberg, C. M. & Waage, P.: "Concerning Chemical Affinity", *Erdmann's Journal für Practische Chemie*, 127, 69-144, **1879**.
- [214] Guldberg, C. M. & Waage, P.: "Studies Concerning Affinity", *Forhandlinger: Videnskabs-Selskabet i Christiana*, 35, **1864**.

7. Appendix

7.1. Materials

Carbon nanoparticles

HiPCO:

Producer:	Unidym (http://www.unidym.com/)
Product:	Purified HiPCO Single Wall CNTs
Purity:	9 wt% TGA residuals
Dimensions:	Hundreds of nanometers in length [114] Diameter distribution around 1 nm

CoMoCat:

Producer:	SWeNT (http://www.swentnano.com/)
Product:	CoMoCat SWeNT Purified Single Walled CNTs (Grade SG)
Purity:	1-15 wt% TGA residuals Enriched with CNTs of (7,6) and (6,5) chirality
Dimensions:	Up to 1 μm in length Diameter distribution around 1 nm

MWCNT small:

Producer:	SES Research (http://sesres.com/)
Product:	Long purified Multi Wall Nanotubes
Purity:	>95% nanotubes vs. amorphous carbon (<2%) Ash content: < 0.2%
Dimensions:	5 – 15 μm in length 10 – 30 nm outer diameter

MWCNT large:

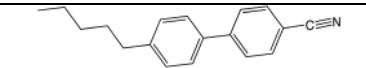
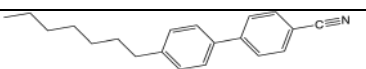

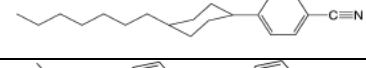
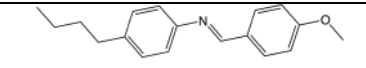
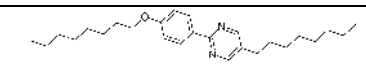
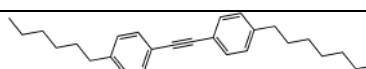
Producer:	SES Research (http://sesres.com/)
Product:	Long purified Multi Wall Nanotubes
Purity:	>95% nanotubes vs. amorphous carbon (<2%)
	Ash content: < 0.2%
Dimensions:	5 – 15 μm in length
	60 – 100 nm outer diameter

C₆₀-Fullerene:

Producer:	SES Research (http://sesres.com/)
Product:	C ₆₀ -Fullerene
Purity:	99,998%

Liquid Crystals

Thermotropic nematics

Code	Structure	Phase sequence [°C]	η [mPa s] [a]	μ [D] [b]	ϵ_r (N/I) [c]
55CB [d]		Cr. 23 N 35 Iso.	29.9@RT	6.3	11.6 / 7.0
7CB [d]		Cr. 30 N 42.8 Iso.	36,9@RT	6.3	10.0 / 6.1
PCH5 [d]		Cr. 31 N 55 Iso.	26@RT	5.9	3.7 / 3.5
PCH7 [d]		Cr. 30 (SmC _x 17) N 59 Iso.	29.4@RT	5.9	5.5 / 3.4
MBBA		Cr. 22 N 48 Iso.	39.6@RT	1.8 -3.1 [e]	3.6 / 3.7
8OPhPy8		Cr.28.5 SmC 55.5 SmA 62 N 68 Iso.	15@63°C	1.3	2.7 / 2.5
6T7		Cr. 20.5 (Sm 18.8) N 29.4 Iso.	23@RT	0.09	2.0 / 1.9
RO-TN-403/015S	Multi-component mixture (<i>n</i> CB, <i>n</i> OCB, <i>n</i> CT, <i>n</i> CPhPy, <i>n</i> PDP, 0.1 wt.-% cholesteryl nonanoate).	Cr. <0 N 81.5 Iso.	78.4@RT	-	5.5 / 4.6
E7	4-component mixture (5CB, 7CB, 8OCB and 5CT).	Cr. <-30 N 58 Iso.	45.5@RT	-	8.5 / 5.7

[a] η = viscosity as measured in a standard cone rheometer. RT = room temperature. [b] μ = molecular dipole moment. [c] ϵ_r = relative dielectric permittivity at 10 kHz and $\pm 2.5^\circ\text{C}$ from the nematic (N) - isotropic (I) transition, in the N case measured along **n**. [d] These mesogens tend to organize into antiparallel dimers. [e] Several conformations have similar energy, the resulting μ ranging from 1.8D to 3.1D.

Cholesterics

Substance	Molecular formula Molar mass [g/mol]	Phase sequence [$^\circ\text{C}$]	Melting enthalpy [kJ/mol]
Cholesteryl nonanoate	$\text{C}_{36}\text{H}_{62}\text{O}_2$ 526.88	Cr. 77 SmA* 79 N* 90 Iso.	23.45 [199]
Cholesteryl oleyl car- bonate	$\text{C}_{46}\text{H}_{80}\text{O}_3$ 681.13	Cr. 26.7 N* 34 Iso. Iso 34 N* 20 Sm*	27.34 [200]
Cholesteryl benzoate	$\text{C}_{34}\text{H}_{50}\text{O}_2$ 490.76	Cr. 145 N* 178 Iso.	33.40 [201]
(S)4-(2-methylbutyl)- 4-cyanobiphenyl CB15	$\text{C}_{18}\text{H}_{19}\text{N}$ 249.35	Cr. 4 Iso Iso -30 N* -54 SmA* [202]	-

Surfactants

Surfactants for isotropic CNT Dispersions

Substance	Molecular formula Molar mass [g/mol]	Micelle shape at low con- centrations	CMC (mmol/L)	Association number	pK _A of conjugated acid
SDS	$\text{C}_{12}\text{H}_{25}\text{NaO}_4\text{S}$ 288.40	spherical	2.3 [203]	62 [203]	-
SDBS	$\text{C}_{18}\text{H}_{29}\text{NaO}_3\text{S}$ 348.48	spherical	1.0 [204]	30 [205]	0.45
SC	$\text{C}_{24}\text{H}_{39}\text{NaO}_5$ 430.55	disklike [121]	3.9 – 6.0 [206]	4 [207]	4.98
SDC	$\text{C}_{24}\text{H}_{39}\text{O}_4\text{Na}$ 414.6	disklike [121]	1.7 – 3.3 [206]	4 [206]	-
DNA	d(GT) ₁₀ 6.413 kDa	Integrated DNA technologies, Inc. (Coralville, Iowa, USA)			

Secondary LC-forming surfactants

Substance	Molecular formula Molar mass [g/mol]	Krafft Temperature [°C]	Phase sequence in water at 25 °C [wt%]
CTAB	C ₁₉ H ₄₂ BrN 364,45	24	I 25 N 28 H
MTAB	C ₁₇ H ₃₅ BrN 333.37	< 20	I 40 H
CEDAB	C ₂₀ H ₄₄ BrN 378.47	< 20	I 31 N 33 H

7.2. Equipment

Centrifuge	Hettich Universal 320R
Dielectric bridge	HP 4192A LF Impedance Analyzer
Differential Scanning Calorimeter	Perkin Elmer Pyris 1
Glue dispenser	Asymptek 402
High Speed Camera	Motion ProX 4
LC cells	E.H.C. liquid crystal cells (planar, 10 µm) Chalmers liquid crystal cells (homeotropic, 9 µm)
Magnetic Stirrer	VWR VMS-C7
Microfluidic device	Fluigent MFCS-FLEX
Microscope	Nikon Eclipse LV100
Microscope spectrometer	Photo Research PR-702A
Raman spectrometer	Horiba JOBIN YVON HR800 Raman Spectrometer with Olympus BX41 optical microscope
Rheometer	Anton Paar Physica MCR-301
Ultrasonic bath	Bandelin Sonorex TK52
Ultrasound processor	Dr. Hielscher UIS250L
UV/Vis spectrometer	Varian Cary 5000

7.3. Procedures

7.3.1. Dispersion procedures

Tip Sonication

Tip sonication was done by immersing the sonotrode tip into the sample, which was immersed in an ice bath for cooling. To assure similar dispersion conditions for every sample care was taken to center the sonotrode in the used vial and to use the same height of immersion for all the samples. Although our procedures allowed comparable results even when using different vials and sample volumes all comparison of results in this thesis are between samples going through the exact same dispersion process.

The different vials used were 1.5 mL Eppendorf cups and 4 mL cylindrical glass vials with a diameter of 1 cm for 1 mL samples, 10 mL cylindrical glass vials with a diameter of 2 cm for 10 mL samples and 25 mL cylindrical glass vials for 20 mL samples. The sonotrode immersion depth was set to the 0.25 mL marker for the Eppendorf cups, half of the sample height for the 4 mL vials and about one 1 cm above the bottom for the larger vials (see Fig. 7.1).

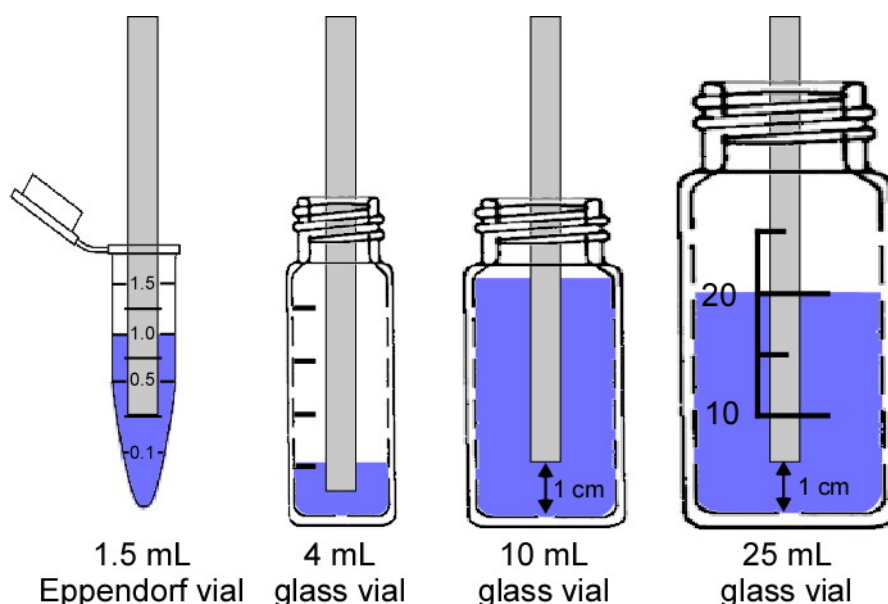


Fig. 7.1: Position of the sonotrode for the vial geometries and sample sizes used.

The sonotrode was used at 100% amplitude corresponding to 12 W delivered to the sample according to the manufacturer. Note that values of energy output of sonotrodes are notoriously flawed as they depend highly on factors such as immersion depth, sample geometry and

sample properties so that even if the Vial Tweeter and the sonotrode nominally have the same energy output one can consider the sonotrode as the method of much higher strength. Note also that the 12 W are the effective energy output as measured by the manufacturer. The energy input into the ultrasonic processor, which is often the value given in literature, in our case is 140 W.

The sonication cycle was continuous for aqueous surfactant solutions and 0.5 for thermotropic LCs in order to avoid phase transitions due to overheating. For sonication times see the following table. In general, sonication times were chosen such that no apparent change in the dispersion quality can be noticed by continued treatment.

Vial type	Sample volume	Sonication time	Medium	Sonication cycle
1.5 ml Eppendorf cup	1 mL	30 min	Thermotropic LC	0.5
			Aqueous surfactant solution	continuous
4 mL glass vial	1 mL	30 min	Thermotropic LC	0.5
			Aqueous surfactant solution	continuous
10 mL glass vial	10 mL	3 h	Aqueous surfactant solution	continuous
25 mL glass vial	20 mL	3 h	Aqueous surfactant solution	continuous

Stirring experiments

Stirring experiments were conducted in 4 mL cylindrical glass vials with a diameter of 1 cm and sample volumes of 1 mL. Two magnetic stir bars of 5 mm x 2 mm were used and the stirrer was set to half its maximum speed.

Vial Tweeter

The Vial Tweeter is specifically built to sonicate Eppendorf vials with higher energy input than an ultrasonic bath while avoiding the potentially destructive high power of a sonotrode. Since nothing is inserted into the sample, in contrast to the case when tip sonication is used, the risk of contamination is also minimized. The device has several sonication sites differing in energy input into the sample (Fig. 7.2). Only the four sites with the highest power were

used. Due to rapid heating of the sample the vial Tweeter was not suitable for thermotropic LCs. CNTs in aqueous surfactant solutions were however sometimes dispersed using the device, with multiple sonication steps using a 0.5 cycle at 100% amplitude for 20 min followed by a 10 minute pause to avoid overheating. Without the pause the heating can lead to melting or bursting of the Eppendorf cups which were closed using additional plastic clips. After every 2 hours of this treatment, thus after 4 x 20 min of sonication, an additional pause of 1 h was made. The treatment was usually run for 12 h over night yielding a total sonication time of 5h and 20 min.

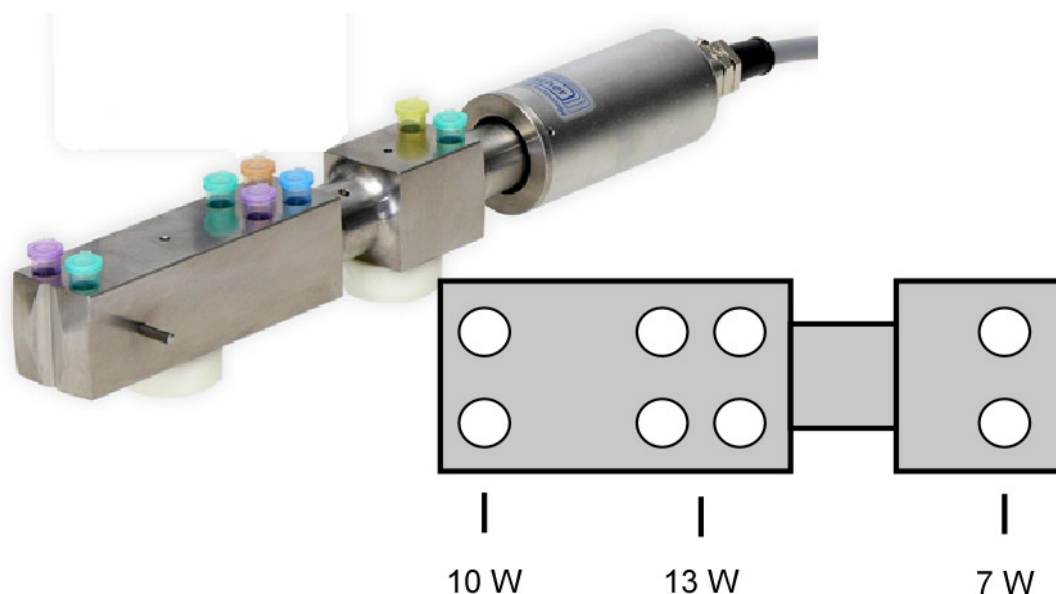


Fig. 7.2: Vial Tweeter and corresponding sonication powers for each set of sonication sites as given by the manufacturer.

7.3.2. Preparation of lyotropic LC/CNT composite

Step 1: Preparation of the isotropic CNT-dispersion in aqueous surfactant solution

The isotropic CNT-dispersion can be prepared via sonotrode treatment or the Vial Tweeter as outlined above. The surfactant to CNT ratio was generally set to 5:1.

Step 2: Preparation of the lyotropic LC/CNT composite

In general 1 mL of isotropic CNT dispersion was given to the right amount of LC-forming surfactant (standard: 28 wt% CTAB or 32 wt% CEDAB) with a 1 cm magnetic stir bar already immersed in the dry powder. The magnetic stir bar should be big enough to homogeneously stir the whole sample. An inclined position in the vial proved advantageous (Fig. 7.3).

The mixture was then carefully stirred so that a slow homogenous stirring of the whole sample was achieved without the formation of foam. Highly viscous parts of liquid crystal with locally increased surfactant concentration that may be sticking to the bottom of the vial during machine stirring, can be removed by stirring the sample manually using a strong permanent magnet (Fig. 7.3). The stirring continued for at least one hour. This was followed by a sonication step in the ultrasonic bath until the polarizer effect could be seen (typically 3 hours). Samples were stored at 30°C to avoid crystallization.

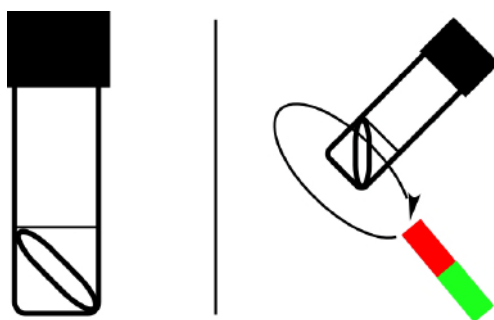


Fig. 7.3: Position of the stir bar in the sample for lyotropic LC/CNT composite production (left), and removal of highly viscous parts of high-surfactant-concentration LC by hand using a permanent magnet.

7.3.3. Checking for polarizer effect

The polarizer effect was checked by slowly sucking the LC/CNT-composite into an optically flat capillary with a thickness of 200 μm , which was fixed to a syringe using shrinking tubes (Fig. 7.4). The polarizer effect can then be confirmed by rotating the sample in front of a linear polarizer (or vice versa). For further use the ends of the capillaries were then sealed using epoxy resin.

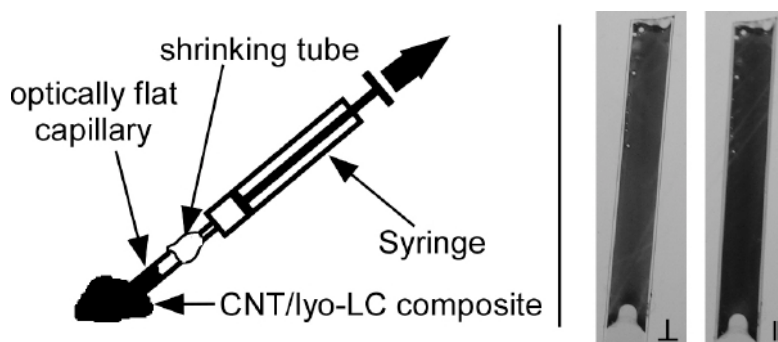


Fig. 7.4: Schematic depiction of the capillary filling process (left) and pictures of the filled capillary with the incident light being polarized perpendicular and parallel to the capillary axis, respectively (right).

7.3.4. Polymerization of lyotropic LCs

The polymerization routine followed published procedures[180]. 28 wt% of acrylate-modified CTAB was mixed with 6% 1,6-hexanediol dimethacrylate as crosslinker and 1 wt% Irgacure 2958 as initiator (in respect to monomer concentration). Oxygen was removed from the used water by a combination vacusuction and flushing with argon. The so-produced lyotropic LC phase could be polymerized by irradiation for about 30 minutes using a UV lamp.

7.3.5. High Speed camera measurements

The increasing opacity of each sample during sonication, due to the continuously improved dispersion of the CNTs, was measured using the image analysis features of the high-speed video camera software (Motion ProX Studio). The total brightness of a $\sim 25 \text{ mm}^2$ area just below the sonotrode was measured in each frame of video since turning on the sonication power, normalizing the value to the initial video frame. For the experiment a water bath was kept on a heating plate and in it were immersed a sample vial with weighed-out dry CNTs (1 mg) as well as a second vial containing 1 mL of the host liquid. The sonotrode was positioned from the start for acting on a liquid filled into the first of these vials. Once the desired bath temperature had been attained a Pasteur pipette preheated with an air gun was used to rapidly transfer the liquid to the vial containing the CNTs and immediately afterwards the video recording and sonotrode treatment were started. Because the LCs have some solvation power on CNTs, the addition of LC to the vial immediately led to a swelling of the CNT powder, making the CNT component look substantially larger in these vials than in the vials with aqueous solvent or NMP, in which no or only negligible swelling took place. Moreover, the mass of swelled CNTs stayed at the vial bottom after addition of the LC, whereas the non-swelled grains in case of the isotropic solvents were distributed throughout the sample as a result of the solvent addition, even before turning on the sonication. In the movie still images shown in chapter 4.2.1, Fig. 4.12 a, these two effects give the false impression that less CNTs would be present in the reference experiments with isotropic solvents but this is not the case. The initial cavitation often produced a brief artifact dip in transmission, particularly dramatic for the case of water as solvent in Fig. 4.12 a. As one might suspect that the required variation in temperature of the liquid host within the experiment would have an impact on the result we performed the experiment with NMP as host at room temperature as well as at 90°C , the latter being above the highest temperature used for the LCs. The results were similar, confirming that the effect of the temperature variations in the experiment is small. This is in fact to be expected

since all liquids are far below their boiling points and it is the distance to this temperature that is thermodynamically relevant.

7.3.6. Percolation measurements

For the percolation measurements a dispersion of 1 mg/mL HiPCO was dispersed in E7 by 24 h of magnetic stirring followed by a tip sonication step. This was followed by centrifugation at 13400 rpm for 30 min using an Eppendorf MiniSpin centrifuge to remove large aggregates and subsequently decantation. The concentration of the supernatant was measured by UV/Vis spectroscopy and a concentration series was produced by stepwise dilution of the sample with pure E7.

For measurement the mixtures were filled into homeotropically (Chalmers cells, 9 μm cell thickness) or planar (E.H.C. cells, 10 μm cell thickness) aligning LC-cells that were wired to the dielectric bridge (Fig. 7.5). Before being filled into the cell every dispersion underwent a brief tip sonication step of 1 min. The measurement program consisted of a DC bias sweep from 0 to 15 V (0.5 V steps from 0 to 3V followed by 1 V steps) with an AC measurement field with a 0.1 V amplitude with frequencies of 5 Hz to 13 MHz. After application of each bias a 10 s pause was set before the start of the measurement in order to reach steady state. The samples were measured at either 30°C in the nematic phase or at 70°C in the isotropic phase.

For reproducible results it is advisable to only work with freshly filled cells, since the mixtures degrade over the time of several measurements, especially when heated into the isotropic phase.

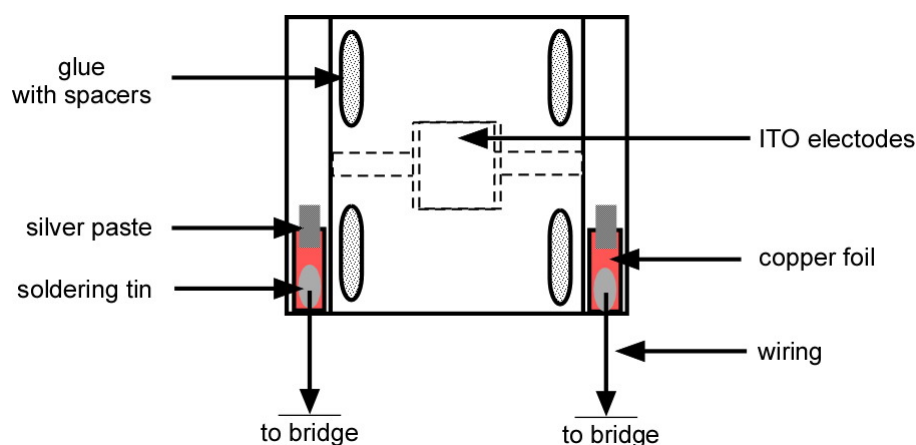


Fig. 7.5: Schematic depiction of a liquid crystal cell used for percolation measurements

7.3.7. UV/Vis Measurements on thermotropic LC/CNT mixtures

Since the turbidity of the nematic phase impairs absorption measurements the samples were heated quickly into the isotropic phase. The cuvette was preheated in the sample holder to a temperature of 10 °C above the clearing point. A 150 μl cuvette with 10 mm light patch was used. The sample was filled in the preheated cuvette and placed in the heated sample holder. Measurement was taken immediately after the absorption became constant, indicating that the sample has reached the isotropic phase. This procedure is only feasible for well-dispersed samples since heating into the isotropic phase will cause aggregation. To ensure fast measurements preheating of the cuvette and small sample volumes are advisable. To obtain a value for the extinction coefficient α we prepared two series of HiPCO CNT dispersions in MBBA and E7, respectively, with concentrations ranging from 0.001 to 0.1 mg mL^{-1} and measured their absorption spectra (Fig. 7.6). The extinction coefficient α at 655 nm wavelength was yielded by dividing the absorption by the sample length and plotting it as a function of CNT concentration. The slope of the linear fit equals the extinction coefficient α_{655} according to the Beer-Lambert law [130,131]

$$A = \log\left(\frac{I_0}{I_1}\right) = \alpha_\lambda cd \quad (7.1)$$

with A the Absorption, I_0 and I_1 the intensity of the incident and transmitted light, respectively, α the extinction coefficient at the specified wavelength, c the concentration and d the path length.

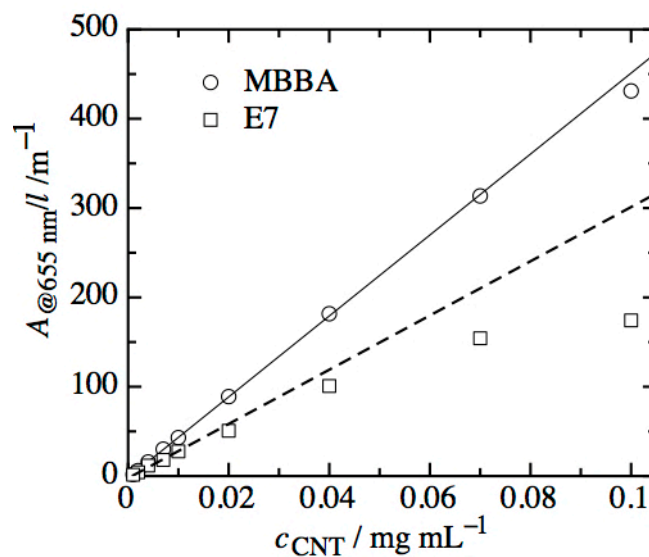


Fig. 7.6: Sample thickness-normalized absorption A/l as a function of wavelength for dispersions of HiPCO in E7 and MBBA, respectively, heated to the isotropic phase just prior to measuring.

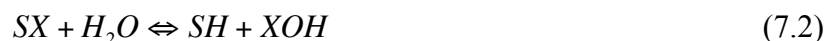
7.3.8. Calculation of dipole moments of thermotropic LCs

The calculations of the dipole moments were done by Dr. Stefan Jagiella from the group of Prof. Frank Gießelmann at the University of Stuttgart. The structures of the molecules and their dipole moments were calculated using the Turbomole program package (TURBOMOLE V6.1 2009, available from <http://www.turbomole.com>.) at the DFT (density functional) level employing the RI-*J* (resolution of identity)[208,209] approximation and the BP86 functional[210] with the def2-TZVP basis set [211,212]. With the exception of MBBA the dipole moments did not depend significantly on the choice of one of the different possible minimum structures with similar energies.

7.4. Additional data

7.4.1. Degrees of protonation of surfactants

If an anionic surfactant SX is brought into water it will dissociate into the species X^+ and S^- . Depending on the acidic strength of the conjugated acid SH some part of the S^- will get protonated by a reaction with the water molecules. Eventually equilibrium is reached which can be expressed by the law of mass action [213,214]:



$$K = \frac{[SH][XOH]}{[SX][H_2O]} \quad (7.3)$$

with the assumption that the concentration of the water $[H_2O]$ stays constant (water in excess) and gets incorporated in the constant K_B and that the concentration of the protonated surfactant $[SH]$ equals $[XOH]$ one gets

$$K_B = \frac{[SH]^2}{[SX]} \quad (7.4)$$

with K_B the base dissociation constant. By defining the degree of protonation p

$$p = \frac{[SH]}{[SX]_0} \quad (7.5)$$

using the original concentration of the non-protonated surfactant $[SX]_0$ follows

$$K_B = \frac{p^2[SX]_0^2}{[SX]_0 - p[SX]_0} \quad (7.6)$$

$$K_B = \frac{p^2[SX]_0}{1 - p} \quad (7.7)$$

$$p^2 + \frac{K_B}{[SX]_0} p - \frac{K_B}{[SX]_0} = 0 \quad (7.8)$$

$$\rightarrow p = -\frac{K_B}{2[SX]_0} \pm \sqrt{\left(\frac{K_B}{2[SX]_0}\right)^2 + \frac{K_B}{[SX]_0}} \quad (7.9)$$

The pK_B value for basic strength is defined as:

$$pK_B = -\log K_B \quad (7.10)$$

and can be derived from the pK_A value of the conjugated acid

$$pK_A + pK_B = 14 \quad (7.11)$$

From this a degree of protonation for surfactants SDBS and SC can be calculated at the concentration of the experiment (12.5 mg/mL). Although the degree of protonation is about 200 times larger for SC than for SDBS they are both in the ppm scale and can be neglected.

	c [mmol/L]	pK_B	p
SDBS	35.9	13.55	1 ppm
SC	29.0	9.02	180 ppm

7.4.2. Viscosity of thermotropic LCs

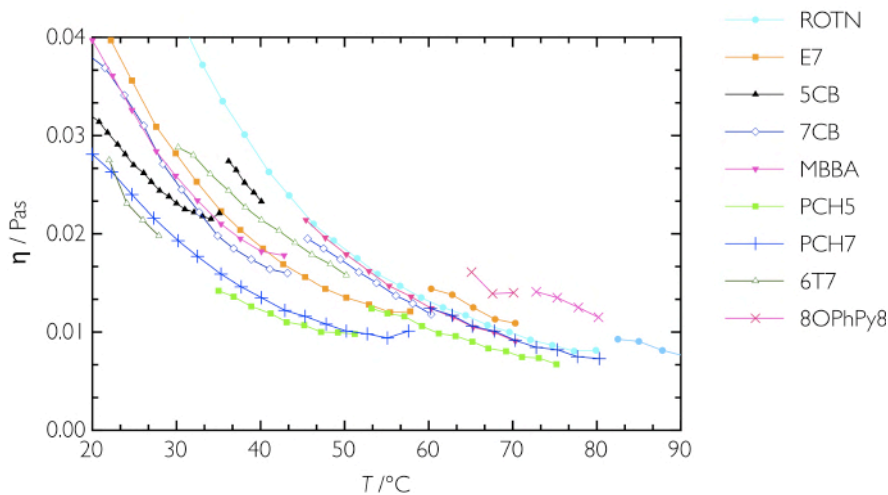


Fig. 7.7: Diagram of the viscosity of the used thermotropic liquid crystals as measured by a standard cone rheometer.

7.4.3. Klopman-Salem Equation

$$\Delta E = -\sum (q_a + q_b) \beta_{ab} S_{ab} \quad \text{first term} \quad (7.11)$$

$$+ \sum_{k < l} \frac{Q_k Q_l}{\epsilon R_{kl}} \quad \text{second term} \quad (7.12)$$

$$+ \sum_r^{\text{occ.}, \text{unocc.}} \sum_s^{\text{occ.}, \text{unocc.}} - \sum_s^{\text{occ.}, \text{unocc.}} \sum_r^{\text{occ.}, \text{unocc.}} \frac{2 \left(\sum_{ab} c_{ra} c_{sb} \beta_{ab} \right)^2}{E_r - E_s} \quad \text{third term} \quad (7.13)$$

with:	q_a and q_b	electron populations un atomic orbitals a and b
	β and S	resonance and overlap integrals
	Q_k and Q_l	total charges on atoms k and l
	ϵ	local dielectric constant
	R_{kl}	distance between atoms k and l
	c_{ra}	coefficient of atomic orbital a in molecular orbital r
	c_{sb}	coefficient of atomic orbital b in molecular orbital s
	E_r	Energy of molecular orbital r
	E_s	Energy of molecular orbital s

The Klopman-Salem Equation describes the interaction energy of two molecules in close proximity. The first term specifies the interaction Energy of occupied orbitals with other occupied orbitals, i.e. the Pauli repulsion. The second term characterizes the electrostatic forces between charged molecules. The third term describes the interaction between unoccupied orbitals of one molecule with occupied orbitals of the other molecule.

8. Curriculum Vitae

Name: Stefan Schymura

Geburt: 14.07.1982 in Ludwigsburg

Ausbildung:

1989 – 1993:	Grundschule Tamm Hohenstange
1993 – 2002:	Albertus-Magnus-Gymnasium Stuttgart Sommer- rain 19 Juni 2002 Abitur
2002 – 2007:	Chemiestudium an der Universität Stuttgart 06. September 2004: Diplomvorprüfung 06. November 2007: Diplomprüfung

Berufserfahrung:

Mai 2007 – Nov. 2007	Wissenschaftlicher Mitarbeiter am Institut für Physikalische Chemie der Universität Stuttgart
Jan. 2008 – März 2011	Wissenschaftlicher Mitarbeiter am Institut für Chemie - Physikalische Chemie der Martin- Luther-Universität Halle-Wittenberg
seit Juli 2011	Wissenschaftlicher Mitarbeiter am Institut für Ressourcenökologie des Helmholtz-Zentrum Dresden-Rossendorf

9. List of Publications

Diploma thesis:

„Dispersionen von Kohlenstoffnanoröhrchen in thermotropen Flüssigkristallen: Präparation, Struktur & Eigenschaften“, Stefan Schymura, *Diploma thesis*, Institute of Physical Chemistry, University of Stuttgart, **2007**

Peer-reviewed articles:

„Gold catalysis: Alkylideneoxazolines and -oxazoles from intramolecular hydroamination of an alkyne by a trichloroacetimidate“, A.S.K. Hashmi, M. Rudolph, S. Schymura, J. Visus, W. Frey, *Eur. J. Org. Chem.* 21, 4905-4909, **2006**

„Carbon nanotubes in liquid crystals as versatile functional materials“, G. Scalia, J. Lagerwall, S. Schymura, M. Haluska, F. Gießelmann, S. Roth, *Phys. Status Solidi B* 244(11), 4212-4217, **2007**

„Macroscopic-scale carbon nanotube alignment via self-assembly in lyotropic liquid crystals“, S. Schymura, E. Enz, S. Roth, G. Scalia, J. Lagerwall, *Synthetic Met.* 159(21-22), 2177-2179, **2009**

„Towards Efficient Dispersion of Carbon Nanotubes in Thermotropic Liquid Crystals“, S. Schymura, M. Kühnast, V. Lutz, S. Jagiella, U. Dettlaff-Weglikowska, S. Roth, F. Gießelmann, C. Tschierske, G. Scalia, J. Lagerwall, *Adv. Funct. Mater.* 20(19), 3350-3357, **2010**

„Filament formation in carbon nanotube-doped lyotropic liquid crystals“, S. Schymura, S. Dölle, J. Yamamoto, J. Lagerwall, *Soft Matter* 7, 2663-2667, **2011**

„Nematic-Smectic Transition under Confinement in Liquid Crystalline Colloidal Shells“, H.-L. Liang, S. Schymura, P. Rudquist, J. Lagerwall, *Phys. Rev. Lett.* 106(24), 247801, **2011**

„Effects of chain branching and chirality on liquid crystalline phases of bent-core molecules: blue phases, de Vries transitions and switching of diastereomeric states“, H. Ocak, B. Bilgin-Eran, M. Prehm, S. Schymura, J. Lagerwall, C. Tschierske, *Soft Matter* 7, 8266-8280, **2011**

„Utilizing the krafft phenomenon to generate ideal micelle-free surfactant-stabilized nanoparticle suspensions“, S. Dölle, B.-D. Lechner, J.H. Park, S. Schymura, J. Lagerwall, G. Scalia, *Angew. Chem. Int. Ed. Engl.* 51(13), 3254.3257, **2012**

„On the effect of carbon nanotubes on properties of liquid crystals“, S. Schymura, G. Scalia, *Phil. Trans. A*, **2013**, in print

Oral presentations:

„Strategies for the radiolabelling of carbon nanoparticles“, S. Schymura, I. Cydzik, A. Bulgheroni, F. Simonelli, U. Holzwarth, J. Kozempel, K. Franke, N. Gibson, Nanosafe 2012, Grenoble, France

„Radiolabelling of engineered nanoparticles – different strategies for Ag⁰-NP, TiO₂-NP and MWCNT“, S. Schymura, H. Hildebrand, I. Cydzik, F. Simonelli, A. Bulgheroni, U. Holzwarth, J. Kozempel, A. Freyer, E. Bilz, K. Franke, N. Gibson, Cycleur Meeting 2012, Ispra, Italy

Poster presentations:

„Dispersions of carbon nanotubes in liquid crystals“, S. Schymura, V. Lutz, U. Dettlaff-Weglikowska, S. Roth, F. Gießelmann, J. Lagerwall, G. Scalia, 36th Topical Meeting on Liquid Crystals, Magdeburg, **2008**

„Carbon nanoparticles in cholesteric liquid crystals“, S. Schymura, J. Lagerwall, 37th Topical Meeting on liquid Crystals, Stuttgart, **2009**

„Filament formation in carbon nanotube-doped lyotropic liquid crystals“, S. Schymura, S. Dölle, F. Schörg, F. Gießelmann, J. Lagerwall, 38th Topical Meeting on Liquid Crystals, Mainz, **2010**

„Towards efficient dispersion of carbon nanotubes in thermotropic liquid crystals“
S. Schymura, M. Kühnast, V. Lutz, S. Jagiella, U. Dettlaff-Weglikowska, S. Roth,
F. Gießelmann, C. Tschierske, J. Lagerwall, G. Scalia, 23rd International Liquid Cryst-
tal Conference, Krakow, **2010**

„Rapid carbon nanotube modification and radiolabelling for particle tracing applica-
tions“, S. Schymura, K. Franke, J. Lippmann-Pipke, NanoNature Clustertreffen,
Frankfurt, **2012**

„Colloidal stability of modified carbon nanotubes“, S. Schymura, S. Weiß, H. Zänker,
K. Franke, Nanosafe, Grenoble, **2012**

„Colloidal Stability of Carbon Nanotubes“, S. Schymura, S. Weiß, H. Zänker, K.
Franke, NanoNature Clustertreffen, Frankfurt, **2013**